Atlas of changes in salt marsh boundaries at selected islands in the West Branch of the Westport River, 1934-2016

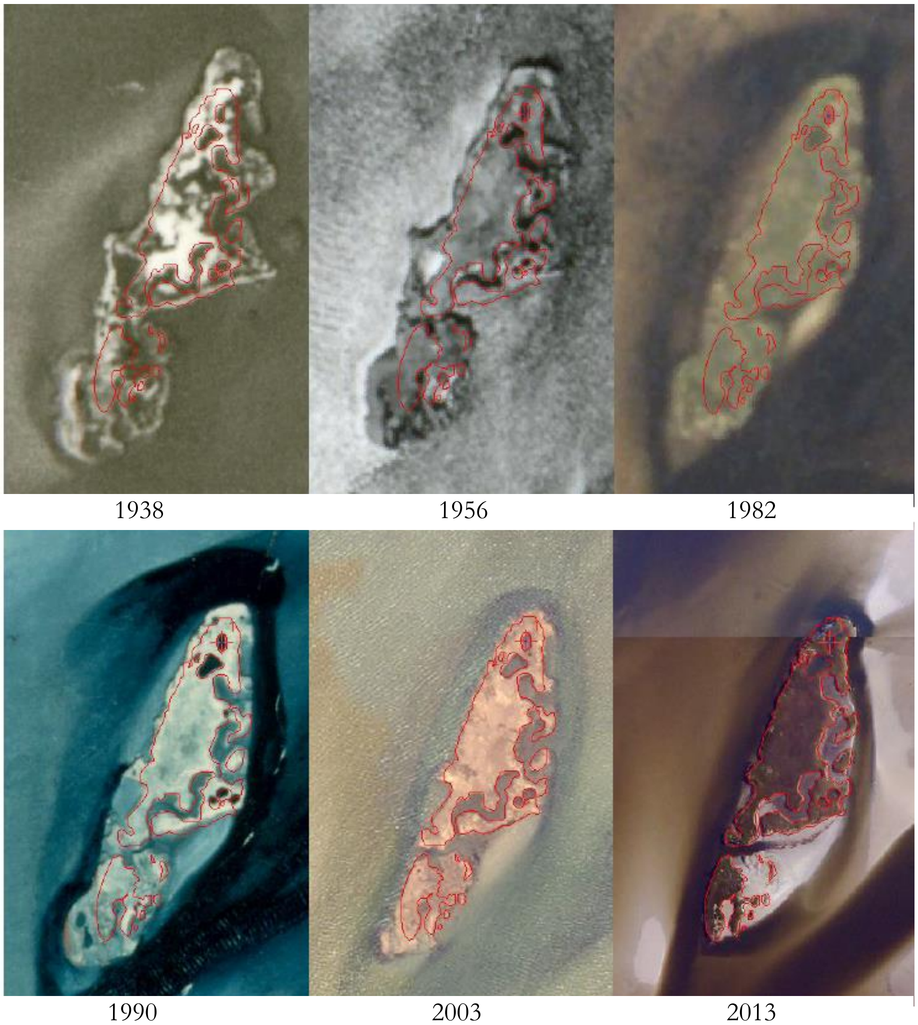

Joseph E. Costa[1] and Molly Weiner[2]

February 2017

[1] Massachusetts Office of Coastal Zone Management, Buzzards Bay National Estuary Program, East Wareham, MA 02538
[2] Buzzards Bay Coalition, New Bedford, MA, 02740

Acknowledgments

Thanks to the Buzzards Bay Coalition and the Westport Fishermen's Association for funding Molly Weiner's work under this project. Thanks also to Tracy Warncke for scanning contact prints of many of the aerials used in this study, and to Bob Boeri, Massachusetts CZM for researching dredging permit information for the Town of Westport with Massachusetts Department of Conservation and Recreation and the U.S. Army Corps of Engineers, and to Paul Curado for operating the UAV and splicing together the imagery which was used to document 2016 conditions. The Buzzards Bay Coalition purchased from NOAA digital scans of several photographs used in this study. Work by the Buzzards Bay National Estuary Program staff was funded by the United States Environmental Protection Agency under assistance agreement CE-96185701 to the Massachusetts Executive Office of Energy and Environmental Affairs.

Suggested citation: Costa, J.E and M. Weiner. 2017. Atlas of changes in salt marsh boundaries at selected islands in the West Branch of the Westport River, 1934-2016. Buzzards Bay National Estuary Program Technical Report. 123pp.

Cover: Aerial images of Bailey Flat from different periods, all with 2013 image marsh boundaries superimposed.

Introduction

Reports of apparent rapid salt marsh loss in the West Branch of the Westport Rivers prompted a collaborative study of representative marsh islands by the Buzzards Bay Coalition in collaboration with scientists from the Woods Hole Research Center/Marine Biological Laboratory Ecosystem Center, the Buzzards Bay National Estuary Program (NEP) and the Westport Fishermen's Association. The planned evaluation included a GIS analysis of historical aerial photographs led by the Buzzards Bay NEP with Buzzards Bay Coalition staff support, and field studies of marsh biomass led by the Buzzards Bay Coalition under the guidance of Linda Deegan and Chris Neill of the Woods Hole Research Center / Ecosystems Center, Marine Biological Laboratory.

This report summarizes the findings of the GIS analysis of changing marsh boundaries, which was undertaken by Buzzards Bay NEP, with support from Buzzards Bay Coalition staff. An analysis of the causes of the more recent accelerated declines in marsh area is addressed separately (Jakuba et al, 2017[3]).

Methods

A cursory review of historical aerial photographs showed that some marsh islands in the West Branch had greater area losses in recent decades than others (for example, Fig. 1 and Fig. 2). To better understand potential drivers of this phenomenon, six different islands with different apparent rates of loss along a north-south gradient in the West Branch of the Westport River were evaluated.(Fig. 3). Marsh islands were delineated by heads-up digitizing of aerial imagery using ArcGIS® software by Esri (ArcMap™ Desktop 10.1). Imagery was rectified and georeferenced, using ArcGIS functions. Polygon areas were calculated in ArcGIS, with some additional analysis completed in an Excel spreadsheet using pivot table functions and regression analysis.

Acquired aerial images taken between December 1938 and May 2015 were evaluated in this study (summary shown in Table 1). In addition, a local unmanned aerial vehicle (UAV) operator provided vertical aerial images of the study sites taken on 27 September (Great Flat 12) and on 5 October 2016 (other sites). A 1934 boundary, inferred from a coastal and geodetic survey chart, was also evaluated to ascertain possible Hurricane of 1938 impacts, but the area derived from this source was not included in the image analysis trends because the 1936 chart tracing of the islands lacked details of the number and size of most smaller pannes and pools evident on aerial images.

The imagery used varied by scale, quality, and image type (black and white, color, and color infrared), tidal elevation, and season. Some of the imagery was available in digital form, and some were contact prints that were purchased at various times and subsequently scanned, generally at 600 to 1200dpi. Most of the imagery had to be georeferenced and rectified in ArcGIS, to match the MassGIS April 2014 base maps. This typically required fine scale transformations for each island. Even imagery already georeferenced was repositioned (generally positional adjustments were less than 10 m), to more precisely match the 2014 base maps.

On aerial photographs, shadows on the east sides of structures indicate the photograph was taken after solar noon; shadows on the west side of structures indicate the photograph was taken before solar noon. The precise time the aerial photograph was taken can be calculated by the shadow angle from true north because this angle equals the solar azimuth-180 degrees. The times the photographs were taken was estimated through an iterative process using the NOAA Solar Position Calculator (http://www.esrl.noaa.gov/gmd/grad/solcalc/azel.html).

[3] Jakuba, R. M. Weiner, J. Costa, L. Deegan, and C. Neill. 2017. Westport River Salt Marsh Loss Study. In preparation.

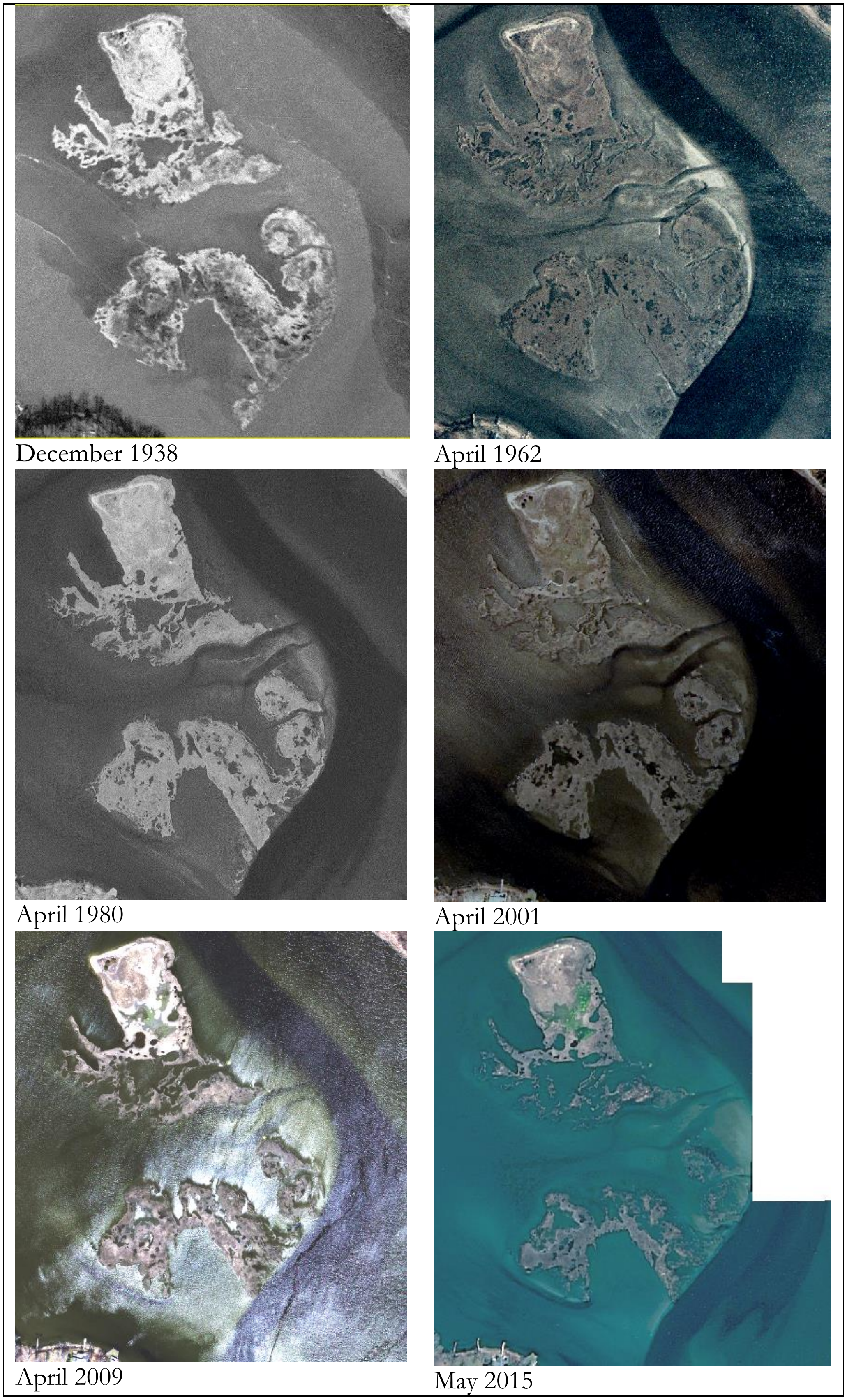

Fig. 1 Sanford Flats A, B, and C

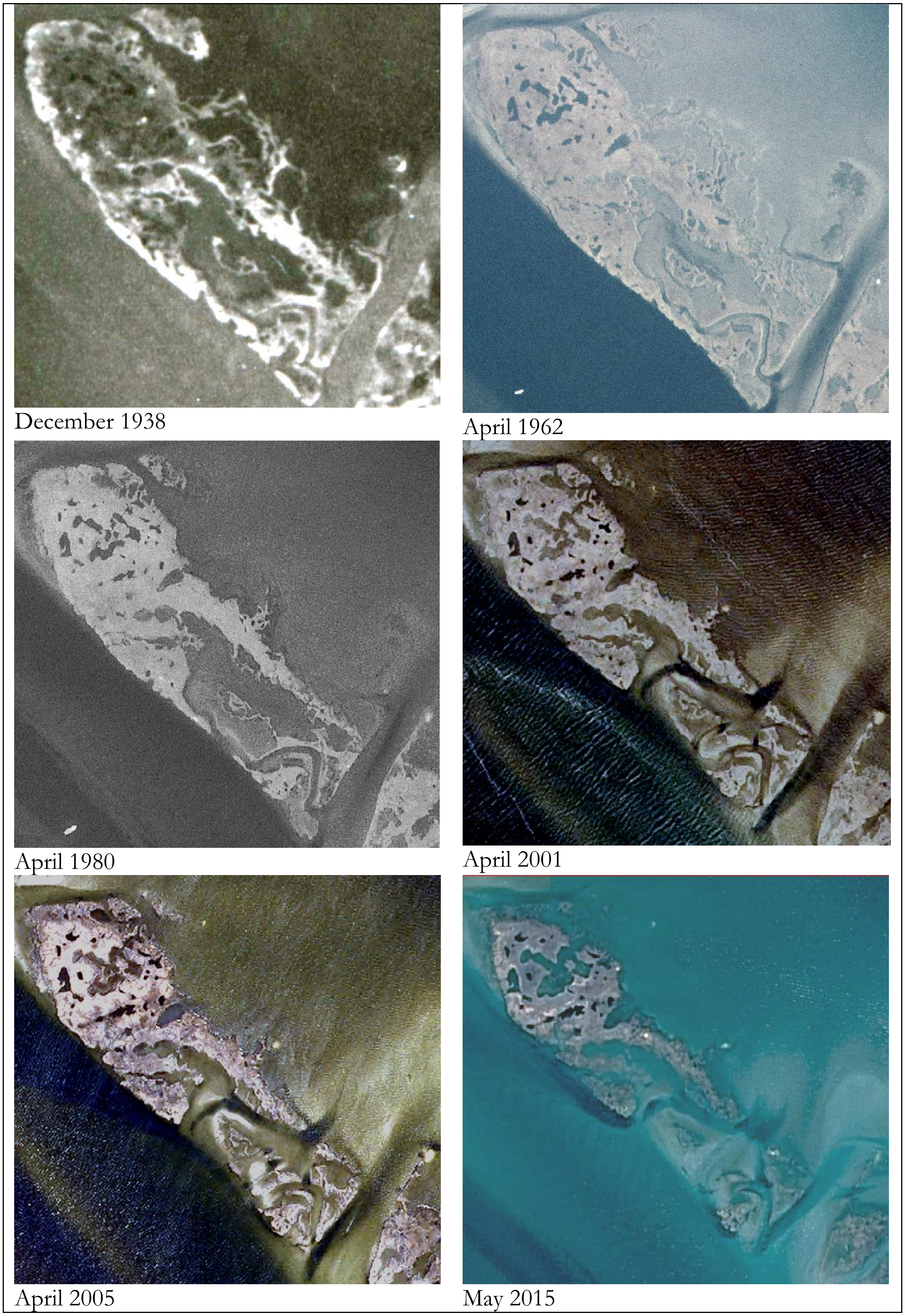

Fig. 2 From North to south, Great Flat 11, 10, 9, and portion of Great Flat 8.

The time that each photograph was taken was used to estimate the predicted tidal conditions at the time of the survey using Dean Pentcheff's WWW Tide and Current Predictor (http://tbone.biol.sc.edu/tide/tideshow.cgi). The tidal elevation was important in interpreting and understanding some photographs, like the 1938 imagery, which was taken within a half hour of a spring high tide in December. At the highest tides (with turbid waters) it is difficult to discern low marsh boundaries, and provides an understanding of potential errors in interpreting differences in area between any two dates.

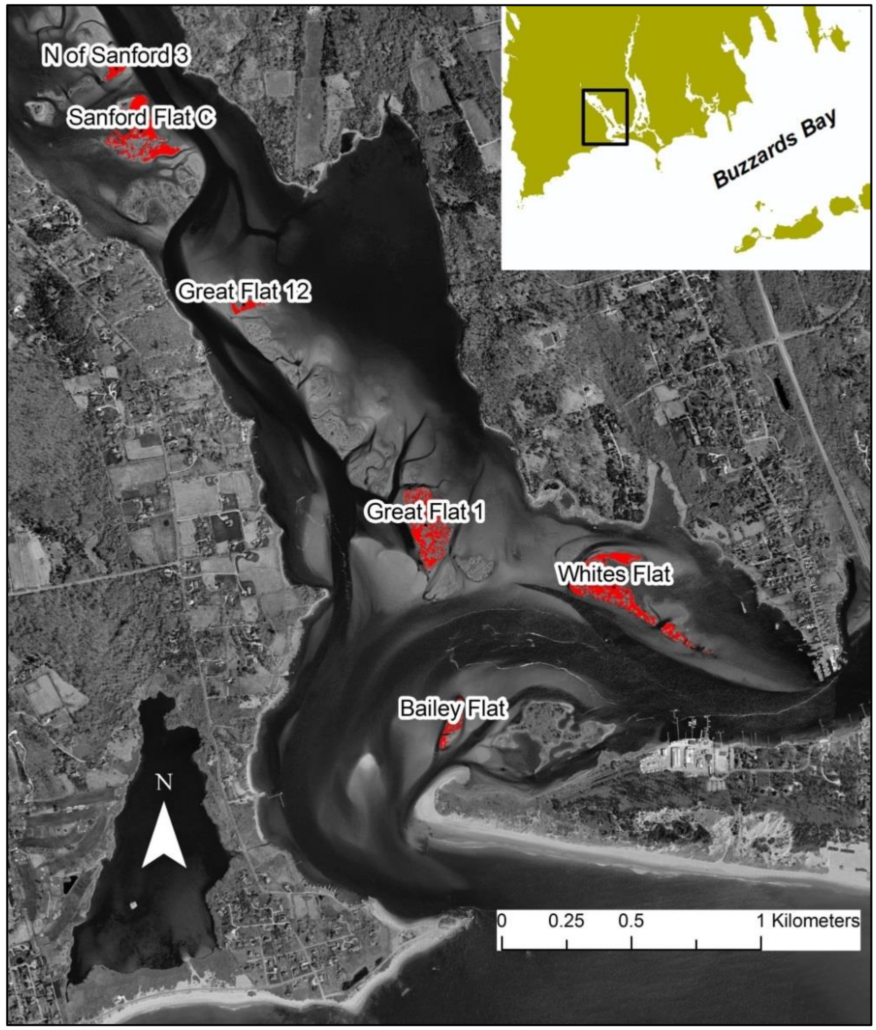

Fig. 3 Salt marsh islands within the West Branch of the Westport River that were evaluated in this study (2015 marsh boundaries shown in red). True north is at the top of all images in this report. The Harbor entrance is at the bottom of the photograph.

Interpretation of the aerial photograph was informed by field observations and past experience in image analysis. The appearance and properties of each raster image was manipulated using ArcGIS tools, typically by stretching the red-green-blue composites with the percent clip or standard deviation display tools, and sometimes by changing contrast and brightness. This approach improved the ability to interpret vegetated and non-vegetated peat areas. Comparison of recent growing season high-resolution color 1/2 m pixel imagery, and the October 2016 UAV imagery (in some cases with less than 10 cm pixel size), together with field visits, proved immensely helpful in interpreting older imagery of poor quality or resolution.

In the analysis of the study sites, it was found that large salt marsh pannes, deep pools, and channels are generally persistent and expanding features in these island marshes, with features surviving decades, or even the entire study period. Changes in these internal marsh features are typically more gradual than changes in the outer marsh boundaries. These features were important for georeferencing imagery for each time step (using feature centers).

In defining the changes in outer and internal marsh boundaries for each image, two key assumptions were applied to interpreting marsh boundary changes in these islands: 1) outer salt marsh boundaries are lost and never recover (especially if the loss was due to undercutting or erosion), and 2) channels and pools only increase in width and diameter over time. Exceptions to these rules of thumb were observed. Notably, the southern island of Bailey Flat (closest to the harbor entrance) was overwashed by sand from storms in 2011 and 2012. By 2015, some small islets were uncovered and appeared revegetated with *Spartina*. Another exception was that in a few instances, it appeared that small shallow pannes in the upper marsh areas appear to have drained and become revegetated.

Table 1. Aerial imagery evaluated in this study.

Date	Source	Type	Comments
1934-11-15	Nautical Survey T-Sheet	Map	1936 map (NOAA T-sheet) drawn from 11/15/1934 aerial photograph 1934-11-15 19:29 UTC 3.49 ft High Tide
1938-12-13	NAR	B&W	NAR downloads and Scanned from contact prints from Costa archive, also available online. Photographs taken approximately 3 months after Hurricane of 1938. Preceding week temperatures above freezing with 4 inches of rain (New Bedford weather data).Shadow angle 8 degrees E of N, time = 17:10 UTC (12:10 EST), Newport Tide: High at 17:29 UTC 3.58 ft High Tide 1938-12-13 17:29 UTC 3.58 ft High Tide
1942-06-??		B&W	Early afternoon photo, shadow, ~+15 degrees of N
1954-04-22	Coast & Geodetic Survey	B&W	Shadow angle 5 degrees W of N, time = 16:33 UTC (11:33 EST) 1954-04-22 15:12 UTC 3.07 ft High Tide 1954-04-22 20:17 UTC 0.48 ft Low Tide
1956-05-01		B&W	Photo time: 12:20 Local Time 1956-05-01 17:08 UTC 2.92 ft High Tide
1962-04-10	Coast & Geodetic Survey	Color	mid morning photo, shadow -74 degrees of N. High Tide: 17:21 UTC 3.28 ft
1964-04-22		B&W	early afternoon photo, shadow +12 degrees of N 1964-04-22 16:01 UTC 0.33 ft Low Tide
1966-09-17	NOS NOAA	Color	HIgh: 14:25 UTC 4.76 ft, Low: 20:06 UTC -0.35 ft
1971-10-08	NOS NOAA	Color	High Tide: 15:24 UTC 4.40 ft
1974-02-27	USGS GS	B&W	High Tide: 16:10 UTC 3.16 ft
1980-04-18	NOS-NOAA	Infra-Red	High tide: 15:15 UTC 3.98 ft; Low: 20:20 UTC -0.18 ft
1981-10-14	NOS-NOAA	Color	Low tide: 18:40 UTC -0.40 ft
1982-06-15	NOS-NOAA	Color	High Tide:19:03 UTC 3.55 ft
1990-04-09	DEP UMASS WCP	Color IR	Low Tide: 17:23 UTC 0.03 ft
1994-06-??	MassGIS	Color	mid-morning photo, shadow ~-55 degrees of N
1994-09-??	NOS-NOAA	Color	Only low resolution images downloadable; photo time 14:06 GMT
1996-04-??	MassGIS HM SIDS	B&W	
2001-04-??	MassGIS	Color	
2001-06-15	DEP Eelgrass Survey	Color	High tide: 2001-06-15 19:32 UTC 3.26 ft
2003-08-15	USDA NAIP	Color	High:14:52 UTC 3.76 ft ; Low: 20:09 UTC 0.19 ft
2005-04-13	MassGIS	Color	April 9 through April 17, 2005 survey period, for 4/13, High: 16:00 UTC 3.02 ft, Low: 20:46 UTC 0.35 ft
2005-06-24	NOAA	Color	Low: 19:39 UTC -0.07 ft
2006-08-07	USDA NAIP	Color	Aug 3 to Aug 11, 2006 survey period; for 08/17, High was 19:28 UTC 3.68 ft
2009-04-15	MassGIS	Color	March 24 to April 26, 2009. 2009-04-15 16:44 UTC 2.81 ft High Tide
2009-09-01	NOAA	Color	August 10 to October 21, NOAA Integrated Ocean and Coastal Mapping (IOCM) initiative 2009-09-01 15:40 UTC 0.63 ft Low Tide
2010-08-27	USDA NAIP	Color	Aug 20 to Aug 29 survey period, for 08/27 Low was at 19:35 UTC 0.24 ft
2012-06-??	NOAA	Color	
2012-09-??	USDA	Color	
2013-06-14	MA DEP-NOAA	Color	Survey was May 28 through Sept 9, 2013, but Westport was 6/14; High: 16:33 UTC 3.29 ft
2013-09-??	USDA	Color	
2014-04-??	MassGIS	Color	
2014-07-18	USDA NAIP	Color	Survey was July 13 to July 29; for 7/18 high was at 17:36 UTC 4.10 ft
2014-09-11	Google Capture	Color	Low was at 19:47 UTC -0.32 ft
2015-05-06	Google Capture	Color	Low at 19:18 UTC 0.21 ft
2015-05-07	WorldView Orthoimagery	Color	see http://www.mass.gov/anf/docs/itd/services/massgis/ortho2015wv-index.pdf; low at 19:18 UTC 0.21 ft
2016-10-06	UAV imagery	Color	

Overall, however, the expansion of pools and channels was continuous over the study period (although rates varied), and the biggest challenge of interpretation was determining whether marsh peat was vegetated, or in water too deep to sustain vegetation. For example, deep pannes and pools (also sometimes called "pond holes" in the literature) in the marsh are generally dark colored. However, when those features became connected by a channel and have appreciable tidal exchange, those deep pannes and pools then appear light in color (Fig. 4). In addition, depending upon the angle of the sun, a deep, darkly colored pool may appear bright in an aerial photograph because of sun glare and glint (Fig. 5). Shallow vegetated pannes were presumed to be excluded from the analysis, but glare of standing water, and seasonality of vegetation can result in inconsistent interpretations.

Other features may also give the appearance of a panne with sunlight reflection. Rafts of drift material on marshes, typically consisting of *Spartina*, macroalgae (especially *Ulva*), and eelgrass wrack can accumulate in large features on the surface of a marsh, creating bright areas that can be mistaken for pannes (Fig. 6). Even osprey platforms, which have been built on marsh islands in Westport since the 1980s, cast shadows that can be mistaken for small pools (Fig. 7).

One island studied had a small area of upland (Sanford Flat C). Upland areas may have trees or clusters of shrubs that can be mistaken for pannes (Fig. 8). Erosion undercutting and ice scour can detach and displace segments of marsh peat, which can create small, detached submerged or emergent island features (Fig. 9).

The aerial image for each date was analyzed irrespective of the resolution or quality of the imagery, and each image represented a time step in the analysis if any changes could be discerned. When imagery of lower quality was evaluated, generally, the boundaries defined in the previous time step were used as the starting point, and changes to those boundaries were made only where there was visible evidence of a boundary shift in the aerial imagery. For example, even an image with poor contrast and resolution may show a distinct boundary in an area of sun glint. Thus, while any particular time step may underestimate actual marsh loss, because 10 dates (or 30 dates for Bailey Flat) of aerial imagery were evaluated for each island, the average of many time steps is most meaningful to characterize average marsh loss trends for that period, and less subject to errors in interpretation when only two dates are compared.

While these rules of thumb of assumed marsh loss were followed in delineating marsh boundaries, some allowance was provided for varying interpretation of live marsh boundary in each image, versus dead marsh peat sloughed off and present just offshore of the live marsh. Images with high resolution had finer detail of marsh boundary irregularities. There were also some distortions of rectified images that resulted in minor inconsistencies in georeferencing. All these factors contributed to minor inconstancies in marsh boundaries for each time step when images were zoomed at high magnification.

There are many potential errors of interpretation using the approach described. Photographs taken during different times of year, different tidal condition, and different effective pixel size can result in boundary changes. For example, it became apparent in reviewing early fall drone imagery, that living marsh boundaries do not always coincide with apparent marsh boundaries as illustrated by Fig. 11. This issue is particularly problematic when comparing imagery taken from different seasons. Another source of error was the resolution and quality of the imagery, or the resolution under which the aerial image was scanned, or whether contact prints were scanned or the source negatives were scanned. If the area of an island happened to apparently increase in area by 1.2% between two time steps separated by a small number of years, this change might as likely be attributed to the limitations of the image interpretation as to any real increase in area. Moreover, in this example, increases in area are generally unlikely, except in a few instances were an area of an island damaged by storms s (e.g. sand overwash), and subsequently showed a modest increase in area (observed on Bailey Flat after 2001. For this reason, the average loss rate loss calculated from the slope across multiple years or decades is the most meaningful comparison between rates of loss among the islands.

The Appendix supplements this report, and contains a figure of every image of every island reviewed, and showing the interpreted boundary and the boundary of the previous time step for those images that were photo interpreted for salt marsh boundary.

Fig. 4 The relative darkness of deep pannes and pools was used as a guide as to understand the degree of tidal connection and water exchange with surrounding waters (May 5, 2016 Google Earth Image of White Island Flat).

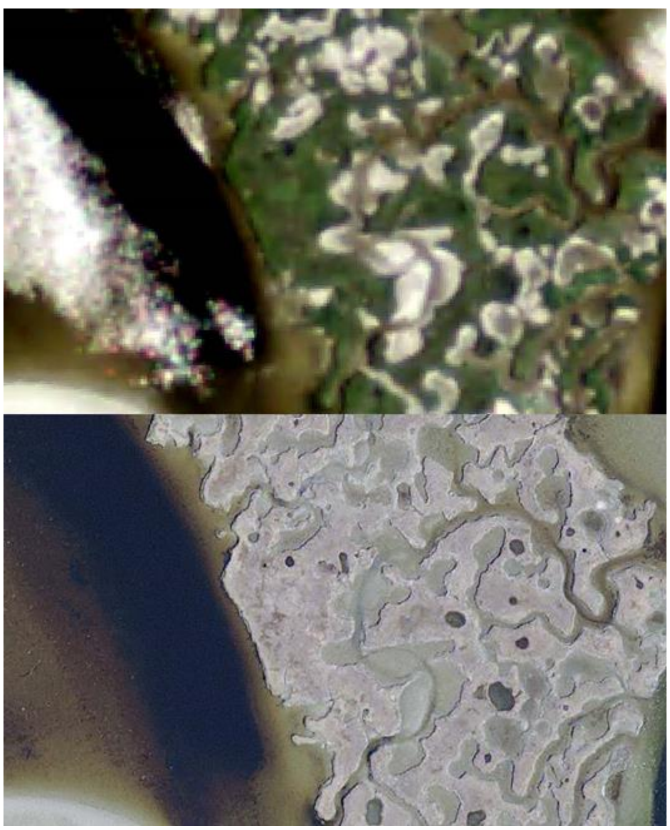

Fig. 5 Top: A portion of Great Flat 1 with appreciable sun glint and glare (September 2014 USDA aerial). Bottom: the same area on an aerial with little glint or glare (April 2014 MassGIS image).

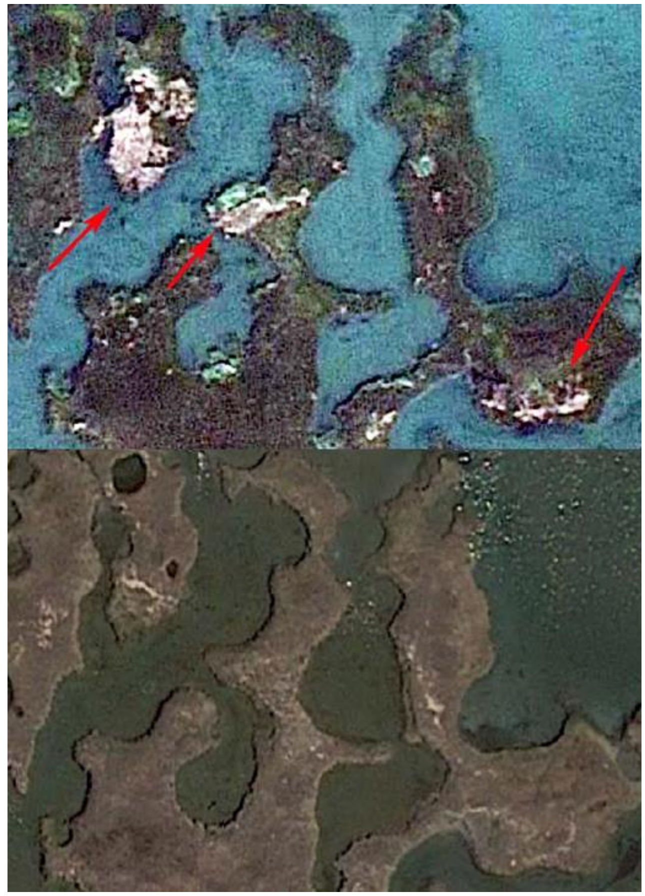

Fig. 6 Accumulated wrack (arrows) can appear as light patches on images of low resolution (Top: stretched color September 2015 USDA image; bottom: May 2015 Google Earth Image.

Fig. 7 An osprey platform or its shadow (arrow left; September 2014 Google Earth image) can be mistaken for a small pool or panne on an image of lesser contrast or resolution (right: May 2015 Google Earth aerial).

Fig. 8 Tree and shrubs (arrow, top; image of September 2014 Google Earth image of Sanford Flat C) can appear to be pannes or pools in images of lesser resolution or quality (bottom: same area on May 1996 MassGIS image).

Fig. 9 Field view versus aerial view of undermined collapsing marsh on the western shore of Bailey Flat.

Top: July 2016 photo courtesy Chris Neill, middle: September 2012 aerial in the same vicinity of good quality and resolution; bottom: May 2015 image of excellent quality and resolution showing precisely the same area but different undermined areas (arrows; scale marker has not moved).

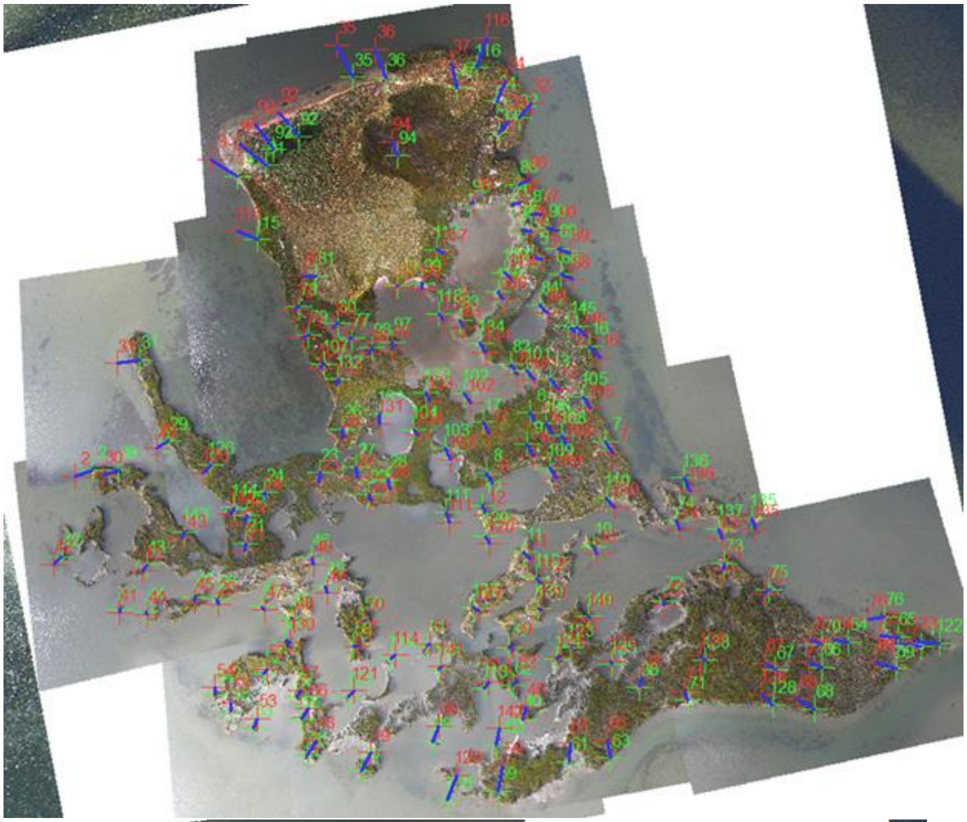

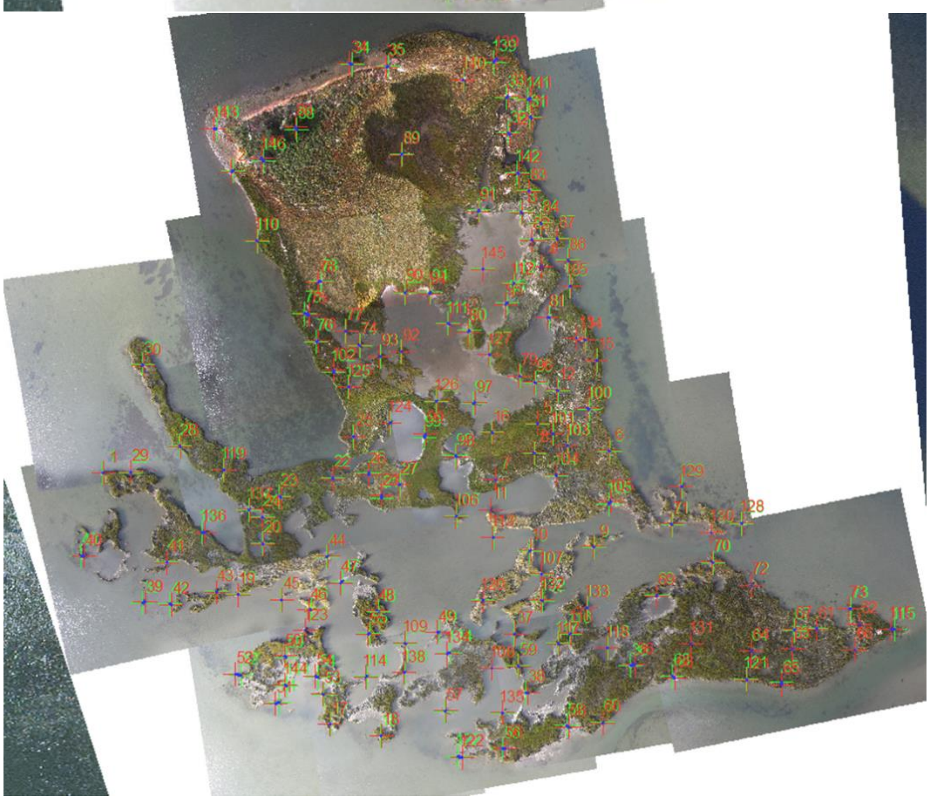

Fig. 10 UAV composite images were ortho rectified to the MassGIS May 2014 base map using a cloud of points, principally set on the center of small features (mostly pools and deep pannes). Top: a simple affine transformation (not used); bottom: 2nd order polynomial transformation (used).

Fig. 11 Example of living marsh boundaries may not coincide with apparent panne boundaries. (top right panne; October 2016 drone image from Sanford Flat C).

Marsh boundaries with respect to tidal and lidar elevations

New England salt marshes are typically classified into three intertidal zones: low, middle, and high marsh based on the assemblage of plant species found in each (e.g., Redfield 1972; Nixon 1982; Bertness, 1992; Donnelly and Bertness 2001). The plant species assemblage in each of these zones is defined by the frequency of tidal flooding and the average inundation time. In Buzzards Bay, the low marsh is dominated by cord grass, *Spartina alterniflora*, and begins roughly at mean sea level (MSL). The middle marsh area, occurring roughly between mean high water (MHW) and mean high higher high water (MHHW) is dominated by *Spartina patens*, *Salicornia* spp., *Distichlis spicata,* and *Juncus gerardii*. The high marsh environment occurs above MHHW, and vegetation includes mid-marsh species as well as the invasive *Phragmites australis*. The transition between the high salt marsh and upland areas include certain characteristic species such as the high tide bush *Iva frutescens*, and switch grass, *Panicum virgatum*. Salt marshes may also grade into freshwater wetlands. The actual real world elevation of all these boundaries with respect to local tidal datums depends on numerous factors ranging from fresh water inputs to levels of eutrophication (Bertness et al. 2002, 2009; Silliman and Bertness, 2004).

In southeastern Massachusetts, the lower depth limit of a salt marsh is generally somewhat above local mean sea level. The upper marsh boundary is defined under the Massachusetts Protection Act regulations (310 CMR 10.0), and under federal regulations (33 U.S.C. 1344, Regulatory Program of the US Army Corps of Engineers, Part 328.3), by the "high tide line"(sometimes called the annual high tide" or "king tide"). This boundary encompasses predicted spring high tides (for the past year) but does not include storm surges. Locally, the high tide line is characterized by the presence of the high tide bush *Iva fructens*. The approximate tidal elevations for Westport using MSL as a datum, and the approximate boundaries of the upper and lower saltmarsh are shown in Fig. 12. Additional details of how these values are calculated are contained in Costa 2013.

In this report, LiDAR elevations were adjusted to the estimated Westport mean sea level elevations using the NOAA software model VDatum 3.2. The particular LiDAR elevation model used in this study (FEMA LiDAR 2006) was also based on a different GEOID (GEOID03) than the current NOAA tidal data (GEOID12B). This difference in was also accounted for in the VDatum model. The VDatum model is valid only to the mouth of the Westport Rivers, not within the estuary. Because it is often the case that tidal range diminishes toward the head of an estuary, the omission of the Westport Rivers, and other uncertainties in the VDatum model means that the upper and lower boundary may vary within the estuary by up to 0.7 feet lower than the HTL elevation at the mouths of the respective estuaries. Details of the application model Buzzards Bay are contained in Costa (2013) and at the Buzzards Bay climate website[4].

[4] See http://climate.buzzardsbay.org/tidal-datums-benchmarks.html, http://climate.buzzardsbay.org/vdatum-elevations-climate.html, and http://climate.buzzardsbay.org/annual-high-tide-elevations.html.

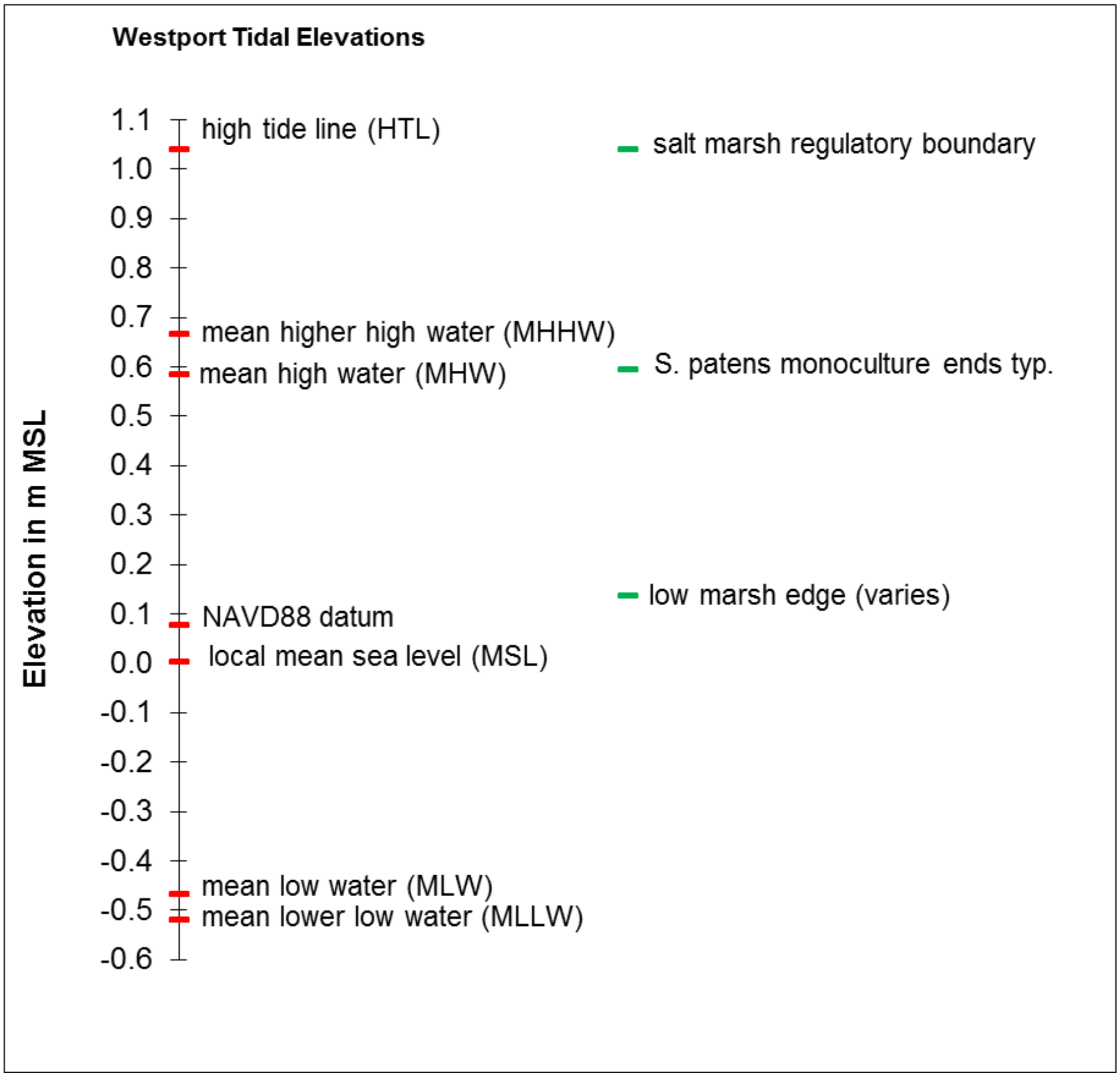

Fig. 12 Estimated tidal elevations for Westport relative to typical salt marsh boundary elevations. Based on Round Hill, Dartmouth tidal data and VDatum 3.2 adjustments for the mouth of the Westport River.

Relevant Physical Factors Associated with Marsh Loss

Relevant physical factors associated with marsh loss include storm damage, coastal erosion, icing, and sea level rise. Salient data for Westport, MA associated with these drivers are summarized below. Marsh loss may also be associated with biological factors like grazing by invasives and nutrient pollution. These drivers will be discussed and evaluated elsewhere.

Tidal records show that mean sea level at Newport RI and Woods Hole, MA tidal have been linearly increasing during the past eighty years, and increasing about 2.7 and 2.8 mm per year, respectively (Fig. 13).

As discussed in the results section, changes in marsh boundaries on some islands appear related to storm damage. Storm damage changes were most evident on Bailey Flat, which is closest to the entrance of the harbor. Potential storm damage to a marsh depends on tidal elevation, wind speed, and wind direction. A summary of major storm events and water elevations are shown in Table 2. Based on press reports, water elevations, erosion to Horseneck Point in the aerial photographs, the Hurricanes of 1938 and 1944, Hurricane Bob (1991), and Hurricanes Irene and Sandy (2011 and 2012; both locally just tropical storms) were likely the most relevant.

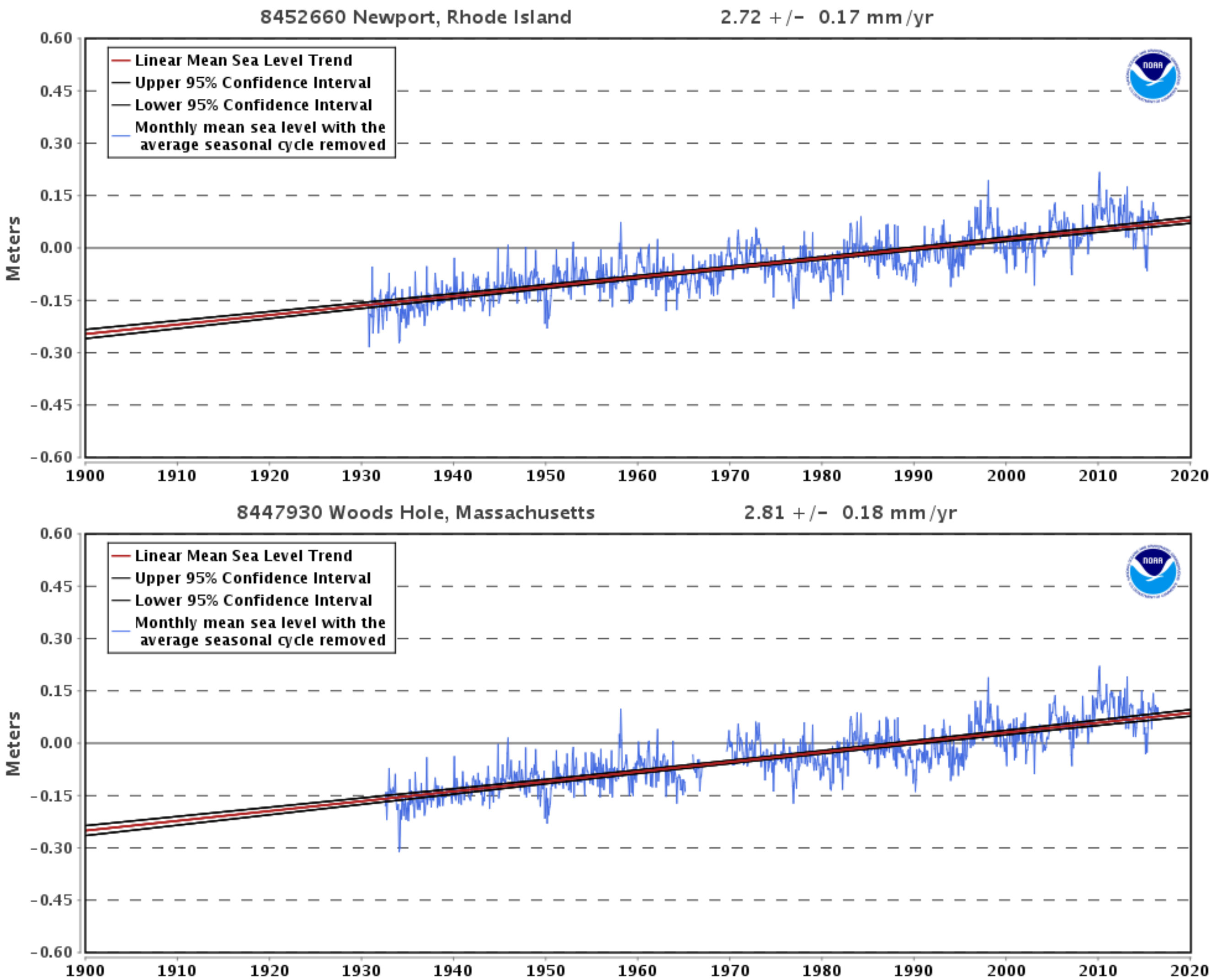

Fig. 13 Sea level rise trends for Newport, RI (top) and Woods Hole, MA (bottom). MSL (0 datum) was calculated for the current tidal epoch.

As shown in Fig. 9, some islands have sites of erosional undercutting caused by tidal flow. Migration of these channels may be the result of some form of natural progressions, or the result of hydrological changes caused by the storms in Table 2. Changes in these estuary channels and meanders were not systematically mapped in this study. Dredging of the harbor navigation channel, including realignment and expansion, also has the potential to affect the movement of natural channels directly connected to the navigation channel. Dredging of the harbor navigation channel was undertaken principally in the 1950s, 1997, and in 2007 (in Table 3), and these dredging activities may be relevant to Bailey Flat and Whites Flat. Whites Flat may have had a small channel cut across it in the early 1950s.

Table 2. Maximum stillwater ocean elevations at the New Bedford hurricane barrier, including historical estimates.

From http://nae-rrs2.usace.army.mil:7777/pls/cwmsweb/cwms_realtime.capeindex, last accessed October 2012

Date	**Comments**	**Ocean Elev. Ft. NGVD**
21-Sep-38	Hurricane of 1938	12.5
14-Sep-44	Hurricane of 1944	8.1
30-Nov-44		6.8
07-Nov-53		6.2
31-Aug-54	Hurricane Carol	11.9
29-Dec-59		5.8
19-Feb-60		6.1
10-Jun-60		6.1
30-Jul-60	Trop. Storm Brenda	6.1
12-Sep-60	Hurricane Donna	6.3
29-Dec-66		6
26-Jan-71		5.3
19-Feb-72		5.3
20-Nov-72		6.1
04-Apr-73		5.4
02-Dec-74		5.7
21-Oct-76		5.4
09-Jan-78		6.3
27-Sep-85	Hurricane Gloria	5.2
25-Nov-85		5.9
05-Dec-86		5.4
10-Jan-87		6.4
23-Jan-87		6.3
04-Dec-90		5.6
19-Aug-91	Hurricane Bob	7.6
31-Oct-91		5.6
10-Jan-97		6.4
01-Nov-97		5.1
12-Dec-00		5.4
17-Oct-01		5.1
06-Nov-02		5.2
09-Dec-05		5.2
28-Oct-06		5.4
16-Apr-07	Nor'easter	5.8
12-Dec-08		5.5
03-Dec-09		5.3
09-Dec-09		5.1
01-Mar-10		5.2
30-Mar-10		5.1
05-Nov-10		5.2
28-Aug-11	Hurricane Irene	5.6
29-Oct-12	Hurricane Sandy	6.8

Table 3. Documented dredging activity in Westport Harbor

Year	Source	DEM #	DEM Info	Date Range	Details/Comments	Quantities
1887	ACOE			June 1887 – July 1887	Construction of a stone-filled timber crib jetty (groin) on the end of Horseneck Point	Unknown
1887	ACOE					(One jetty built)
1891	ACOE			Sept 1891 – Oct 1891	Reconstruction and extension of the Horseneck Point Jetty with a rubble stone design – 150 feet long	Salvaged stone and 230 tons new stone
1893	ACOE			May 1893	Improvement dredging of a 10-foot MLW Entrance Channel for 1,100 feet through the inlet into the harbor at 33 feet wide to secure a 7-foot channel 100 feet wide	6,500 cy
1955	DEM/DCR	1472			Westport Harbor- Town Wharf dredged 1955	
1956	DEM/DCR	1675			Westport Harbor, year of work assumed	
1957	DEM/DCR	1738			Westport Harbor 1957 dredging	
1958	DEM/DCR	1845			Westport Harbor 1958 dredging	
1997	DEM/DCR	2794			Westport Harbor, Westport River & Point 1997 dredged	
2000	DEM/DCR	3340	D		Westport River design 2000	
2007	DEM/DCR	3580	F		Westport River federal 2007, see ACOE info	
2007	DEM/DCR	3697	C		Westport River Bid Protest, no work presumed	
2007	DEM/DCR	3709	F		Westport Harbor fed project, see Army Corps info	
2007	DEM/DCR	3752	G		Harbor Fall 2007	
2007	ACOE, Fall River Herald			November 2007 – December 2007	Maintenance dredging to 7 Feet MLLW and improvement dredging to -9 Feet MLLW of an entrance channel for 9,700 feet through the inlet into the Harbor at 150 to 200 Feet Wide; FRH: 200-foot-wide by 4,800-foot-long channel, completed in 2007, in fall 2009, phase 2 at Westport Docks completed.	1,523 cy maintenance 14,010 cy improvement
2009	DEM/DCR	3716	C		Westport River, spring 2009, see Army Corps 2007 permit, prob. phase 2 work	

Results

All marsh islands studied showed appreciable loss during the eighty-year study period with net loss from 1938 ranging from a 25% decline for Whites Flat to roughly a 65% percent decline for both Bailey Flat and Great Flat 12 (Fig. 14). Generally, the trends were roughly liner for the entire period, although all but one island has shown accelerated losses after 2012, and seemingly unrelated to the long-term local relative sea level rise trend (Fig. 15). The greatest losses in marsh area generally occurred on the shores of the islands, with some of the most dramatic changes occurring adjacent to tidal channels. However, exceptions to this generalization include a large die-off in the center of Sanford Flat after 2001, and the north (lee) side of Great Flat 12. In general, losses not adjacent to tidal channels occurred in the lowest elevation marsh areas on the islands. Details of the specific trends for each island are summarized in the sub-sections below.

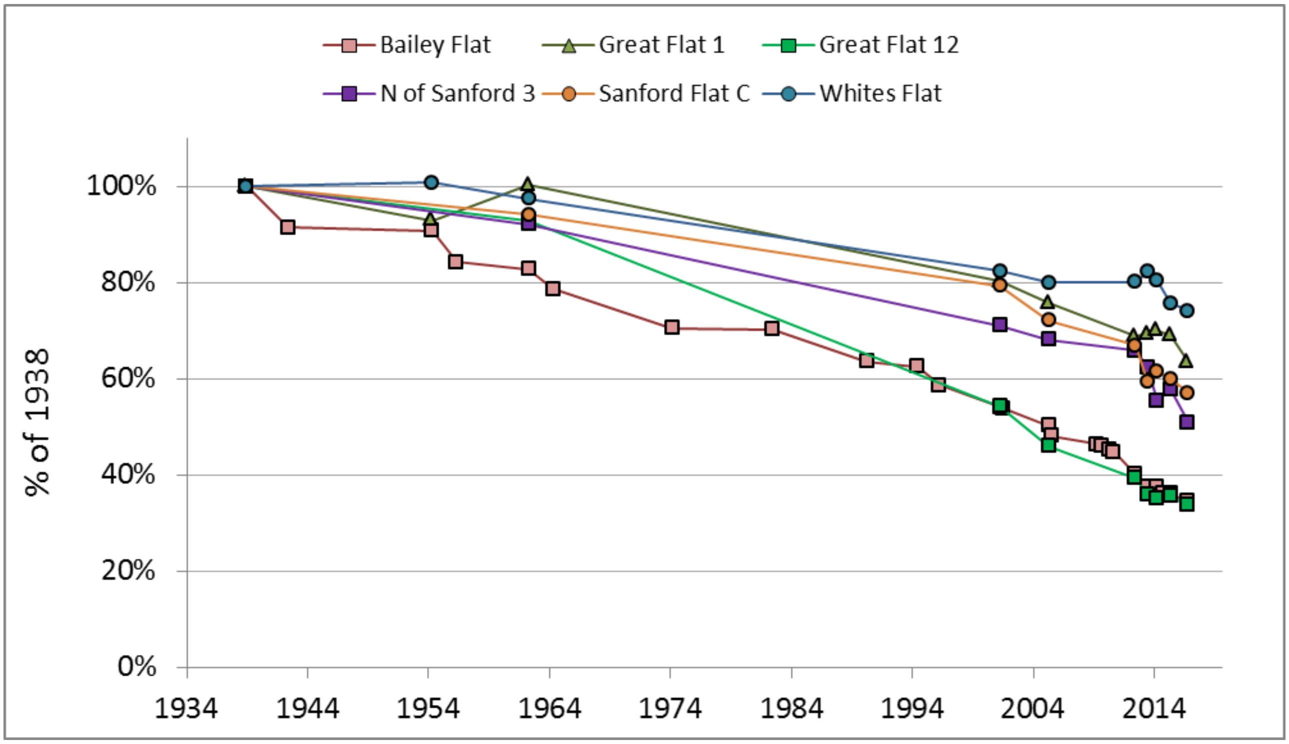

Fig. 14 Decline in area from the 1938 imagery of the six marsh islands studied.

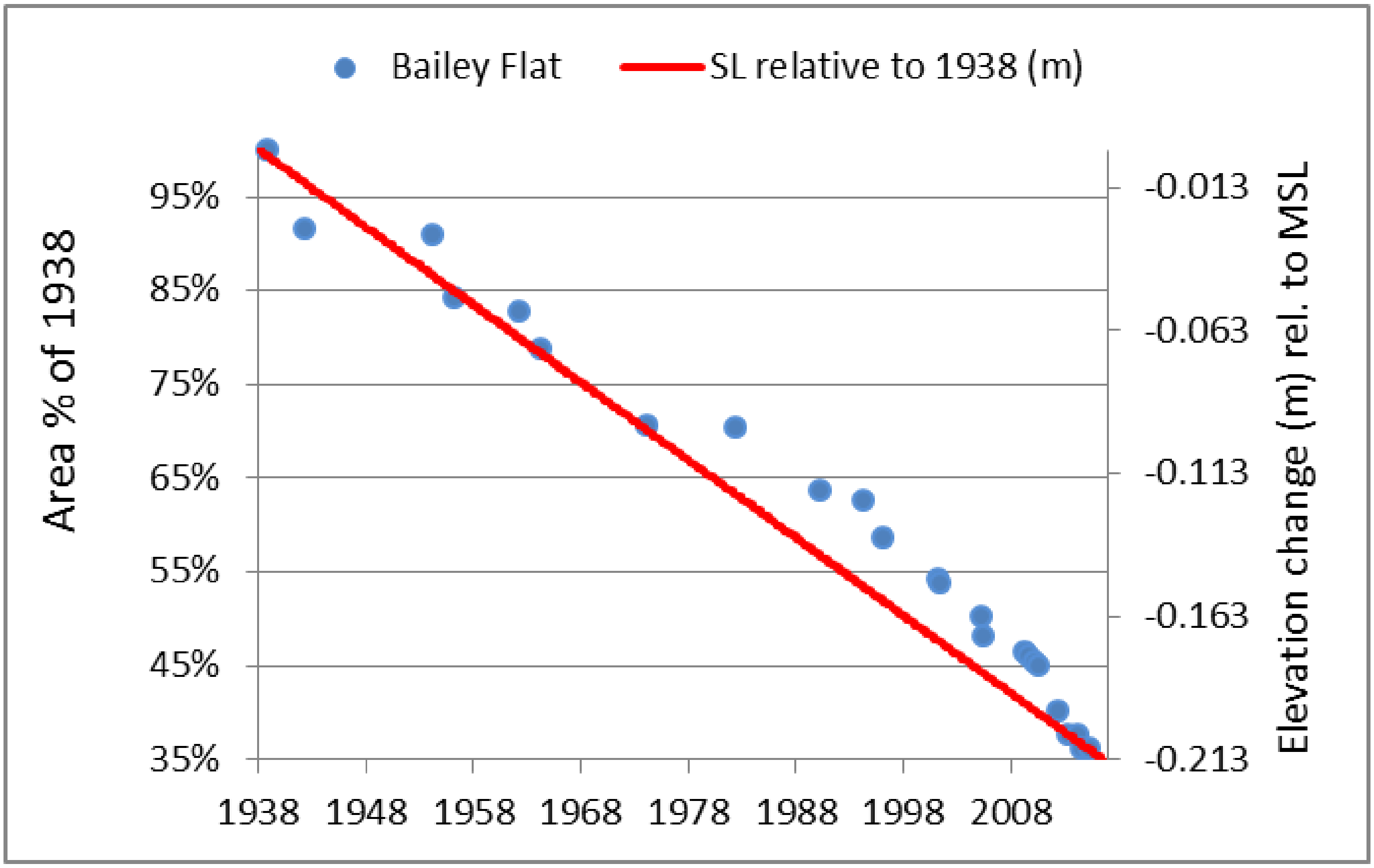

Fig. 15 Change in Bailey Flat area as a percent of 1938 area superimposed with effective elevation decline from relative sea level (curve from Fig. 13, Newport, RI).

Bailey Flat

Bailey Flat is the southernmost salt marsh island in the West Branch of the Westport River, and the island closest to the entrance of the Westport Rivers. This island had among the highest percent loss in area among the six salt marsh islands studied, with a net loss of 69% if 1934 is used as the starting point (Fig. 16), and 65% using the aerial images between 1938 and 2016 (Fig. 15). The greatest area losses occurred on the southern and southwest portions of the island, and the northern end of the island (Fig. 17). The driving factors in these losses appeared to be the migrations of channels, undercutting the marsh bank (as illustrated in Fig. 9), and an overwash of storms of the southern island, particularly because of storms during several storms during 2009 to 2012, which also caused appreciable loss of shoreline at Horseneck Point (Fig. 18).

A 2006 LiDAR image of Bailey Flat shows generally low marsh elevations on the south and eastern shores of the island, and the highest marsh elevations on the western shore (Fig. 19), with much of the island between LiDAR elevation 0.7 and 1.2 feet. Elevation seems to have little bearing on the rates of shoreline recedence as most of the losses are related to tidal channel undercutting. In fact, the lower elevation area on the southern edge of what is now the northern island (small arrow in Fig. 19) had one of the slowest rates of salt marsh loss on the island. Until recently (and only after the separation of the two island halves), there was never a channel abutting this marsh area. Given most of the documented marsh loss on this portion of shoreline occurred after the separation of the islands, this feature suggests that channel undercutting is the principal driver of marsh loss at Bailey Flat. This pattern is even seen at a small scale. Whenever a channel breaks through a small peninsula of the island, marsh loss along the channel and adjacent areas increases appreciably.

While Fig. 16 shows that the loss of salt marsh is generally linear over the eighty-year record evaluated, an analysis of trends for three different periods of the data (Fig. 20) suggests that salt marsh loss is in fact increasing. More specifically, trends between 1934 and 1994 (with an average 0.67% annual loss rate) suggest the island would disappear by 2082. However, trends for more recent data suggest that island loss is accelerating (between 2012 and 2016 this rate increased to 1.2% per year). The higher loss rate suggests the island will disappear by 2036 if this current trend continues. Of course, the most recent losses were likely partly driven by storm damage to the southern island, but even excluding the most recent imagery, the island would still likely disappear by 2047 based on the 1994 to 2012 trends.

The area of the island lost between the 2005 and 2016 aerial images was superimposed on the 2006 LiDAR data to calculate the 2006 elevation areas lost in the subsequent decade (Fig. 21). As shown, most of the areas lost were the lowest elevations of the marsh, but there was also a node of higher elevations lost. These higher elevation losses likely represent a combination of marsh bank undercut and lost, and expansion of pannes and channels in the higher elevations of the marsh.

All images reviewed for Baileys Flat, both interpreted and not interpreted, are shown in Figs, A1through A26 in the Appendix.

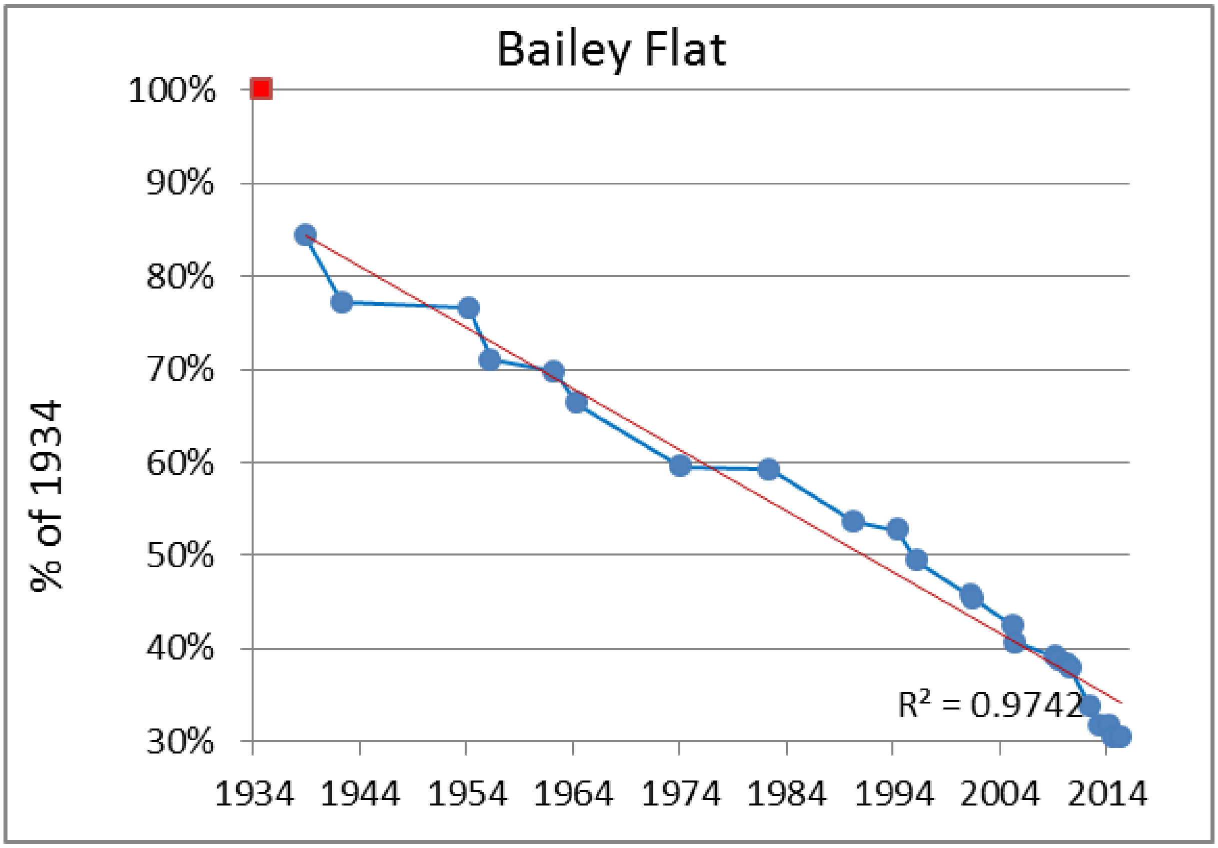

Fig. 16 Area of Bailey Flat salt marsh vegetated areas based on an analysis of 24 aerial images (circles), and the 1936 chart boundary (square; derived from a 1934 aerial survey as plotted here) shown for comparison. Red line is the least squares linear regression for all images evaluated (excludes the 1934-based aerial map boundary).

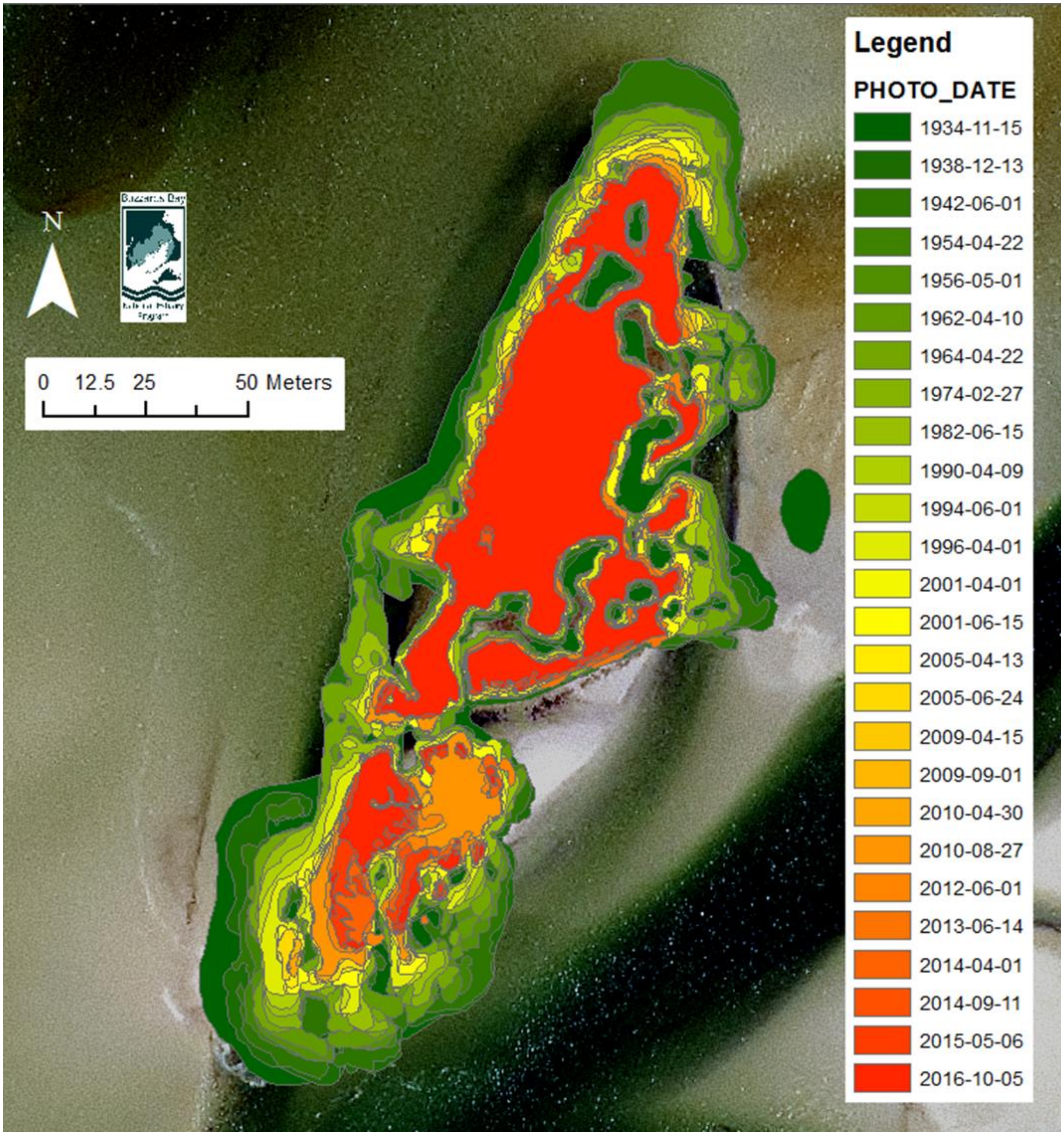

Fig. 17 Composite of estimated vegetated salt marsh boundaries for Bailey Flat for each aerial photograph interpreted for the study.

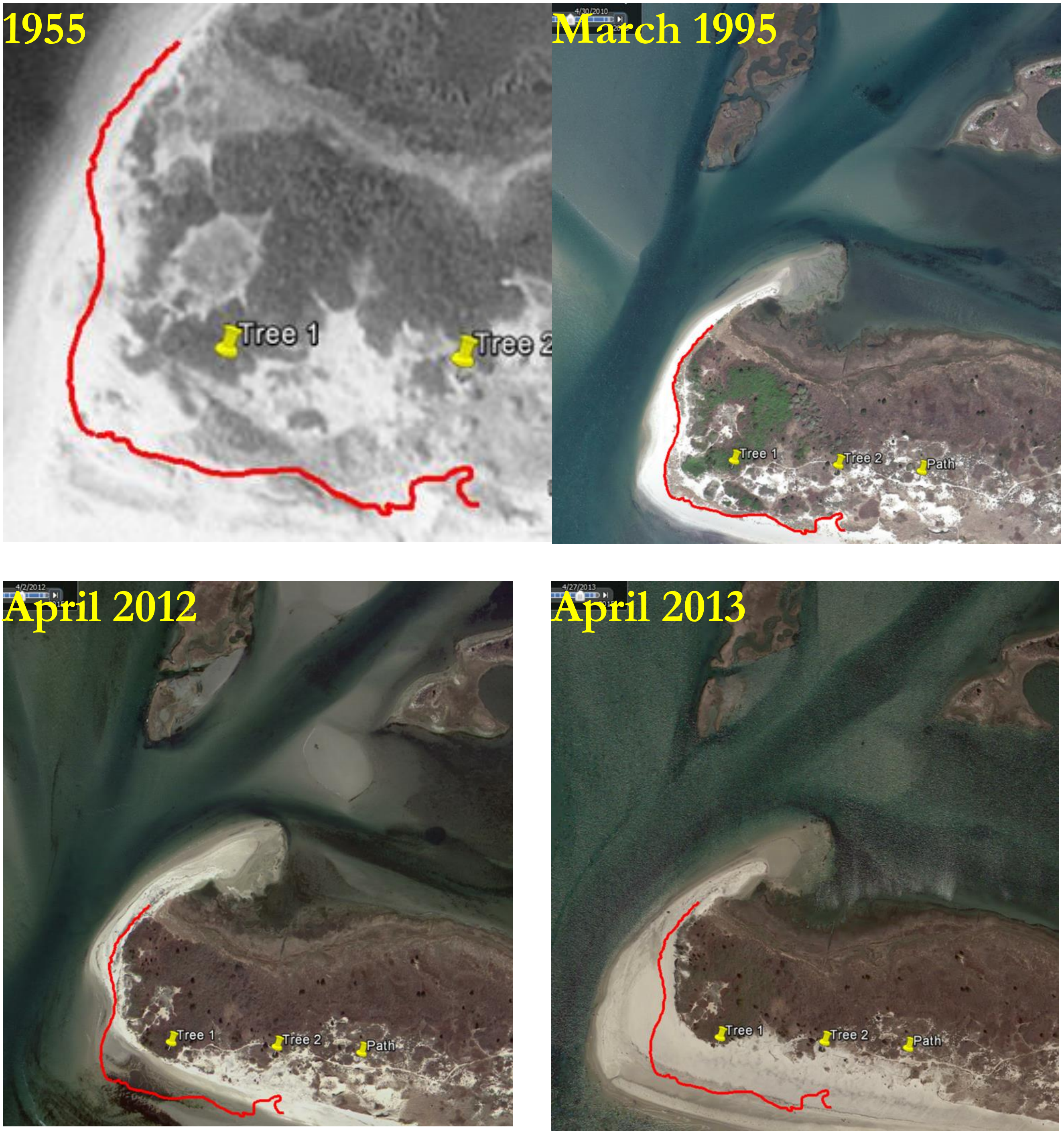

Fig. 18 The western shoreline of Horseneck Point on four dates (red boundary on each shows the dune vegetation boundary from the 1995 imagery. Note apparent shifts in channel configurations and sand overwash area on the southern island of Bailey Flat.

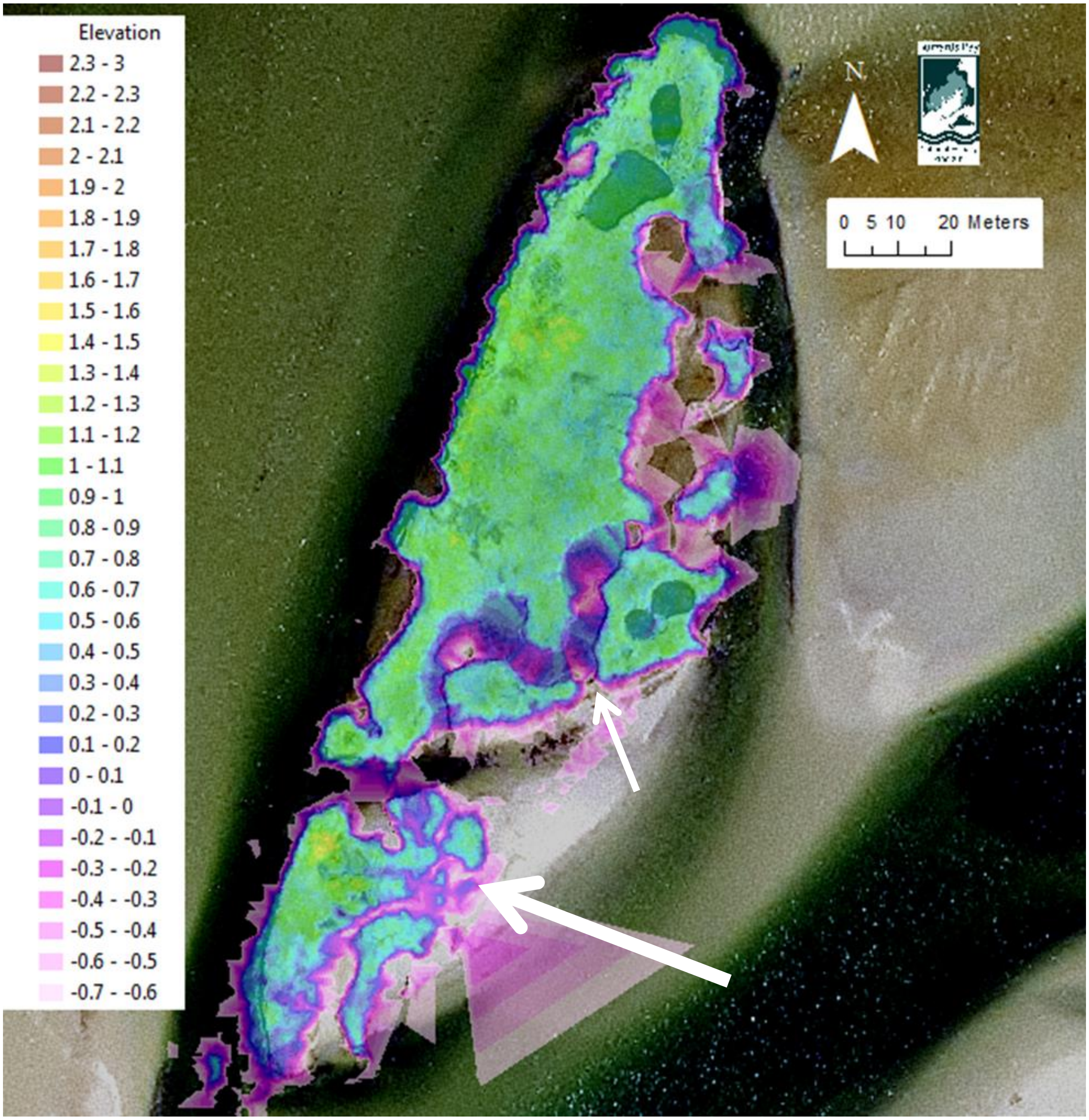

Fig. 19 LiDAR elevations of Bailey from 2006. The low elevation vegetated marsh area at the large arrow was largely overwashed and destroyed by three strong storm events between 2010 and 2012. See text for small arrow.

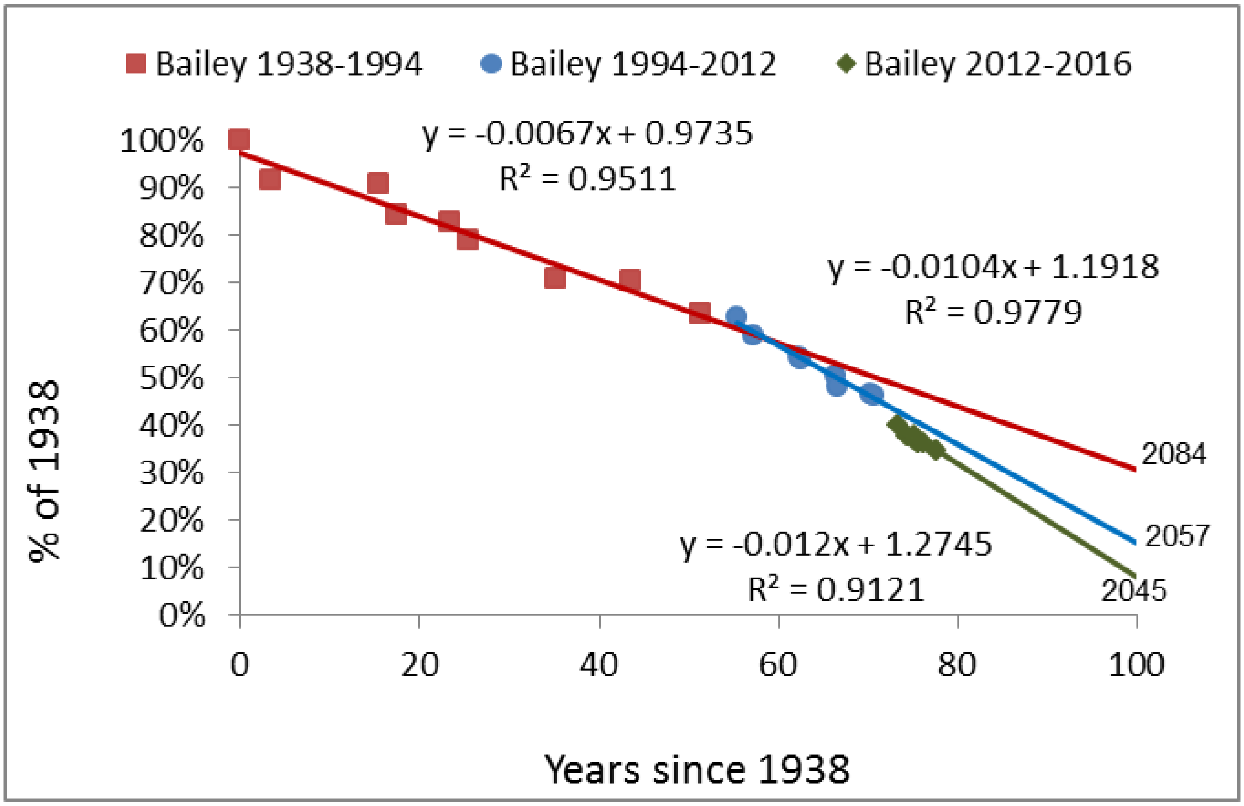

Fig. 20 Piecewise linear regression of salt marsh loss showing rates of marsh loss for three different periods (breakpoints arbitrary). Years show the extrapolated date of island disappearance based on trends for the three periods.

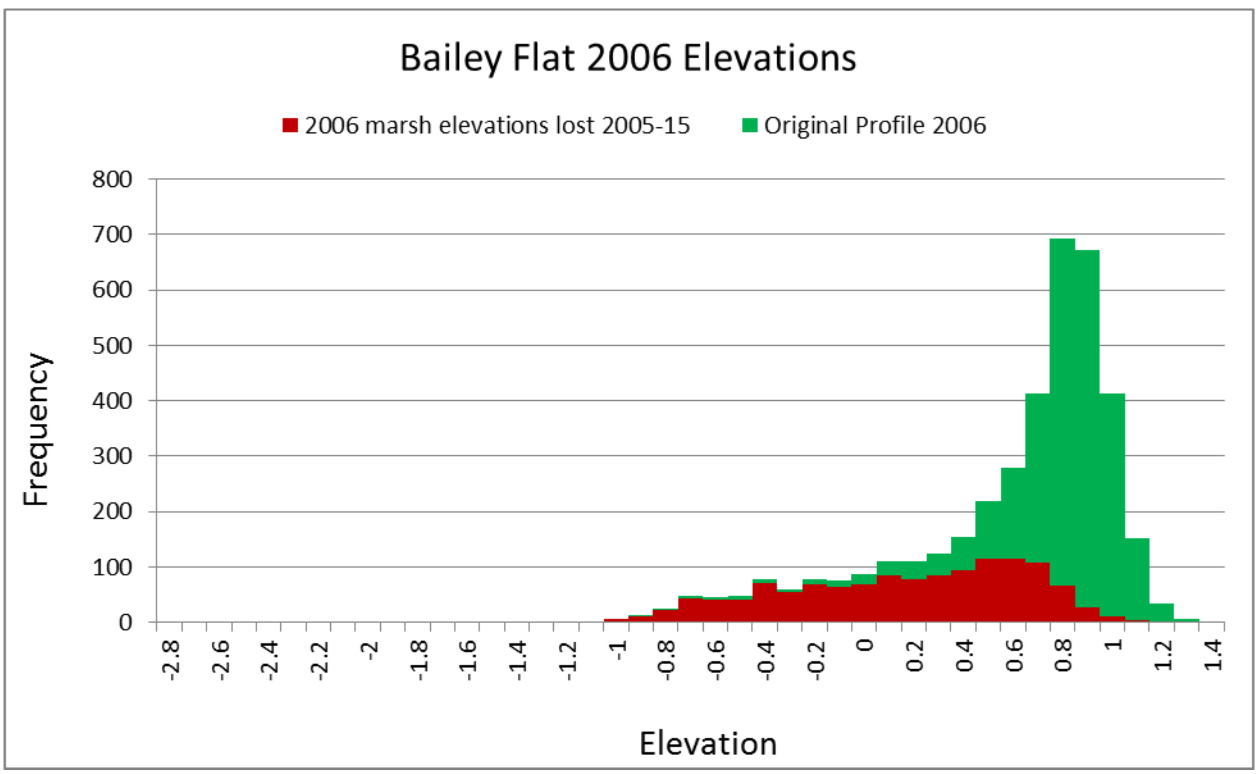

Fig. 21 Frequency histogram of 4 m^2 pixels (red = elevation lost) on Bailey Flat after 2005 based on the 2006 LiDAR elevations.

Whites Flat

Whites Flat had one of the lowest rates of marsh loss, with most of the area losses occurring due to erosion from a tidal channel in the northwest corner of the island, and a result of two breaks in the island (arrows in Fig. 22). The center break in the island began in the 1950s, and because of the linear form of this channel, the original break appears to be a dredged feature (see Fig. A29 in the Appendix).

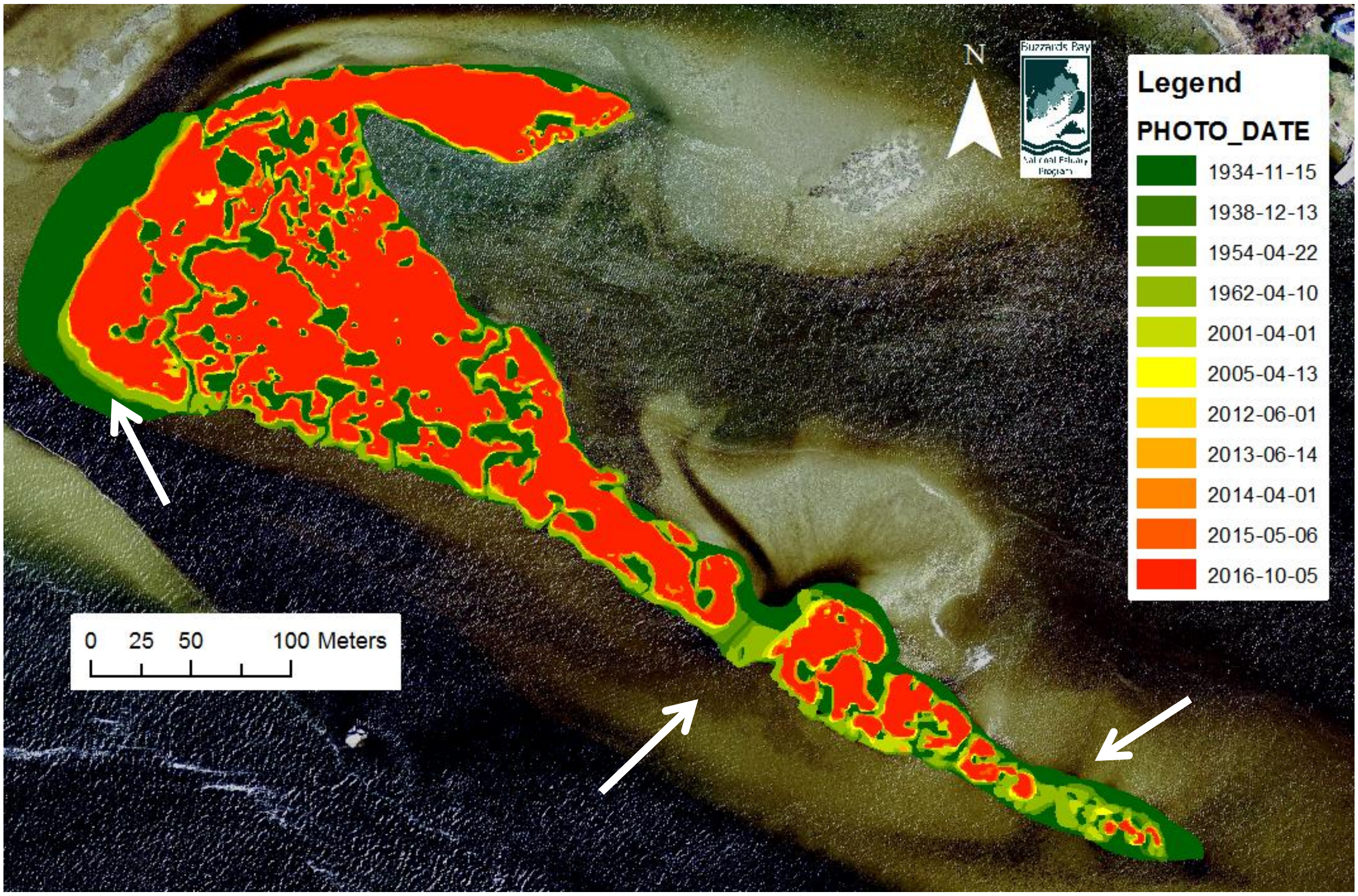

Fig. 22 Composite of estimated vegetated salt marsh boundaries for Whites Flat for each aerial photograph interpreted for the study.

Although the LiDAR for the flight track on the north side of the island was problematic from possible turbulence, the elevation of the island appeared mostly between LiDAR elevation 0.5 and 1.0 feet (Fig. 23). Between 1938 and 2005, Whites Flat lost marsh area at a rate of 0.33 % per year, between 2009 and 2016 this rate increased to 1.8% per year (Fig. 24).

All images reviewed for Whites Flat, both interpreted and not interpreted, are shown in Figs. A27 through A44 in the Appendix.

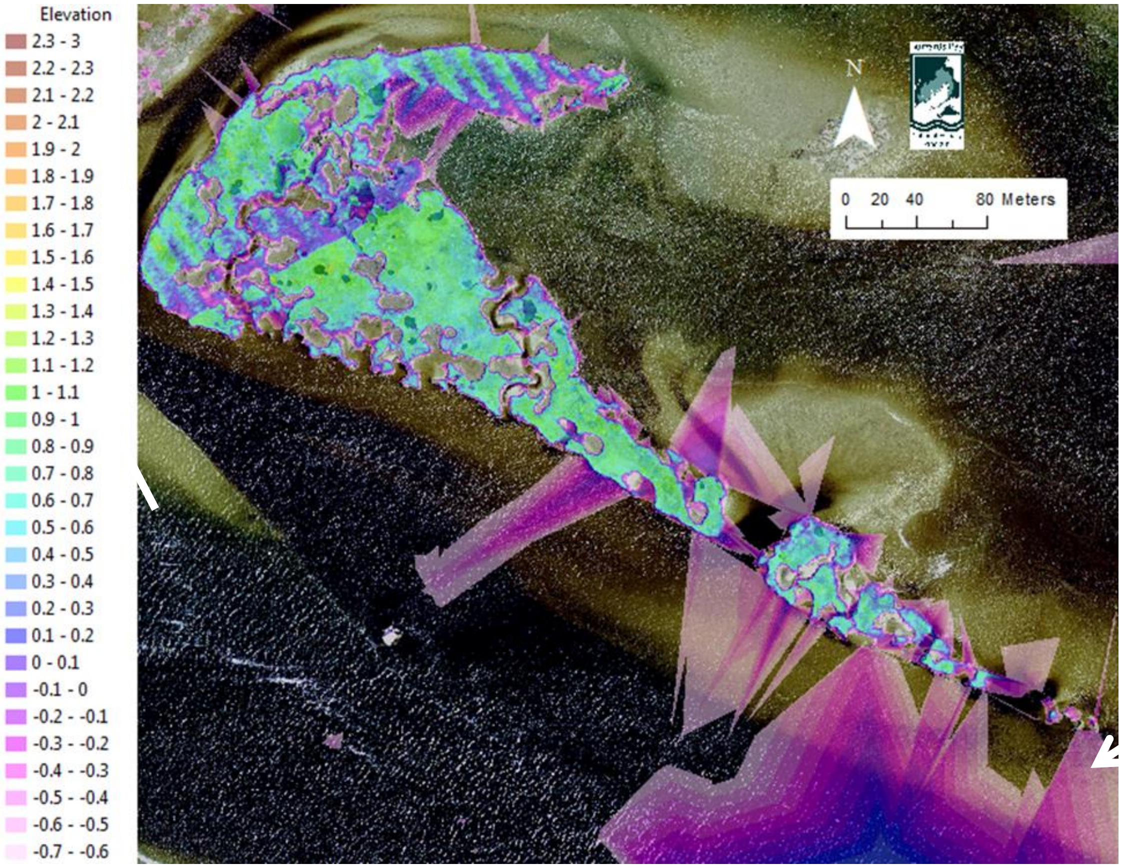

Fig. 23 2006 LiDAR elevations of Whites Flat.

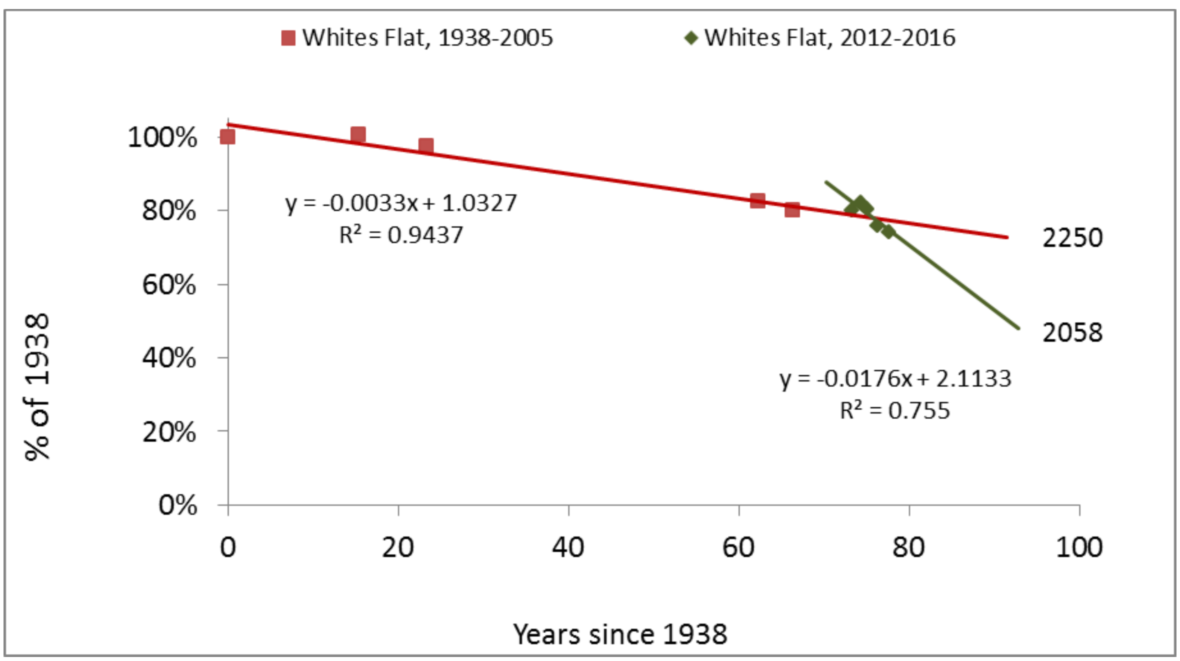

Fig. 24 Rate of area loss on Whites Flat between 1938 and 2005 compared to the rate between 2012 and 2016, with estimated date of island disappearance based on extrapolating trends for each period.

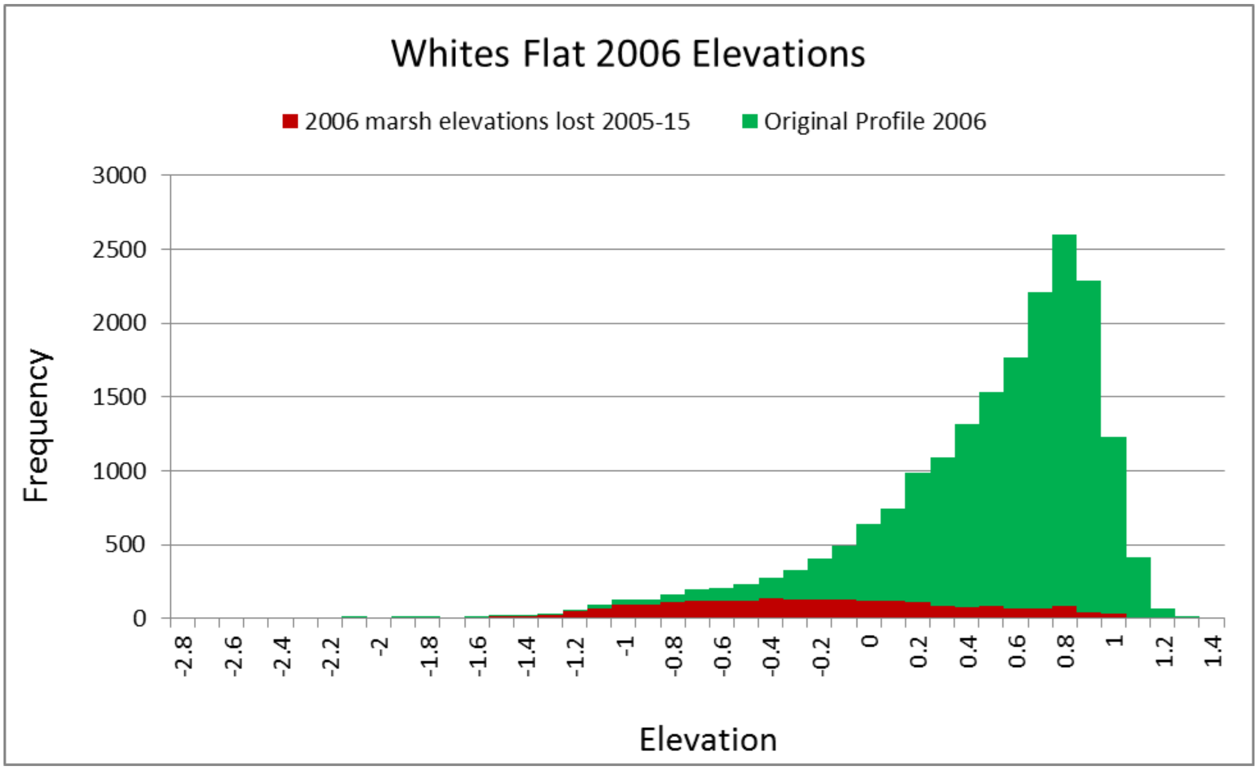

Fig. 25 Frequency histogram of 4 m^2 pixels (red = elevation lost) on Whites Flat after 2005 based on the 2006 LiDAR elevations.

Great Flat 1

Great Flat 1 had the second lowest net loss of marsh area, behind Whites Flat. Like Bailey Flat, the apparent marsh loss suggested by boundary differences between the 1934 boundary inferred from the NGS 1936 T-sheet and the post Hurricane of 1938 December 1938 aerial image, suggest that the southern portion of the island may have been damaged by the Hurricane of 1938 (Fig. 26). Alternatively, there is also the possibility that there was a resulting shift in the tidal channels on the south and west sides of the island, which accelerated erosion in those areas.

Great Flat 1 had higher average elevation than most of the islands studied, with much of the marsh loss between LiDAR elevation 0.5 and 1.0 feet (Fig. 27). Most of the losses on the western edge of the island, which happened to have the highest elevation, and the southeast border of the island, may be related to tidal channel undercutting. The northwest corner of the island appears to be more rapidly diminishing, and this happens to be one of the lowest elevation areas of the island, with most of the area below LiDAR elevation 0.5 ft. Most of the marsh area losses of Great Flat 1 were observed between 1938 and 2005, with an average rate of 0.36 % per year. However, between 2009 and 2016, the rate of loss increased to an average 1.2% per year (Fig. 28).

Although not precisely quantified, Great Flat 1 appeared to have the greatest loss rate derived from expanding panne and channel area, principally due to the extensive number of pannes in the island. All images reviewed for Great Flat 1, both interpreted and not interpreted, are shown in Figs. A45 through A60 in the Appendix.

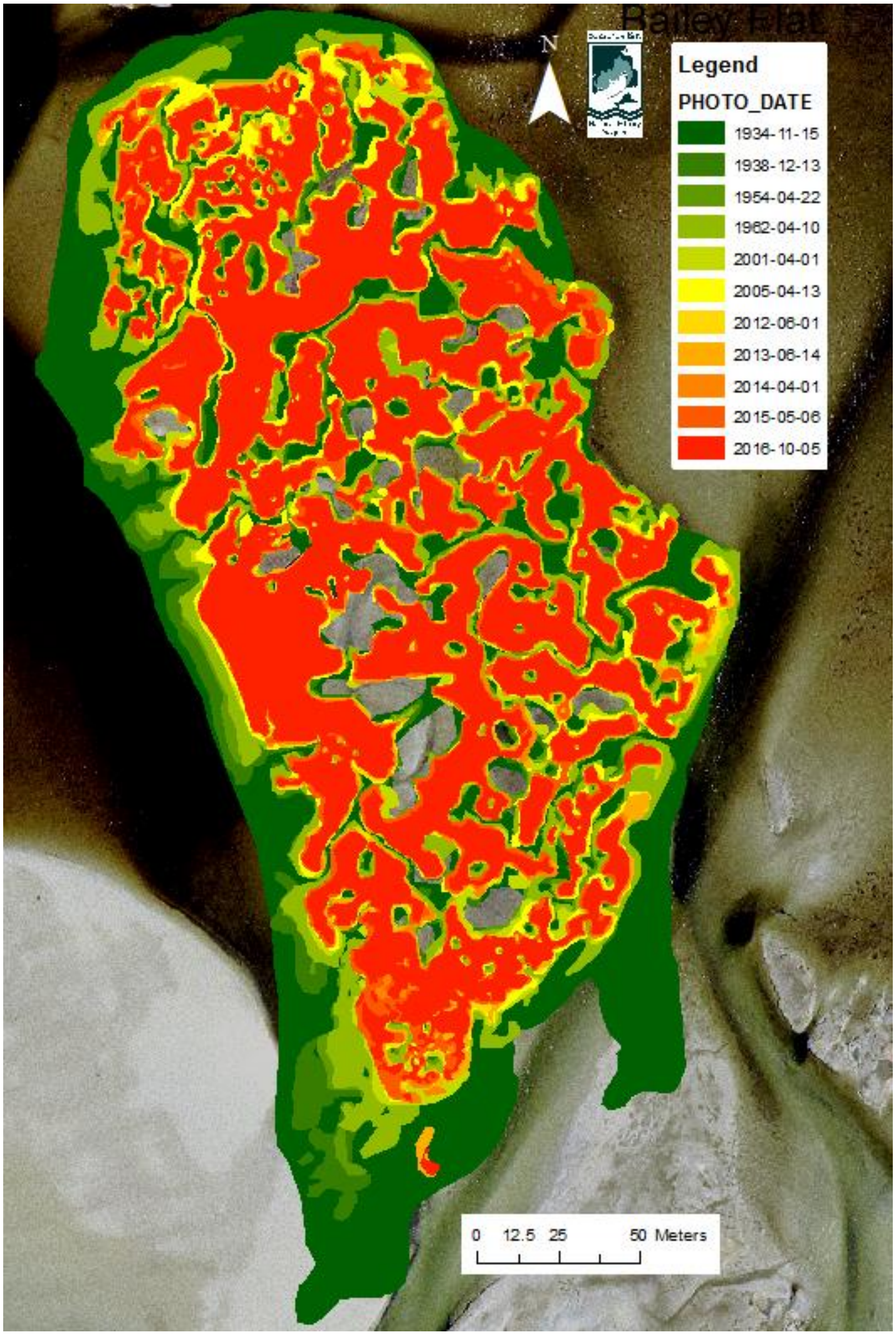

Fig. 26 Composite of estimated vegetated salt marsh boundaries for Great Flat 1 for each aerial photograph interpreted for the study.

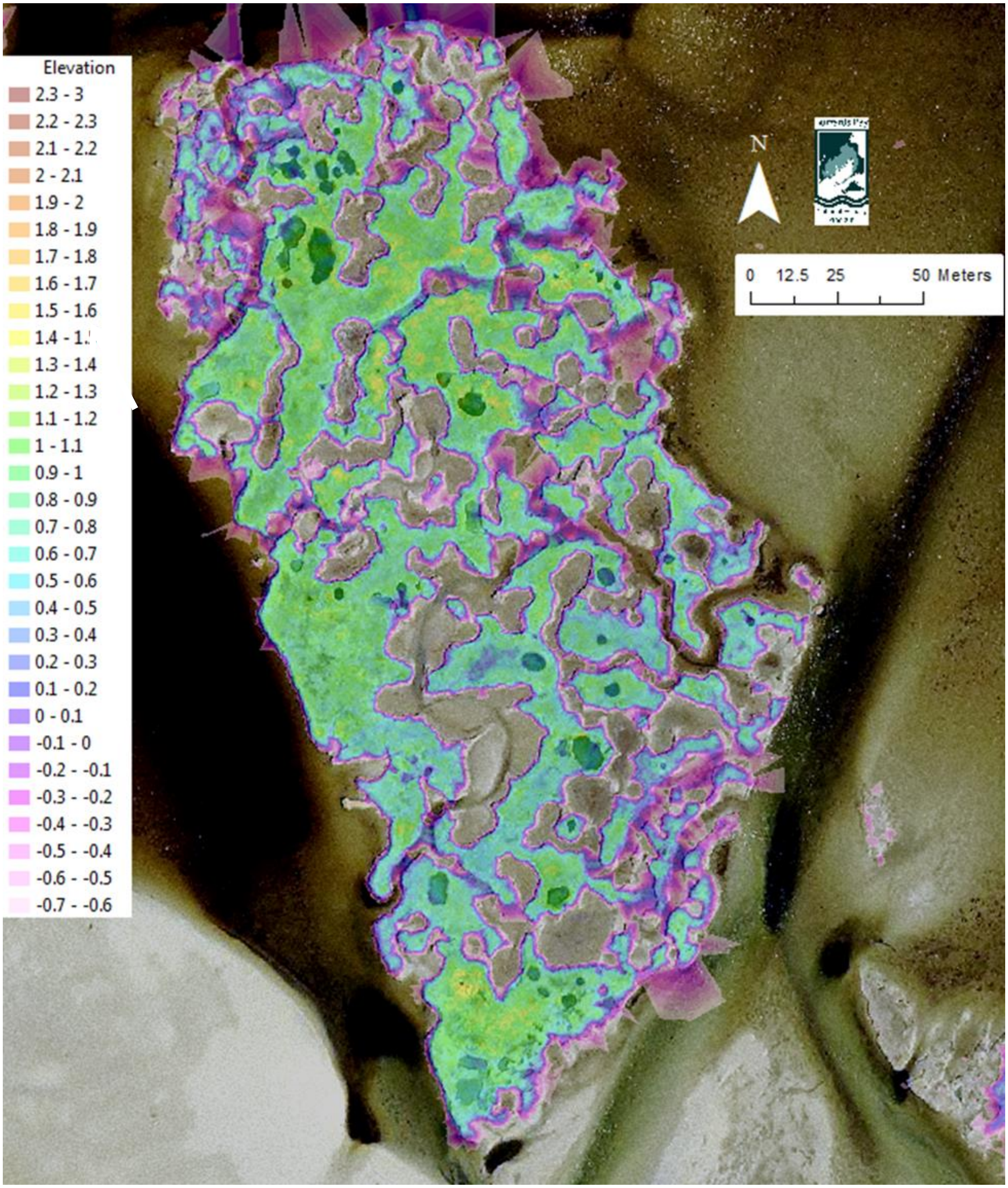

Fig. 27 2006 LiDAR elevations of Great Flat 1.

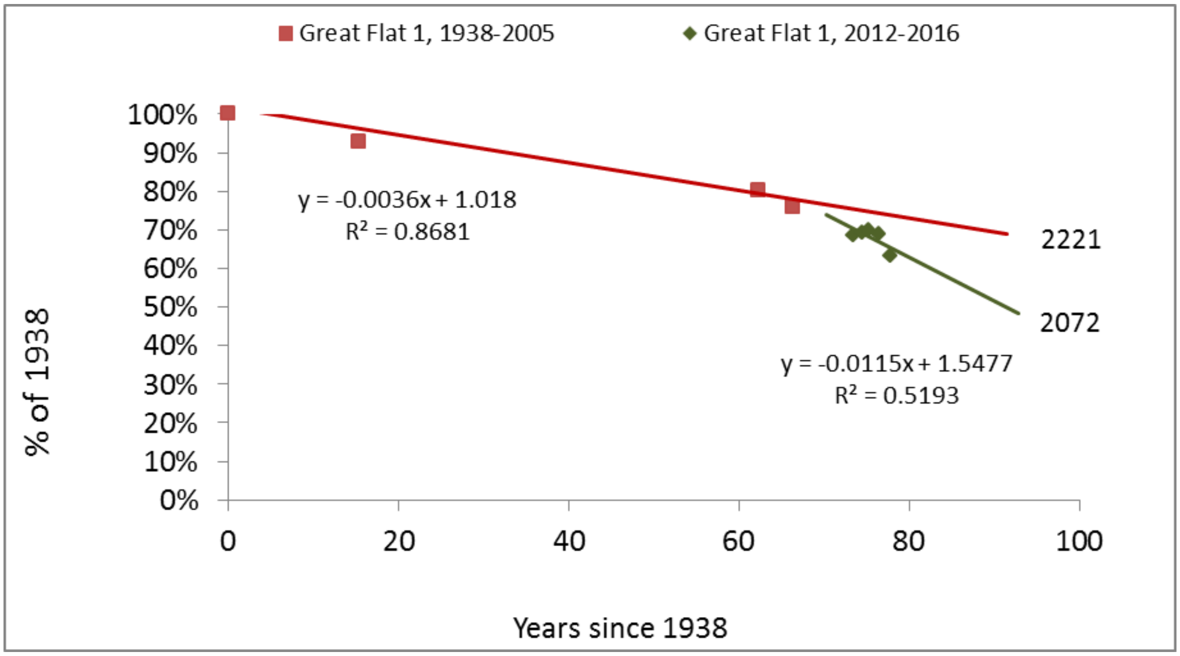

Fig. 28 Rate of area loss on Great Flat 1 between 1938 and 2005 compared to the rate between 2012 and 2016, with estimated date of island disappearance based on extrapolating trends for each period.

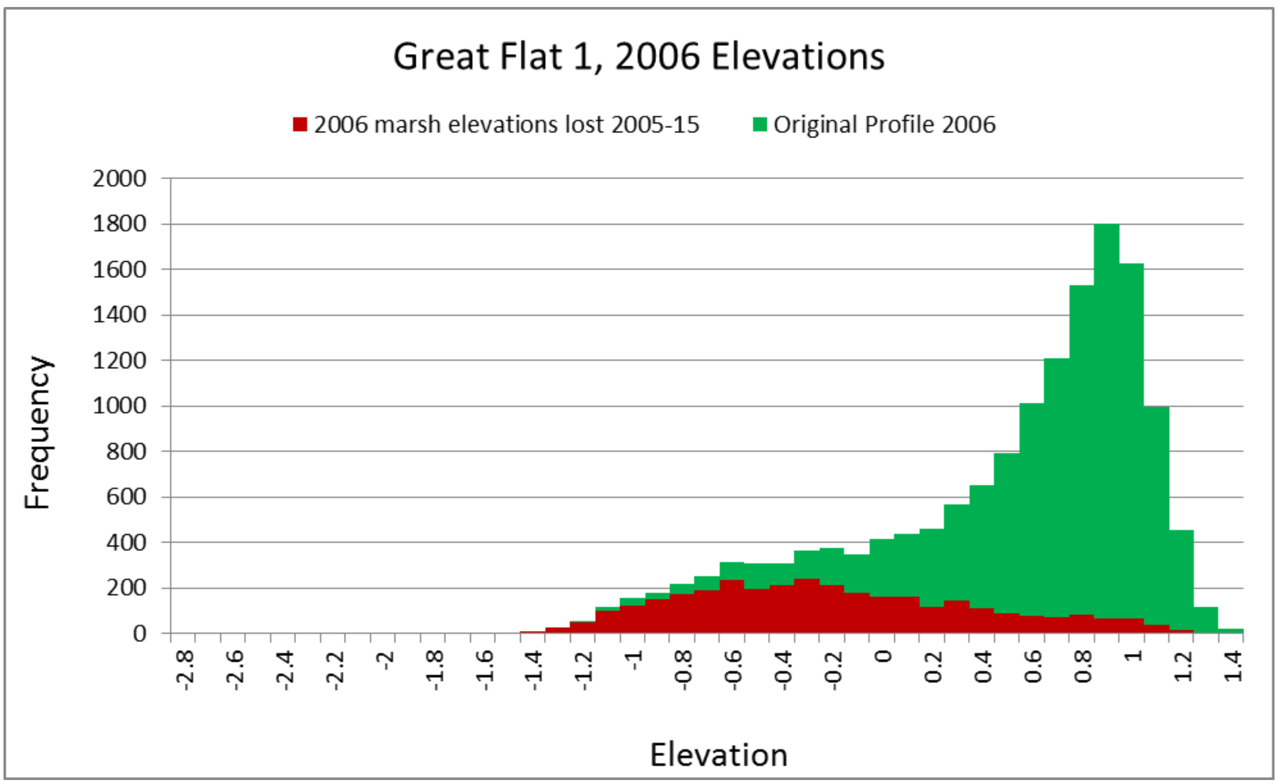

Fig. 29 Frequency histogram of 4 m^2 pixels (red = elevation lost) on Great Flat after 2005 based on the 2006 LiDAR elevations.

Sanford Flat C

Sanford Flat C is the only salt marsh island studied that had an area of upland (uncolored portion of Fig. 30). It is also notable in that it was the only island that exhibited a large loss in the center of the island, the result of the expansion and merging of three large pannes in a low area (arrow, Fig. 30). The island also had a network of low marsh islets on the south that have also had appreciable loss.

One of the most striking aspects of the LiDAR data for Sanford Flat C was that most of the islets on the south side of the island were less than LiDAR elevation 0.0 feet (Fig. 31; these islets were likely mostly submerged during the LiDAR flight, so the lower depth of *Spartina* survival here is unknown). The vegetation density observed in the UAV imagery is notably sparse. This area has experienced the greatest loss in area with much of the loss in areas not adjacent to tidal channels. The low elevation of this area suggests this area is most vulnerable to sea level rise. Between 1938 and 2005, Whites Flat lost marsh area at a rate of 0.40 % per year, between 2009 and 2016 this rate increased to 1.8% per year (Fig. 32).

The area of the island lost between the 2005 and 2016 aerial images was superimposed on the 2006 LiDAR data to calculate the 2006 elevation areas lost in the subsequent decade (Fig. 33). As shown, most of the areas lost were the lowest elevations of the marsh, but there was also a node of higher elevations lost. These higher elevation losses likely represent a combination of marsh bank undercut and lost, and expansion of pannes and channels in the higher elevations of the marsh.

All images reviewed for Sanford Flat C, both interpreted and not interpreted, are shown in Figs A61 through A80 in the Appendix.

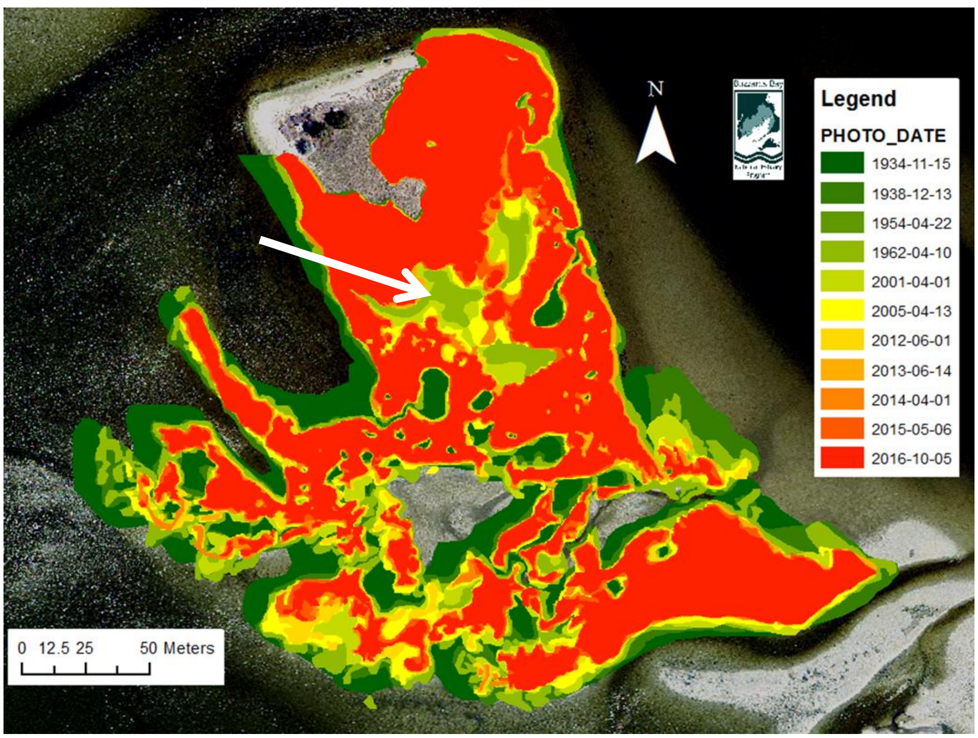

Fig. 30 Composite of estimated vegetated salt marsh boundaries for Sanford Flat C for each aerial photograph interpreted for the study. Arrow shows the local of three large and expanding pans appearing principally after 2001.

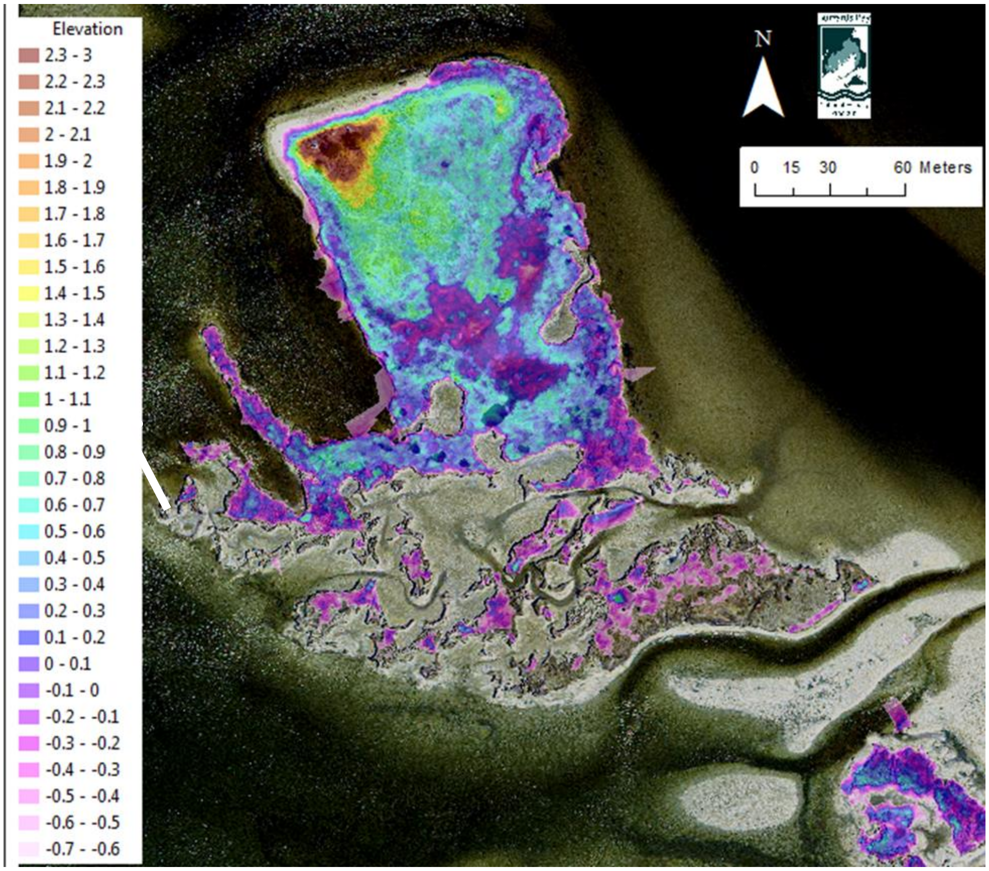

Fig. 31 2006 LiDAR elevations of Sanford Flat C.

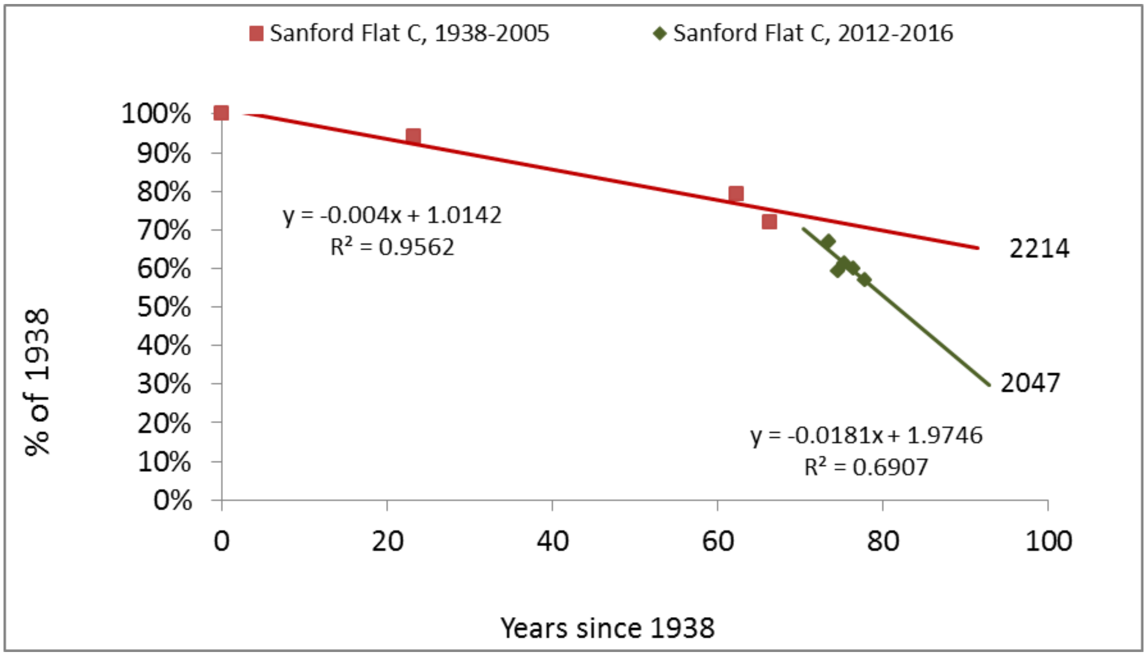

Fig. 32 Rate of area loss on Sanford Flat C between 1938 and 2005 compared to the rate between 2012 and 2016, with estimated date of island disappearance based on extrapolating trends for each period.

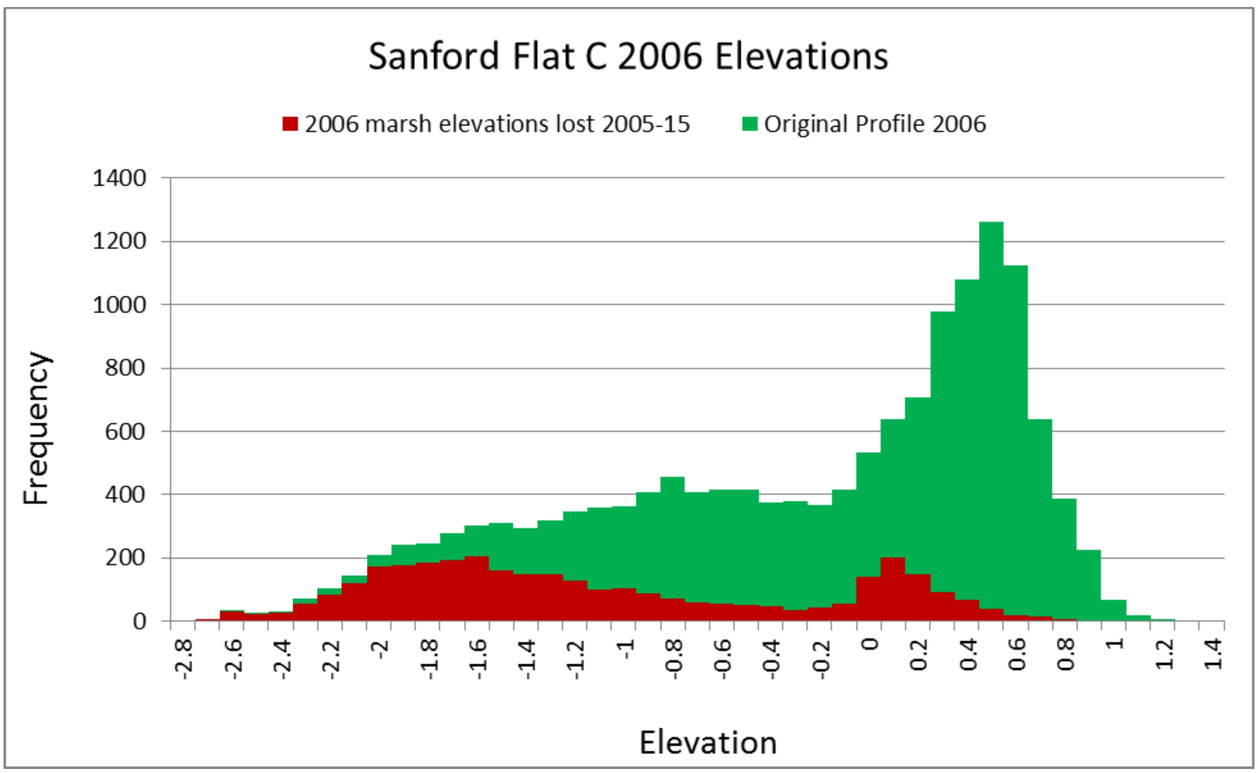

Fig. 33 Frequency histogram of 4 m^2 pixels (red = elevation lost) on Sanford Flat C after 2005 based on the 2006 LiDAR elevations.

Great Flat 12

Great Flat 12 had a dramatic loss of area between the 1962 image and 2001 for the interpreted photos (Fig. 34), with the actual loss occurring between 1982 and 1996 as shown in the uninterpreted images (see Fig. A88 and Fig. A89 in the Appendix). Hurricane Bob occurred during this time (1991), and may have played a role, but certainly other factors may have contributed to the loss during this period.

Great Flat 12 had the lowest average elevation of any island with LiDAR elevation elevations mostly between 0.3 feet and -0.5 feet (Fig. 35). Like the low marsh areas at the southern end of Sanford Flat C, the vegetation density observed in the UAV imagery is notably sparse. The low elevation profile of the island suggest that, among all the islands studied, Great Flat 12 is the most vulnerable to future sea level rise. Great Flat 12 was the only island studied where the rate of area loss was not significantly greater in recent years than over the earlier historical trend. Between 1938 and 2005, Great Flat 12 lost marsh area at a rate of 0.83 % per year, between 2009 and 2016 this rate increased to 1.1% per year (Fig. 36).

All images reviewed for Great Flat 12, both interpreted and not interpreted, are shown in , are shown in Figs A81 through A100 in the Appendix.

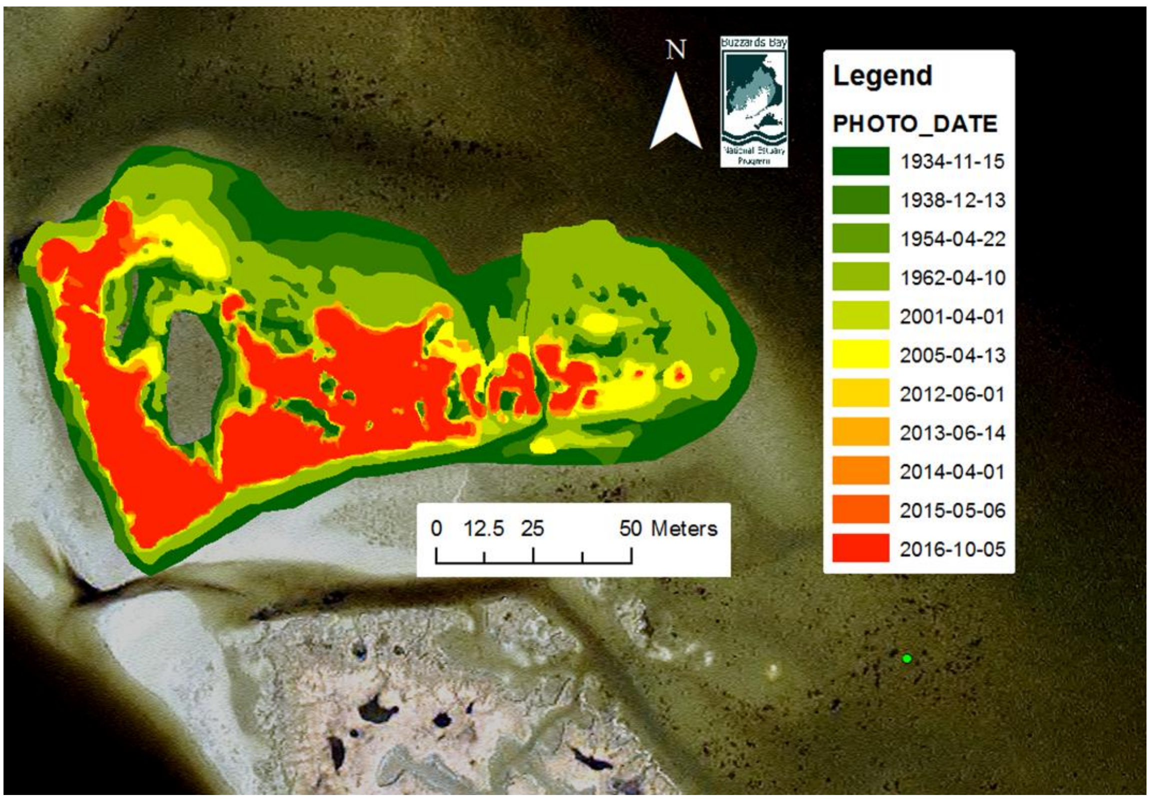

Fig. 34 Composite of estimated vegetated salt marsh boundaries for Great Flat 12 for each aerial photograph interpreted for the study.

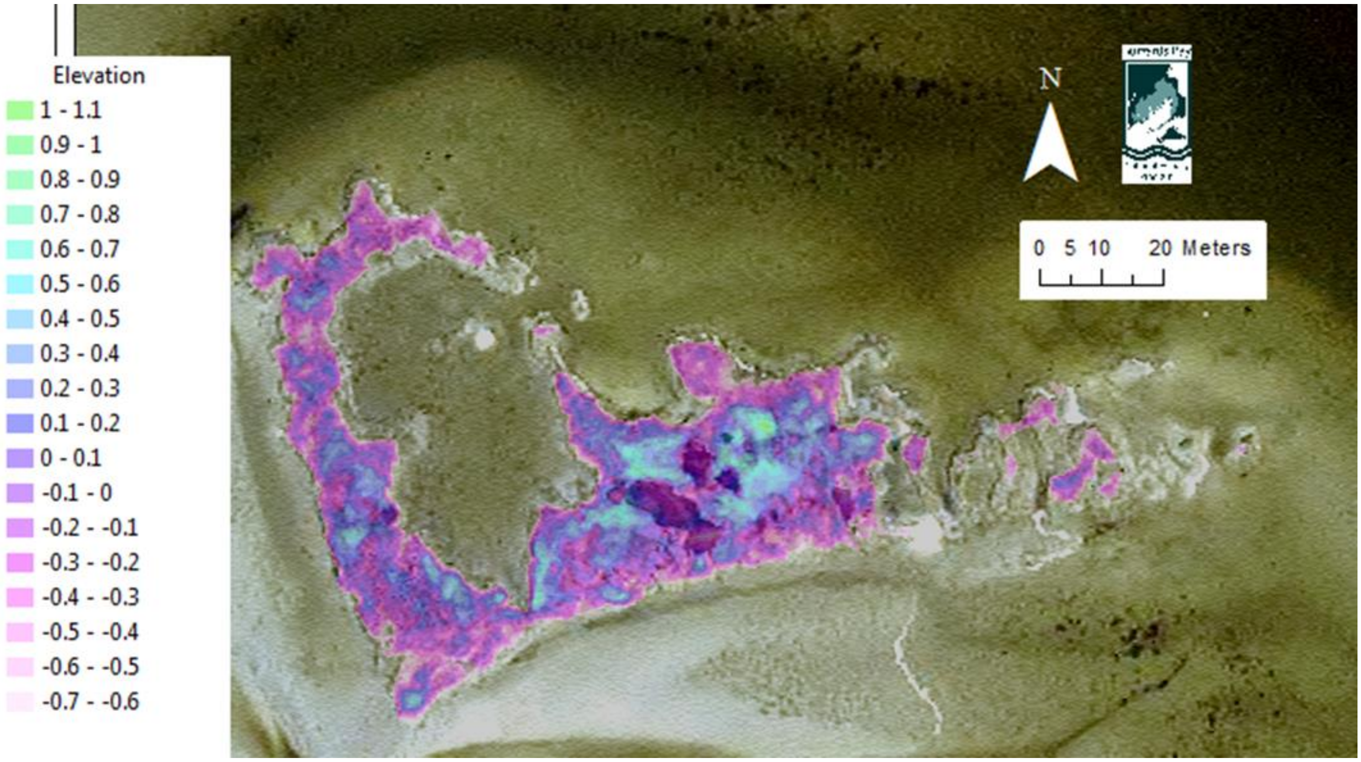

Fig. 35 2006 LiDAR elevations of Great Flat 12.

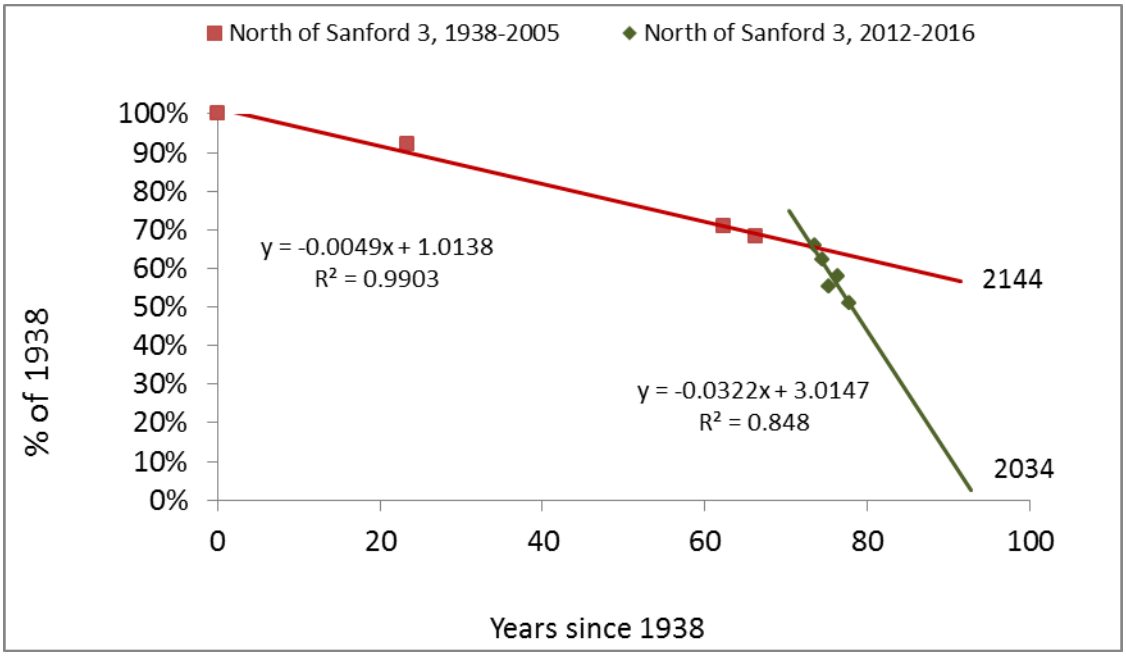

Fig. 36 Rate of area loss on Great Flat 12 between 1938 and 2005 compared to the rate between 2012 and 2016, with estimated date of island disappearance based on extrapolating trends for each period.

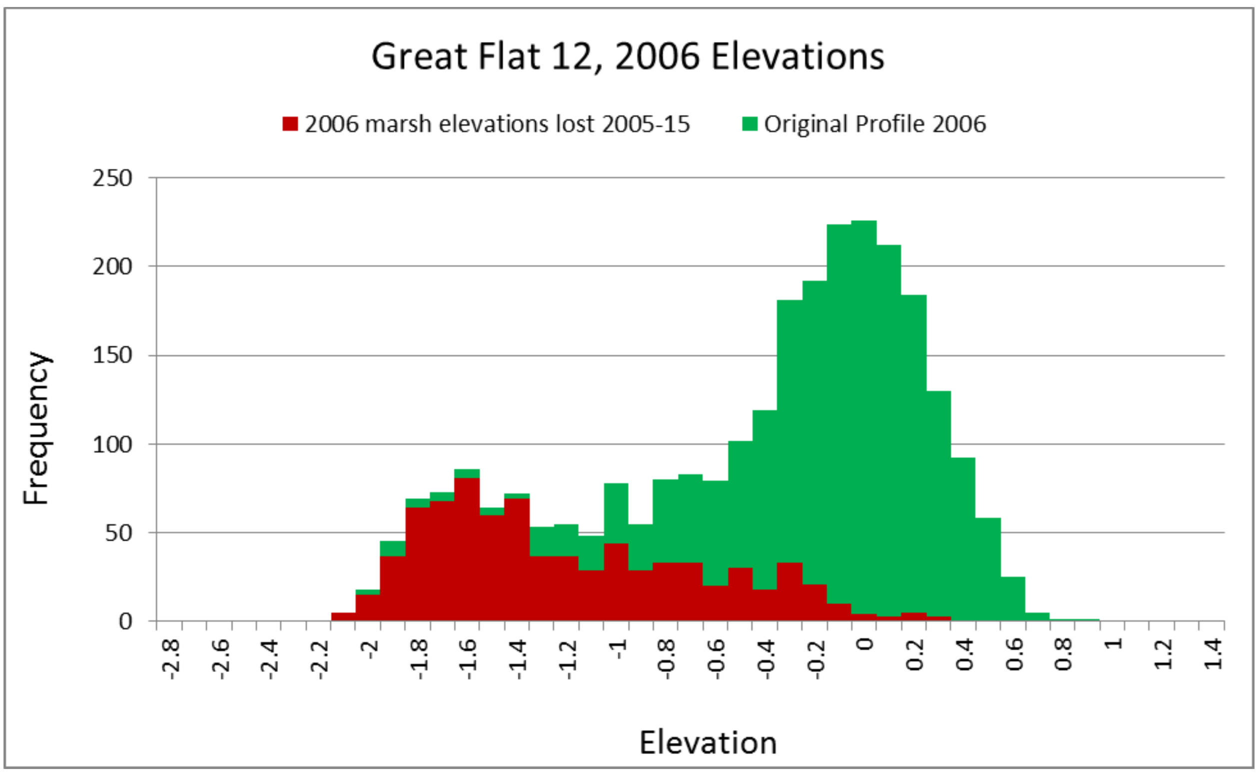

Fig. 37 Frequency histogram of 4 m^2 pixels (red = elevation lost) on Great Flat 12 after 2005 based on the 2006 LiDAR elevations.

North of Sanford 3

North of Sanford 3 had the smallest relative area of pannes of any island, and most of the observed marsh loss occurred on the northeast coast adjacent to a main tidal channel (Fig. 38). The islands marsh was mostly between LiDAR elevation 0.2 and -0.3 feet (Fig. 39). Most of the historical losses on the island were on the northeast corner of the island adjacent to river tidal channels. North of Sanford 3 exhibited one of the lower historical rates of marsh area loss, but now has the highest recent rates of loss (by nearly double). Between 1938 and 2005, North of Sanford 3 lost marsh area at a rate of 0.50 % per year, between 2009 and 2016 this rate increased to 3.2% per year (Fig. 40).

All images reviewed for North of Sanford 3, both interpreted and not interpreted, are shown in Figs A101 through A116 in the Appendix.

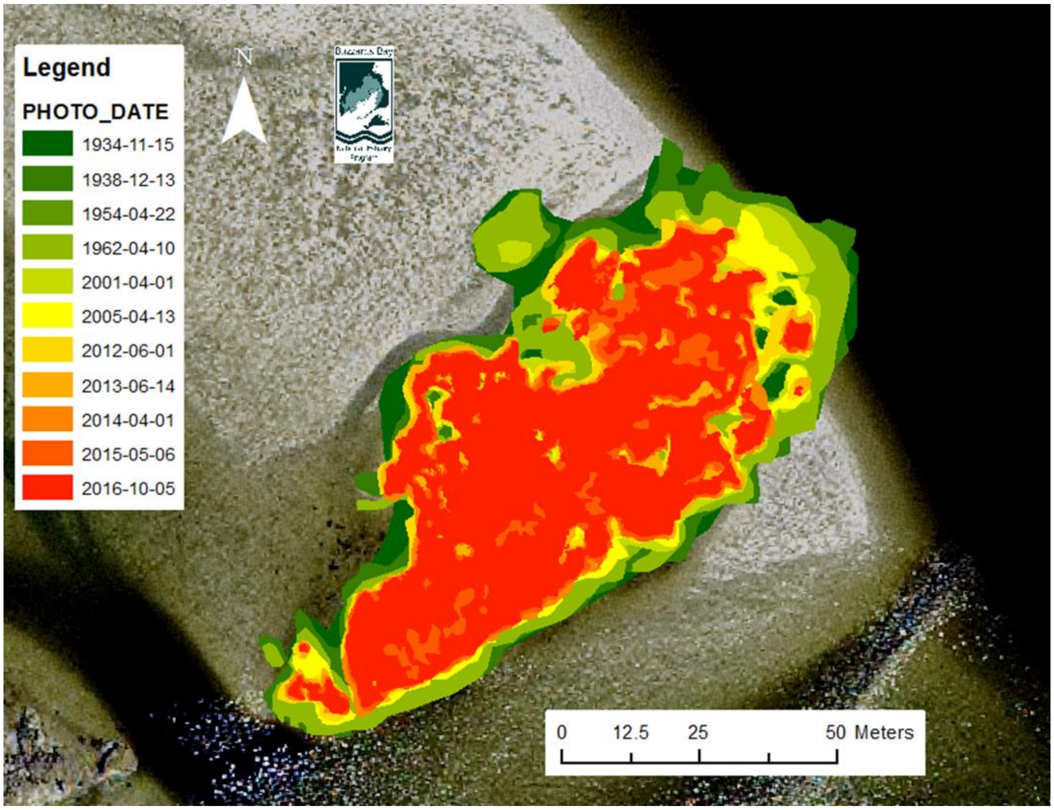

Fig. 38 Composite of estimated vegetated salt marsh boundaries for North of Sanford 3 for each aerial photograph interpreted for the study.

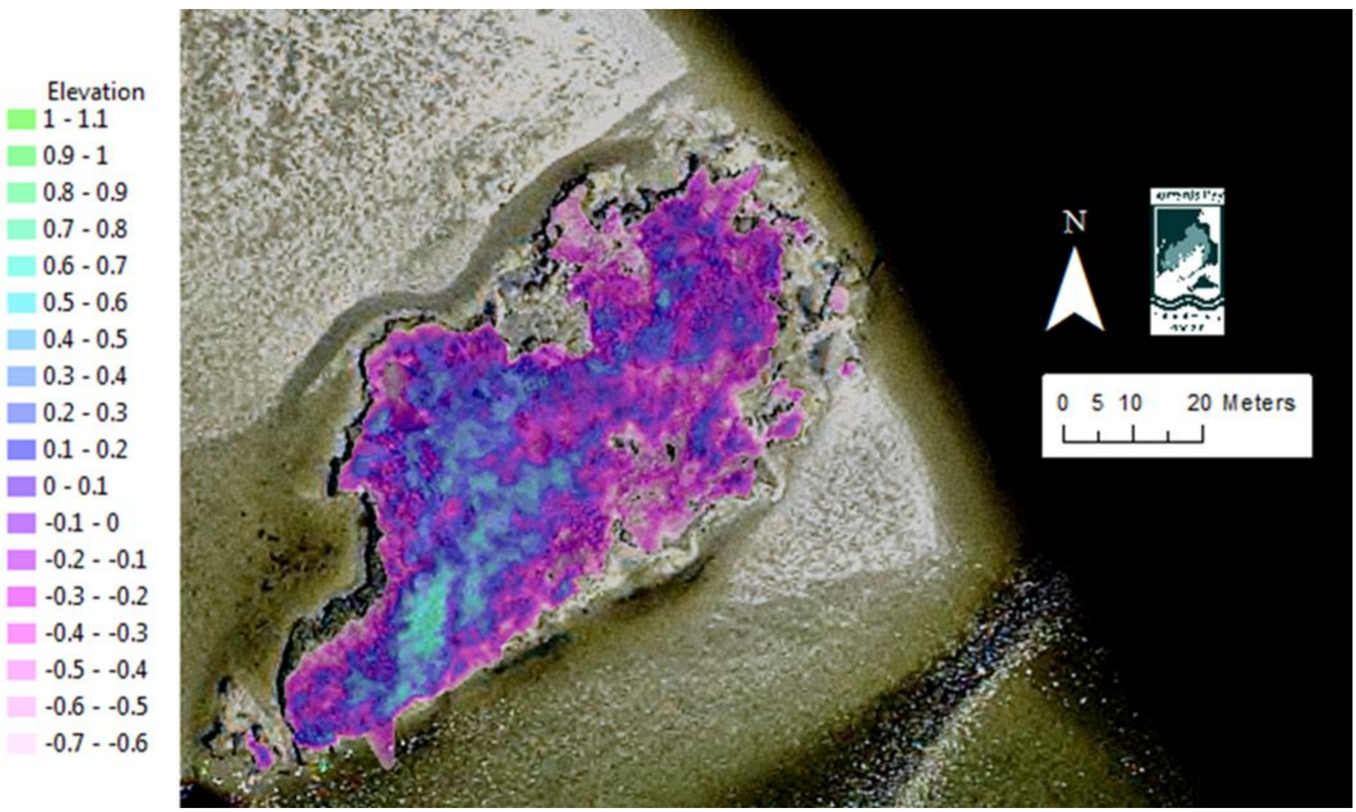

Fig. 39 2006 LiDAR elevations of North of Sanford 3.

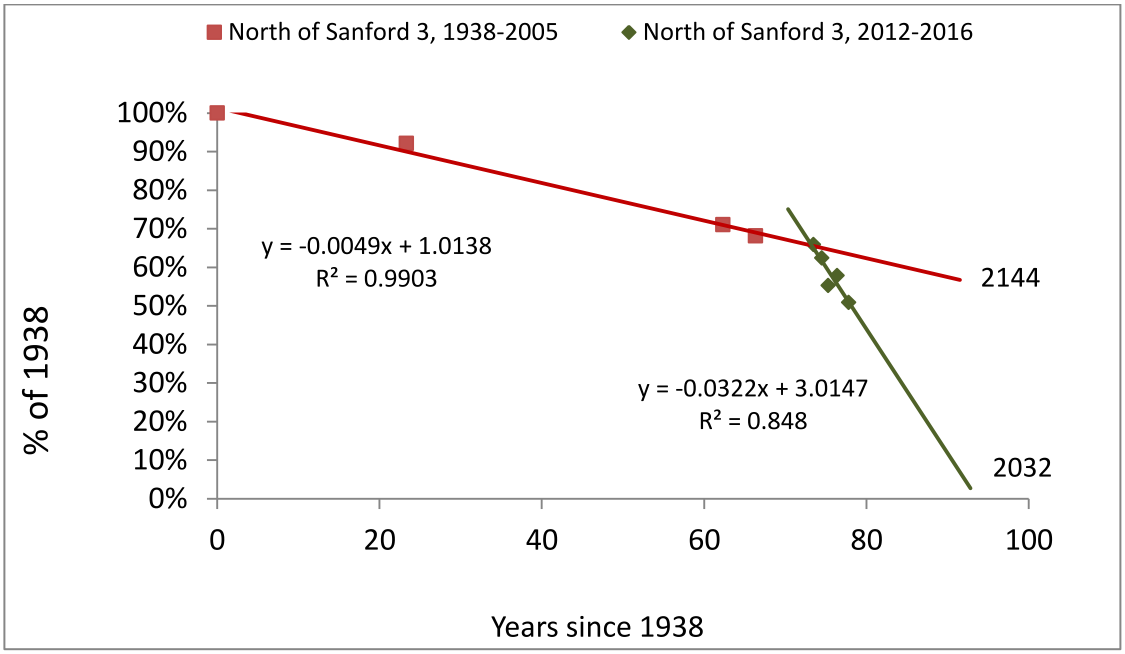

Fig. 40 Rate of area loss on North of Sanford 3 between 1938 and 2005 compared to the rate between 2012 and 2016, with estimated date of island disappearance based on extrapolating trends for each period.

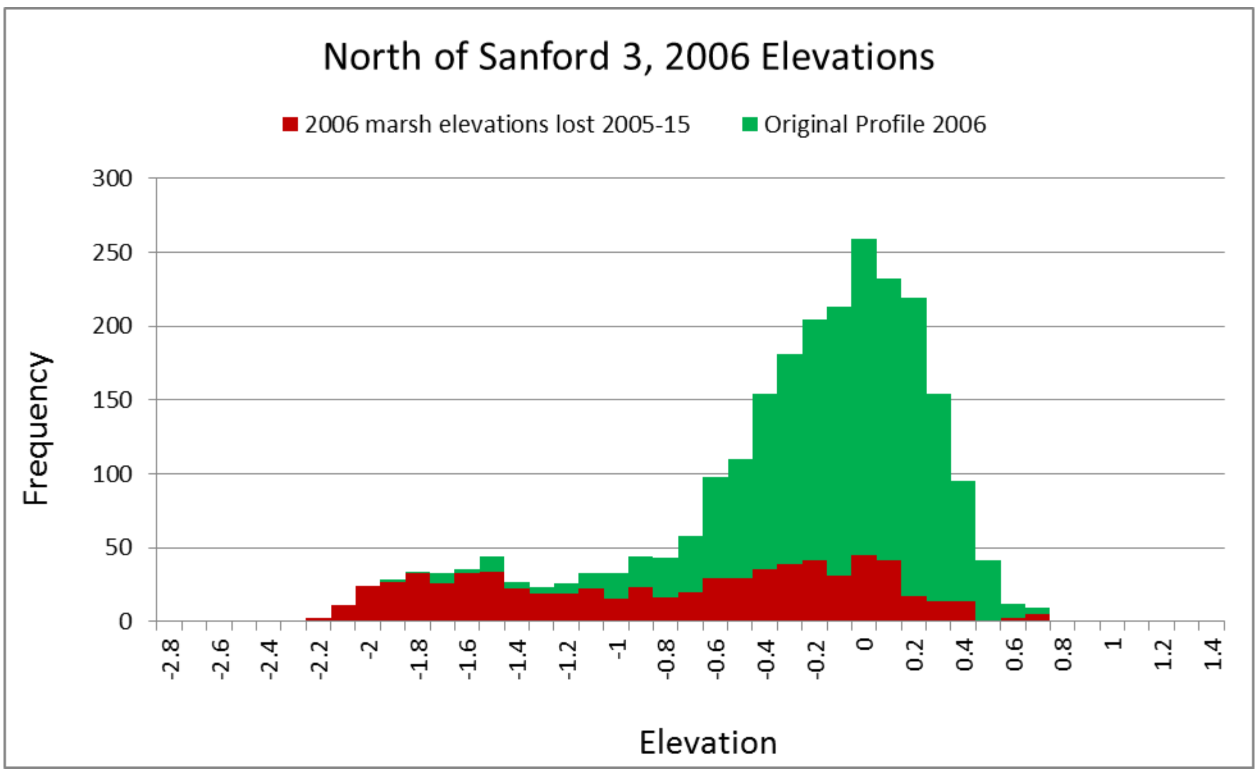

Fig. 41 Frequency histogram of 4 m^2 pixels (red = elevation lost) on North of Sanford 3 after 2005 based on the 2006 LiDAR elevations.

Discussion

Since the end of the last ice age, sea level has risen more than 400 feet. During that time, marshes have been lost or migrated inland. During the past several thousand years, sea level rise has been considerably slower, but sea level rise has likely remained the principal cause of salt marsh loss and inland migration. These patterns of salt marsh change are compounded by other physical factors including storm damage, coastal erosion, and icing. Biological factors such as grazing by invasives crabs and nutrient pollution may also be contributing factors. Marsh islands without upland areas lack a path of marsh retreat and marsh habitat at these sites are most vulnerable to sea level rise, and these marsh islands will eventually be lost. An analysis of changes in salt marsh boundaries alone cannot resolve the relative contribution of sea level rise compared to other contributing physical and biological factors in the cause of these losses.

The greatest challenge of this study was delineating the presumed living marsh boundary. While this boundary is relatively apparent on recent summertime imagery of high resolution, in older early spring images, for any given island, there are likely numerous potential errors in the interpretation of the living marsh boundary. These errors are compounded by differences in tidal elevations, image resolution, and problems of georeferencing the imagery. For these reasons, changes in the area of a marsh island between two successive time steps should be interpreted with caution. Instead, trends over multiple time steps are most meaningful because the various errors inherent in the analysis tend to average out, especially over periods of ten years or more.

Although the rates of loss varied among the islands during the 20th century, for the most part the losses of the islands appear linear, perhaps punctuated by specific erosion events associated with severe storms. Most of the islands also showed an apparent increase in area loss after 2005, some dramatically so. Strong storms marked this period, including a strong nor'easter in 2007, the remnants of Hurricane Floyd and Irene in 2011 and 2012 respectively, and severe icing from January to March 2015. Storm damage alone cannot explain the observed patterns because some islands in the more protected upper estuary saw losses that equaled or exceeded losses to marshes in the lower estuary, closer to the more exposed estuary entrance. The relative importance of physical disturbances and biological processes as compared to the underlying patterns of losses due to sea level rise warrants further study. Because the extrapolated trends in the figures of marsh area loss coincides with a period of multiple disturbances (after 2005, and principally for 2012-2016), care should be taken in interpreting the findings. Whether the recent rates of loss will continue is uncertain, therefore there is considerable uncertainty in the reliability of decadal projections based on less than five years of data.

The histograms of the marsh losses at 0.2-foot interval for each island shown in the Results section define clear differences in the patterns of loss on each island, and may shed light on the different rates of marsh loss on each island. Table 4 summarizes this data using a somewhat arbitrary LiDAR elevation of -0.5 feet as a dividing line (compare to Fig. 12). This analysis affirms the anomalously high rate of loss of higher elevations of Baily Flat (30% of the area greater than -0.5 feet) compared to the other sites. This pattern is explained by the channel erosion undercutting of the high "spine" of the island.

Table 4 also shows a low percent loss of Sanford Flat C below -0.5 feet. This pattern might be related to the fact that this island has a very large fraction of its area in the elevation range of -1.0 to -0.5 feet. Contributing to this apparent pattern of loss may be the fact that dead marsh peat at its southern border may have been persisting longer than similar low marsh areas to the south, giving the appearance of a slower rate of loss.

Table 4. Comparison of marsh loss above and below LiDAR elevation 0.5 feet. Areas in sq. meters of hectares as noted.

	2005 Area <-0.5	2005 Area >=-0.5	2016 Area <-0.5	2016 Area >=-0.5	Area <-0.5 % loss	Area >=-0.5 % loss	2005 total pts ha	2005 ha from polygons	2016 total pts ha	2016 ha from polygons
Bailey Flat	206	5,720	18	3,984	-91.2%	-30.3%	0.59	0.59	0.40	0.41
Sanford Flat C	8,063	14,441	4,542	12,995	-43.7%	-10.0%	2.25	2.28	1.75	1.81
Whites Flat	1,592	27,935	512	25,640	-67.9%	-8.2%	2.95	2.93	2.62	2.72
North Sanford 3	894	2,826	332	2,354	-62.9%	-16.7%	0.37	0.37	0.27	0.27
Great Flat 12	1,445	2,628	453	2,438	-68.6%	-7.2%	0.41	0.40	0.29	0.30
Great Flat 1	1,970	20,696	389	17,336	-80.3%	-16.2%	2.27	2.25	1.77	1.88

We acknowledge there are limitations inherent in this LiDAR data. One issue we did not correct for was that MSL increases somewhat as one goes up the estuary, and MLLW and MHHW are also compressed. Consequently, the -0.5 feet elevation is not precisely at the same tidal elevation for all islands. However, given the proximity of the islands to each other, the tidal elevation correction factor may be small.

Overall, on each island, the area lost during the 2005 to 2016 period appears largely defined by how much area of the island was less than -0.5 feet to begin with, coupled with whatever additional causes (storms, erosion, or potential biological factors) might be exacerbating underlying river-wide average trends associated with sea level rise.

Atlas of changes in salt marsh boundaries at selected islands in the West Branch of the Westport River, 1934-2016 Appendix:
Inventory of aerial images interpreted or reviewed.

Joseph E. Costa and Molly Weiner

Final February 2017

In the following figures, true north is at the top of the photograph, and in many cases, the images were enhanced using various image control features in ArcGIS.

Bailey Flat

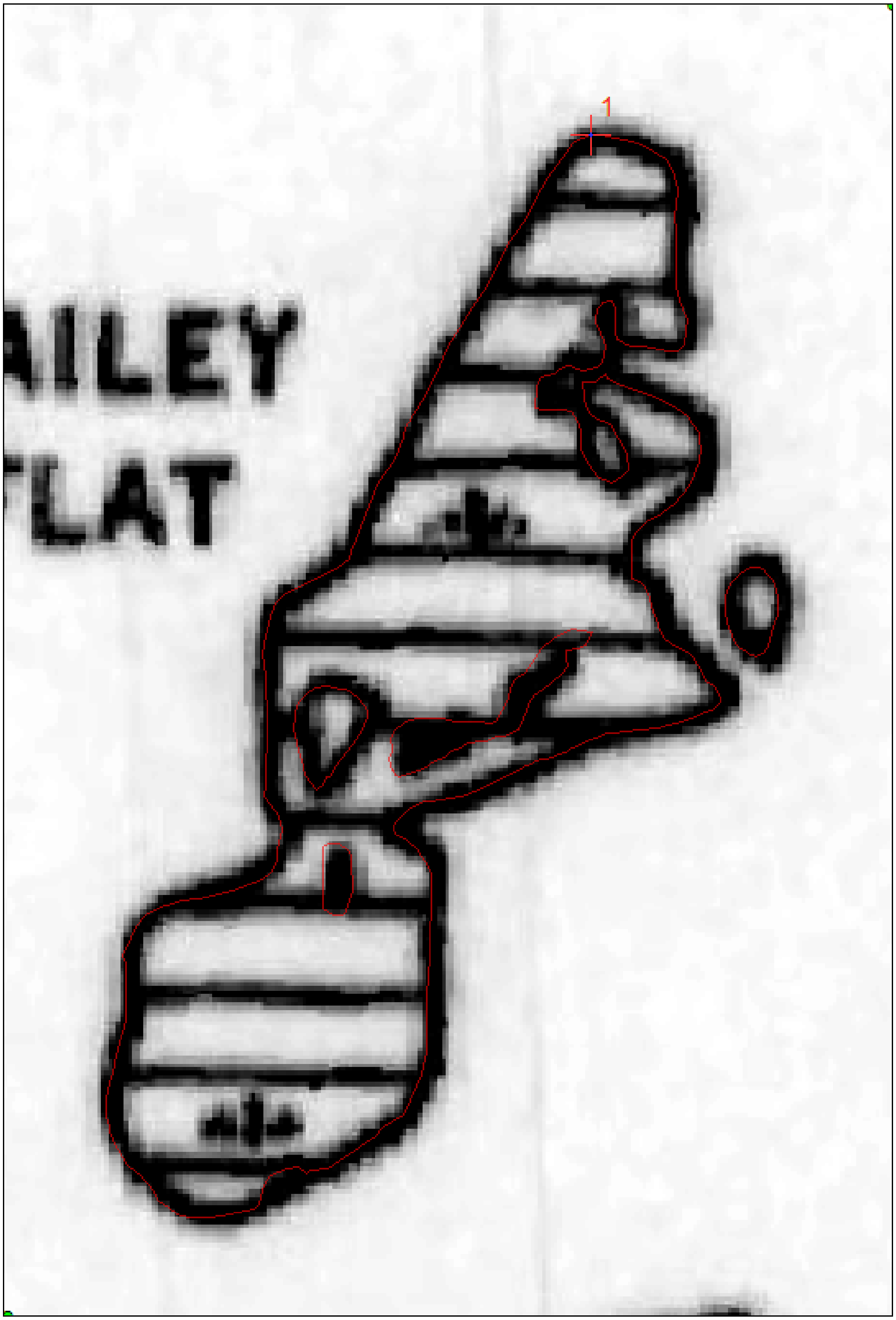

Fig. A1 Bailey Flat November 1934 boundary on Nautical T-sheet based on 11/15/1934 aerial. The irregular vertical lines in the north and south end of the islands represent the marsh grass symbol on the maps.

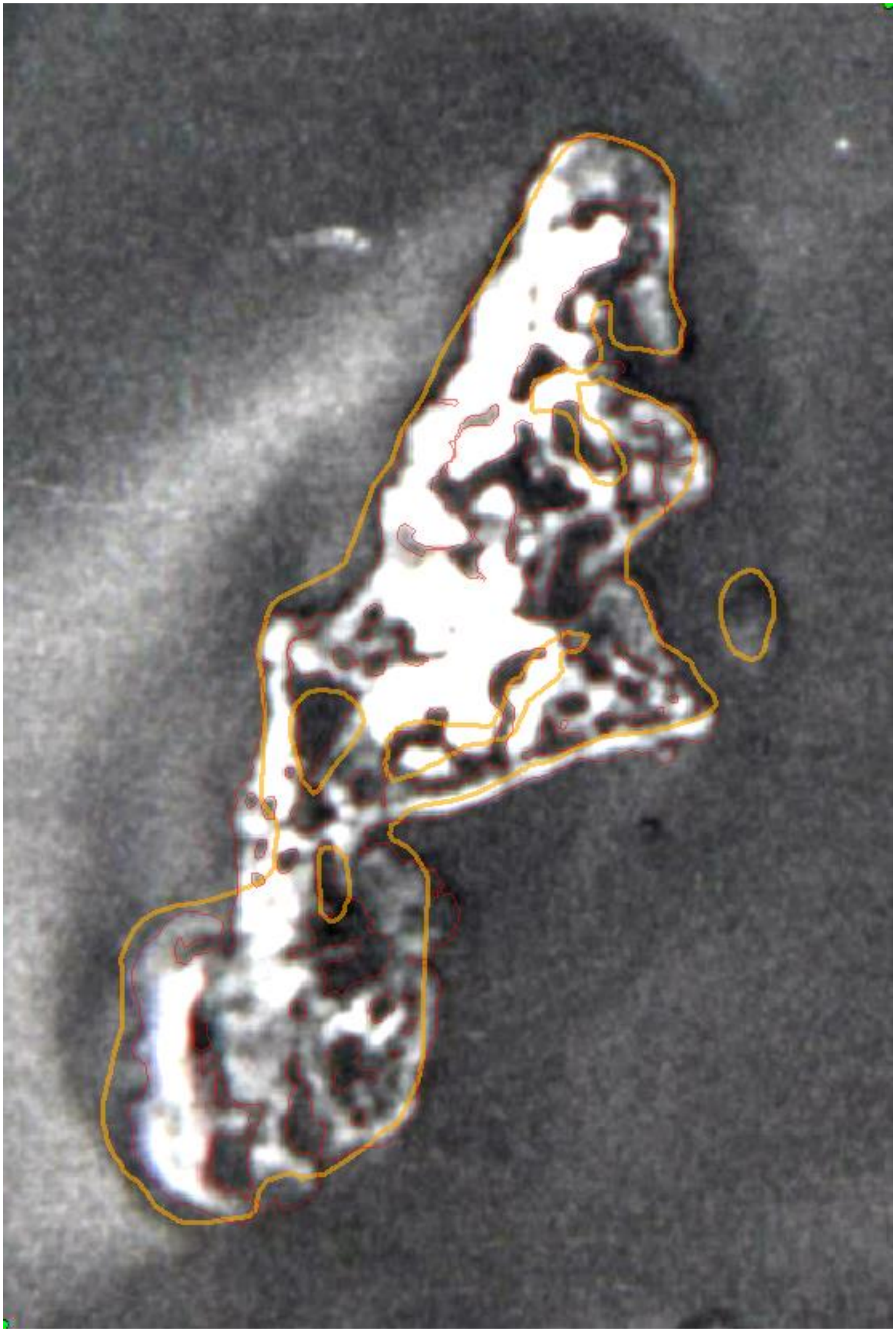

Fig. A2 Bailey Flat December 1938 boundaries (red) on source photograph; previous presumed November 1934 boundaries in orange from Nautical T-Sheet. The small island (center right) was presumed lost in the hurricane of 1938, with just a peat mound remaining.

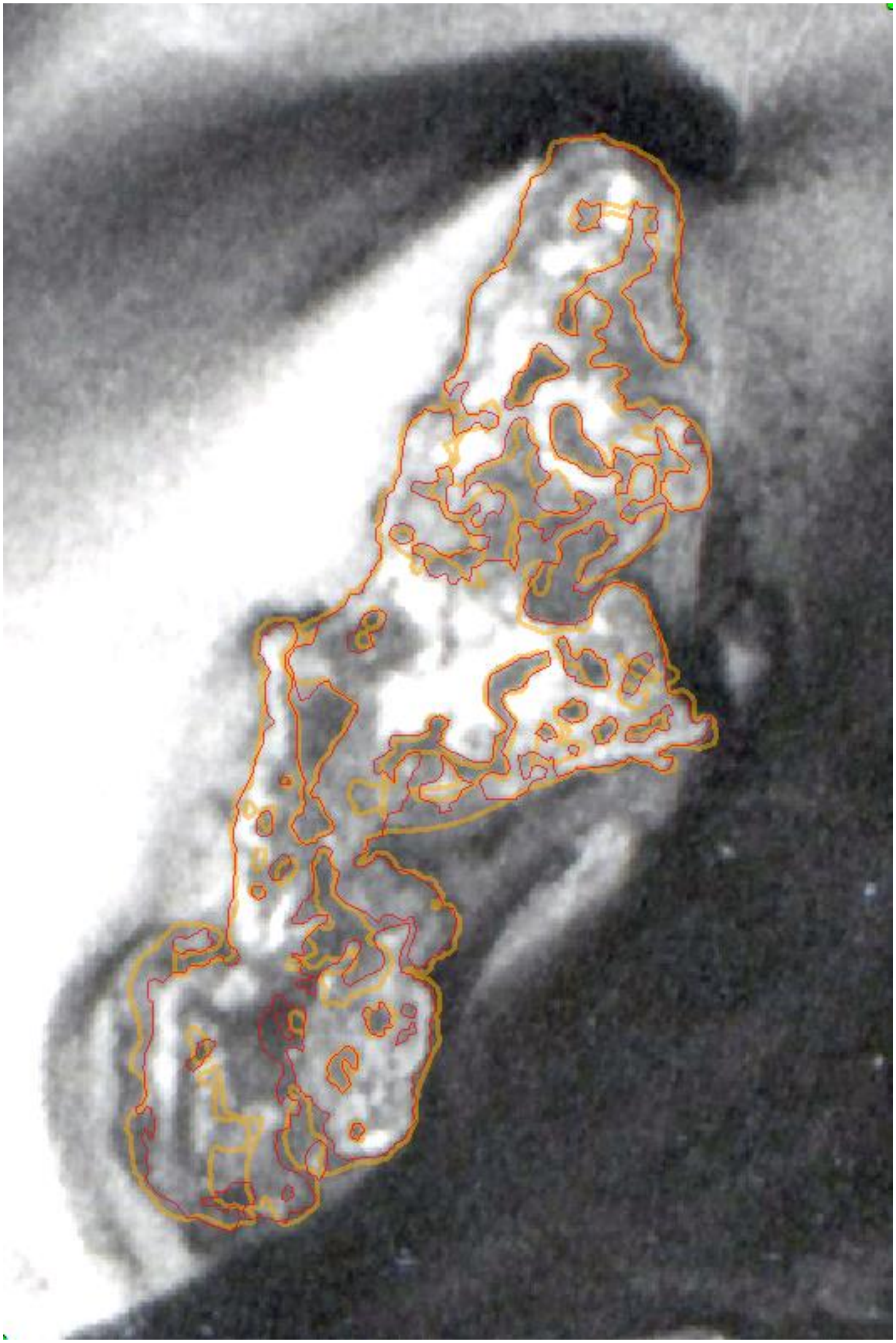

Fig. A3 Bailey Flat June 1942 boundaries (red) on source photograph; previous December 1938 boundaries in orange.

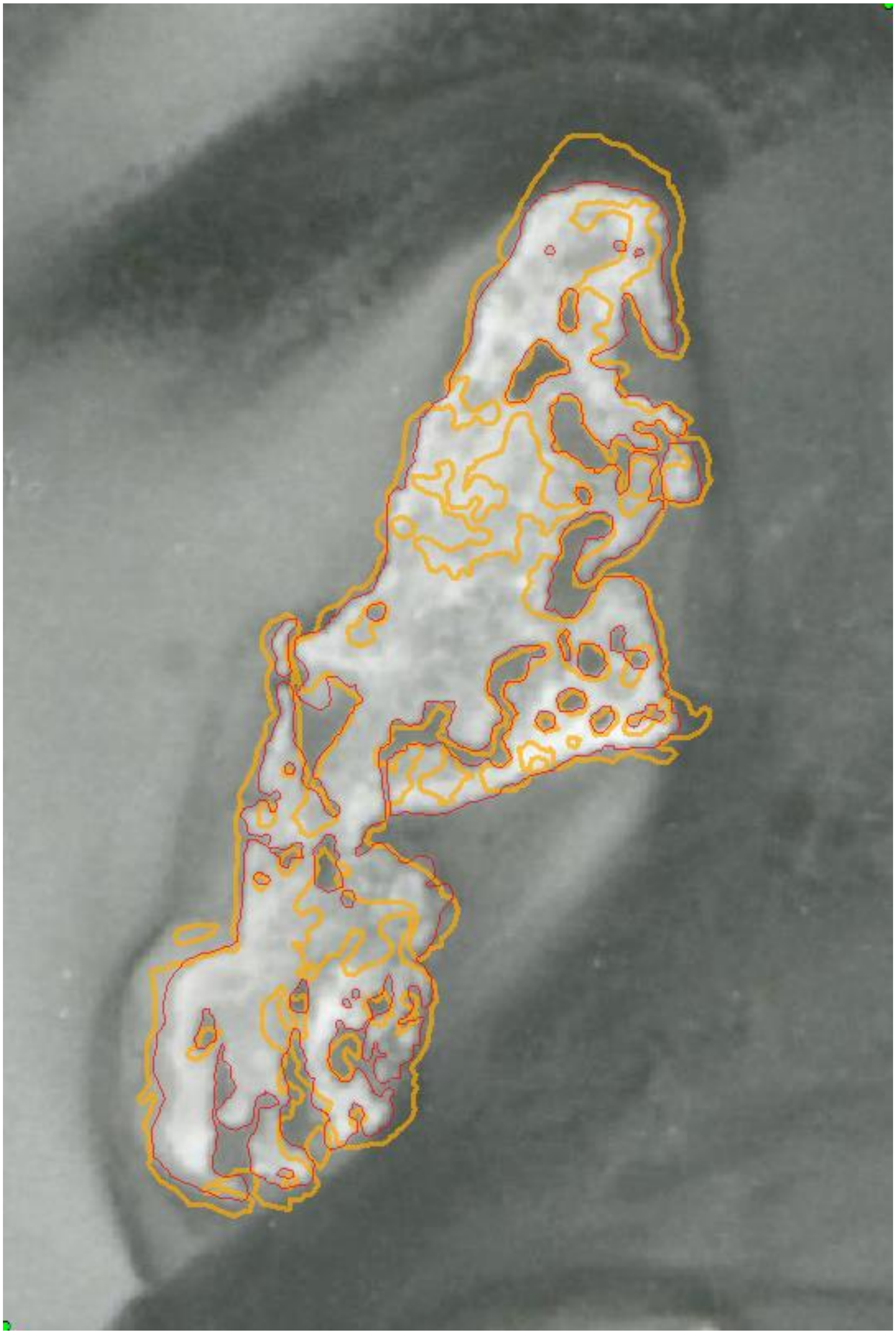

Fig. A4 Bailey Flat April 1954 boundaries (red) on source photograph; previous June 1942 boundaries in orange. Note that some large internal features at the north end of the island appear to have disappeared.

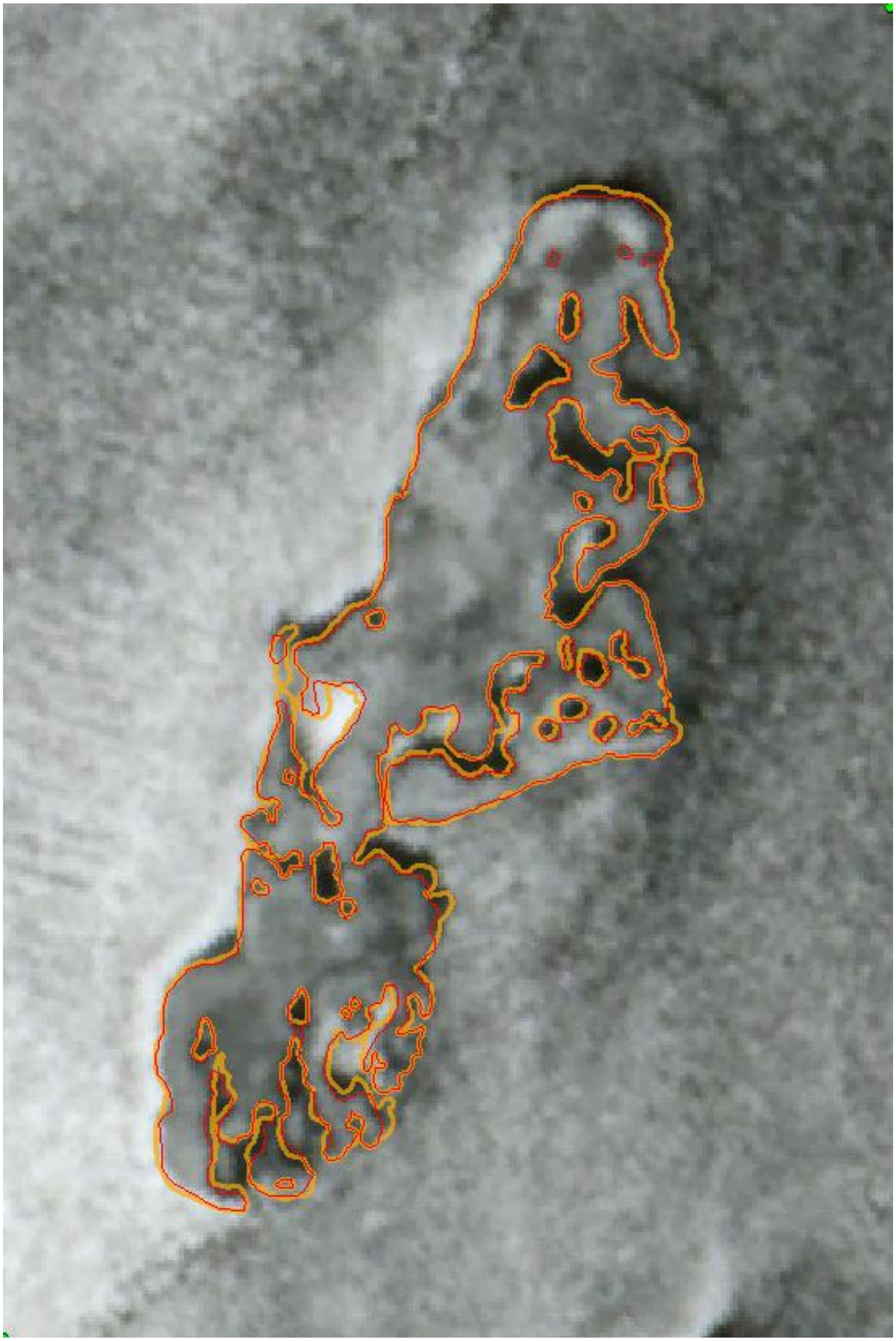

Fig. A5 Bailey Flat May 1956 boundaries (red) on source photograph; previous April 1954 boundaries in orange.

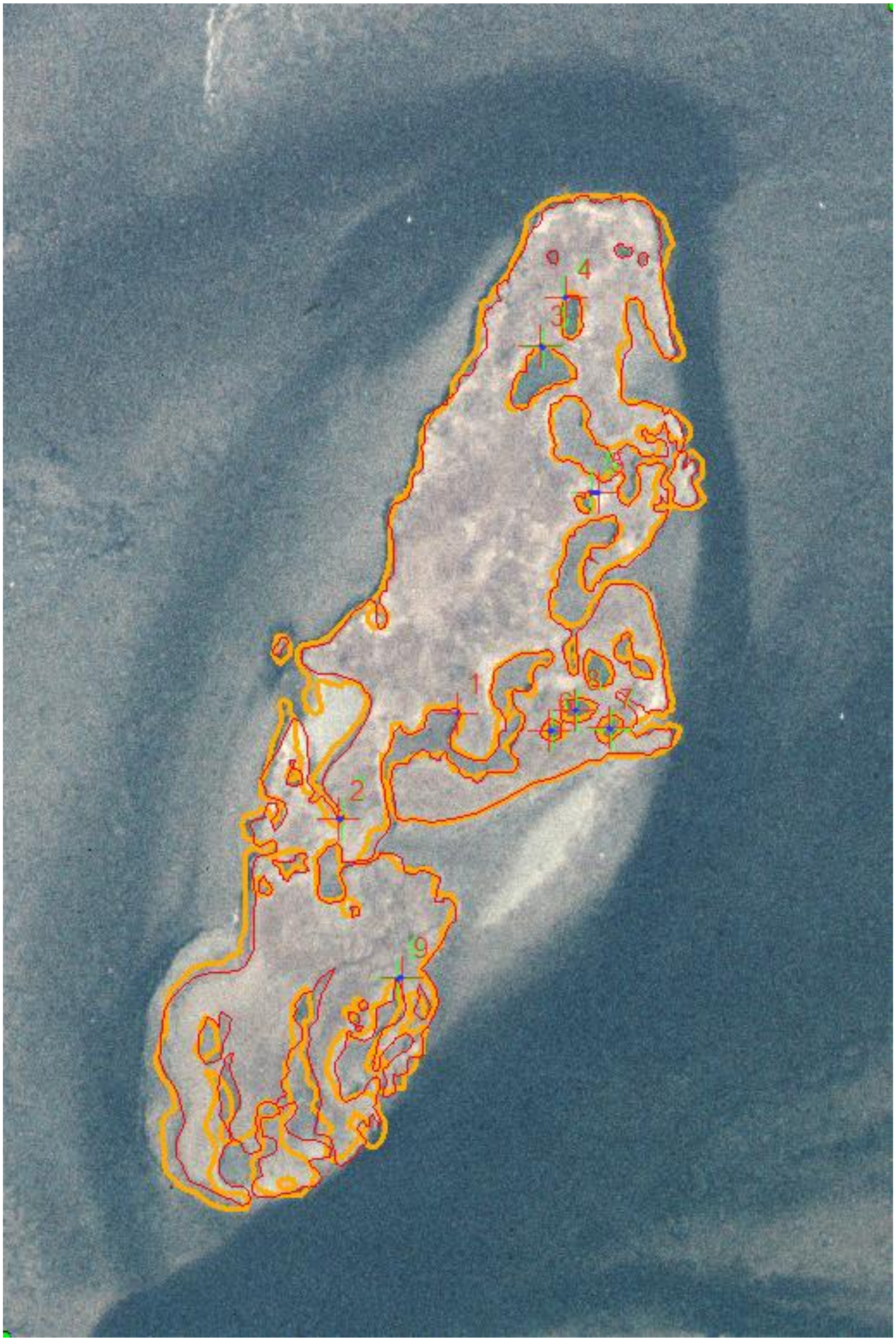

Fig. A6 Bailey Flat April 1962 boundaries (red) on source photograph; previous May 1956 boundaries in orange.

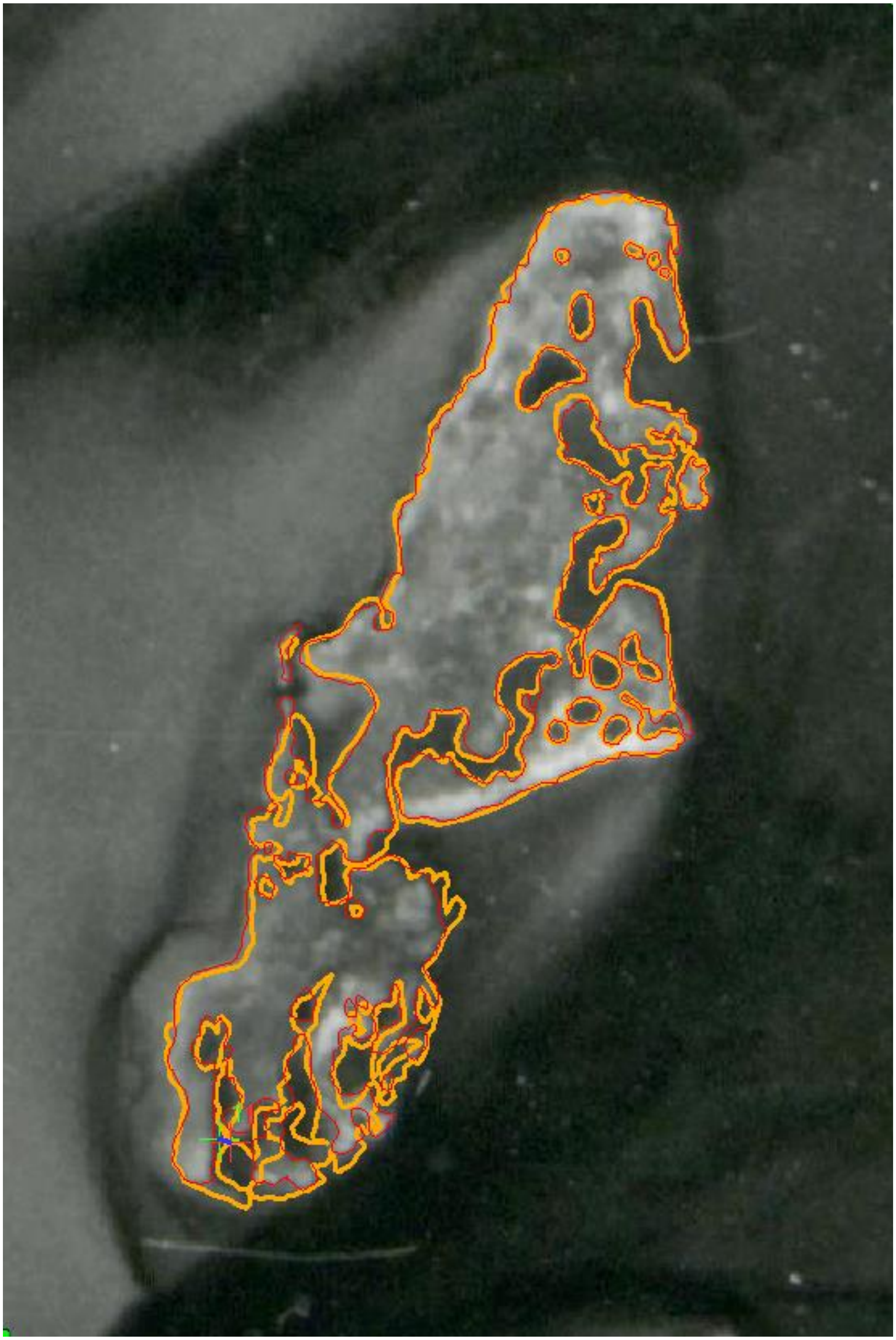

Fig. A7 Bailey Flat April 1964 boundaries (red) on source photograph; previous April 1962 boundaries in orange.

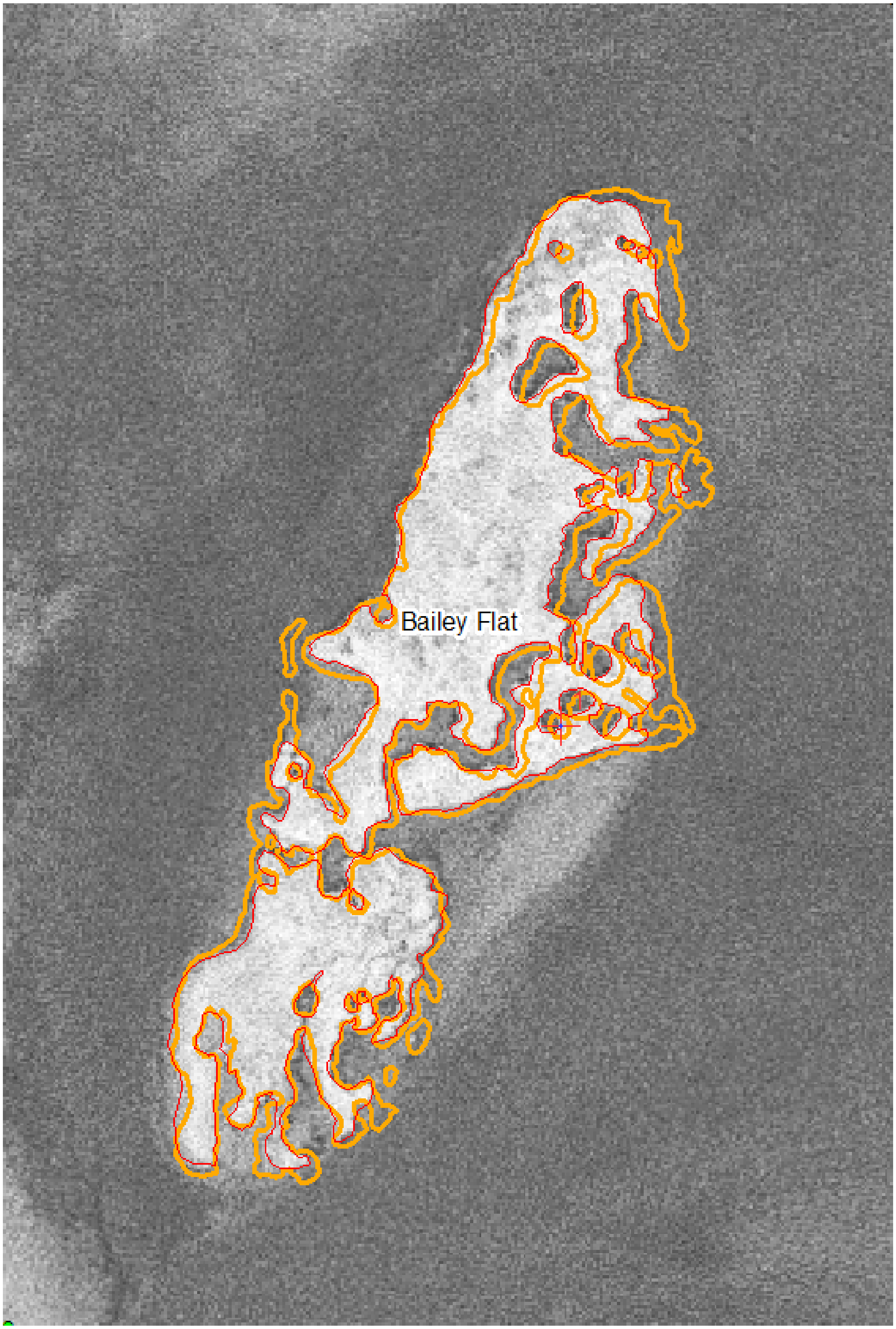

Fig. A8 Bailey Flat February 1974 boundaries (red) on source photograph; previous April 1964 boundaries in orange.

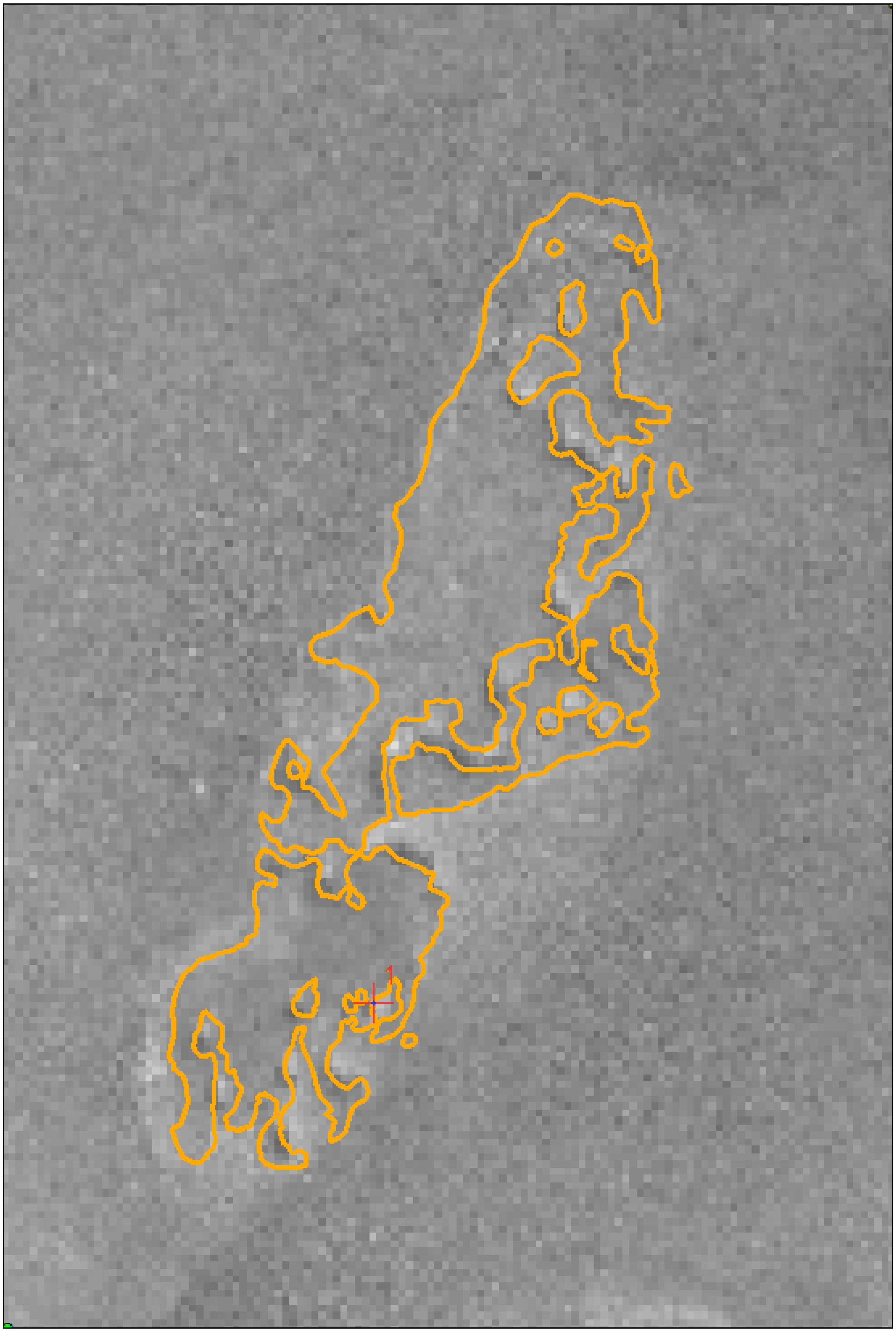

Fig. A9 An April 1980 photograph of Bailey Flat was not interpreted. The previous February 1974 boundaries are shown in orange.

Fig. A10 Bailey Flat June 1982 boundaries (red) on source photograph; previous February 1974 boundaries in orange.

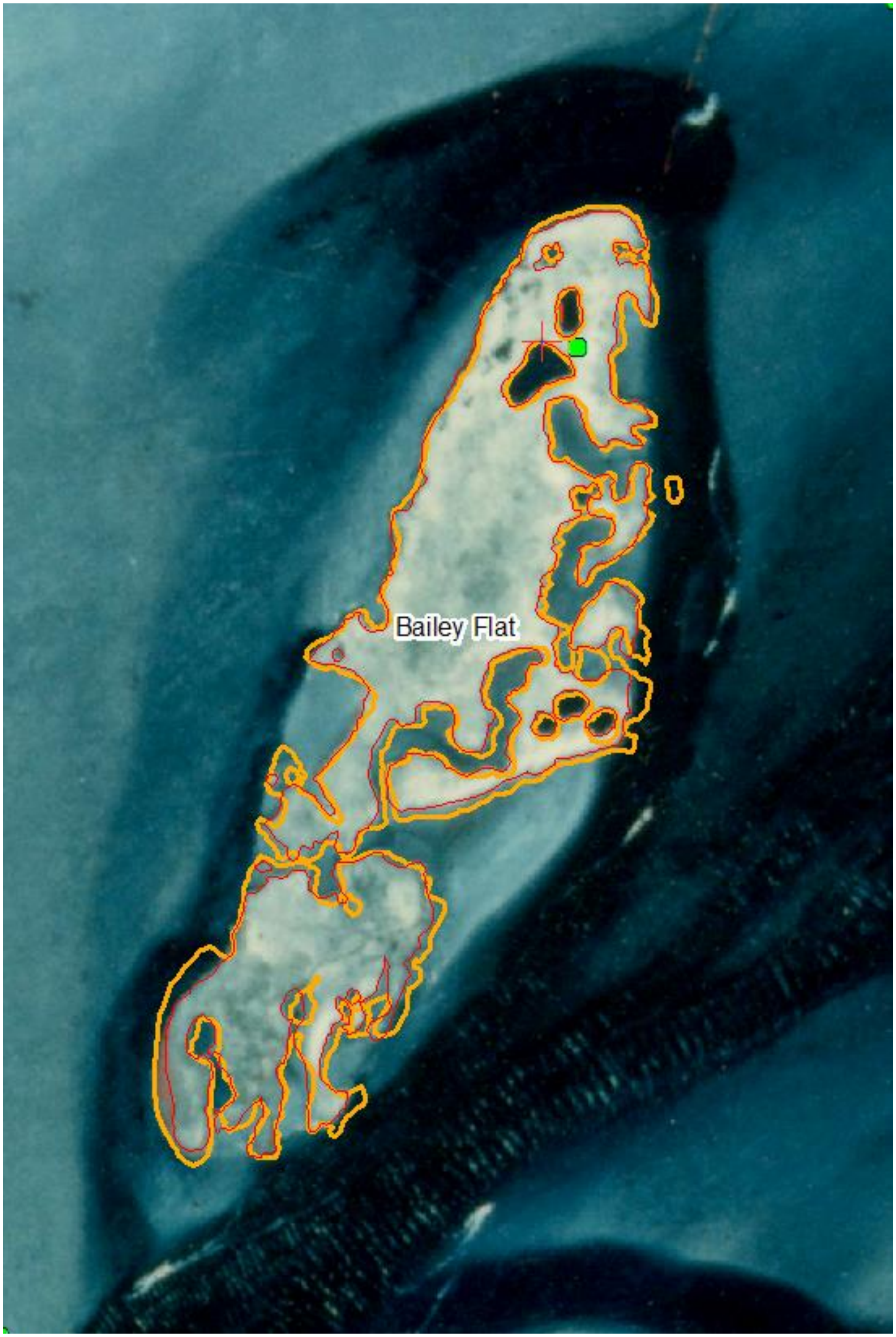

Fig. A11 Bailey Flat April 1990 boundaries (red) on source color-infra red photograph; previous June 1982 boundaries in orange. Green chlorophyll-rich areas appear as red, and the bright red fringe on the southwest corner of the island was interpreted as green algae on the peat in front of the live marsh, a feature common on similar low intertidal areas today.

Fig. A12 Bailey Flat June 1994 boundaries (red) on source photograph; previous April 1990 boundaries in orange.

Fig. A13 Bailey Flat April 1996 boundaries (red) on source photograph; previous June 1994 boundaries in orange.

Fig. A14 Bailey Flat April 2001 boundaries (red) on source photograph; previous April 1996 boundaries in orange.

Fig. A15 Bailey Flat June 2001 boundaries (red) on source photograph; previous April 2001 boundaries in orange.

Fig. A16 Bailey Flat April 2005 boundaries (red) on source photograph; previous June 2001 boundaries in orange.

Fig. A17 Bailey Flat June 2005 boundaries (red) on source photograph; previous April 2005 boundaries in orange.

Fig. A18 Bailey Flat April 2009 boundaries (red) on source photograph; previous June 2005 boundaries in orange.

Fig. A19 Bailey Flat September 2009 boundaries (red) on source photograph; previous April 2009 boundaries in orange.

Fig. A20 Bailey Flat August 2010 boundaries (red) on source photograph; previous September 2009 boundaries in orange.

Fig. A21 Bailey Flat September 2012 boundaries (red) on source photograph; previous August 2010 boundaries in orange.

Fig. A22 Bailey Flat June 2013 boundaries (red) on source photograph; previous September 2012 boundaries in orange.

Fig. A23 Bailey Flat April 2014 boundaries (red) on source photograph; previous June 2013 boundaries in orange.

Fig. A24 Bailey Flat September 2014 boundaries (red) on source photograph; previous April 2014 boundaries in orange.

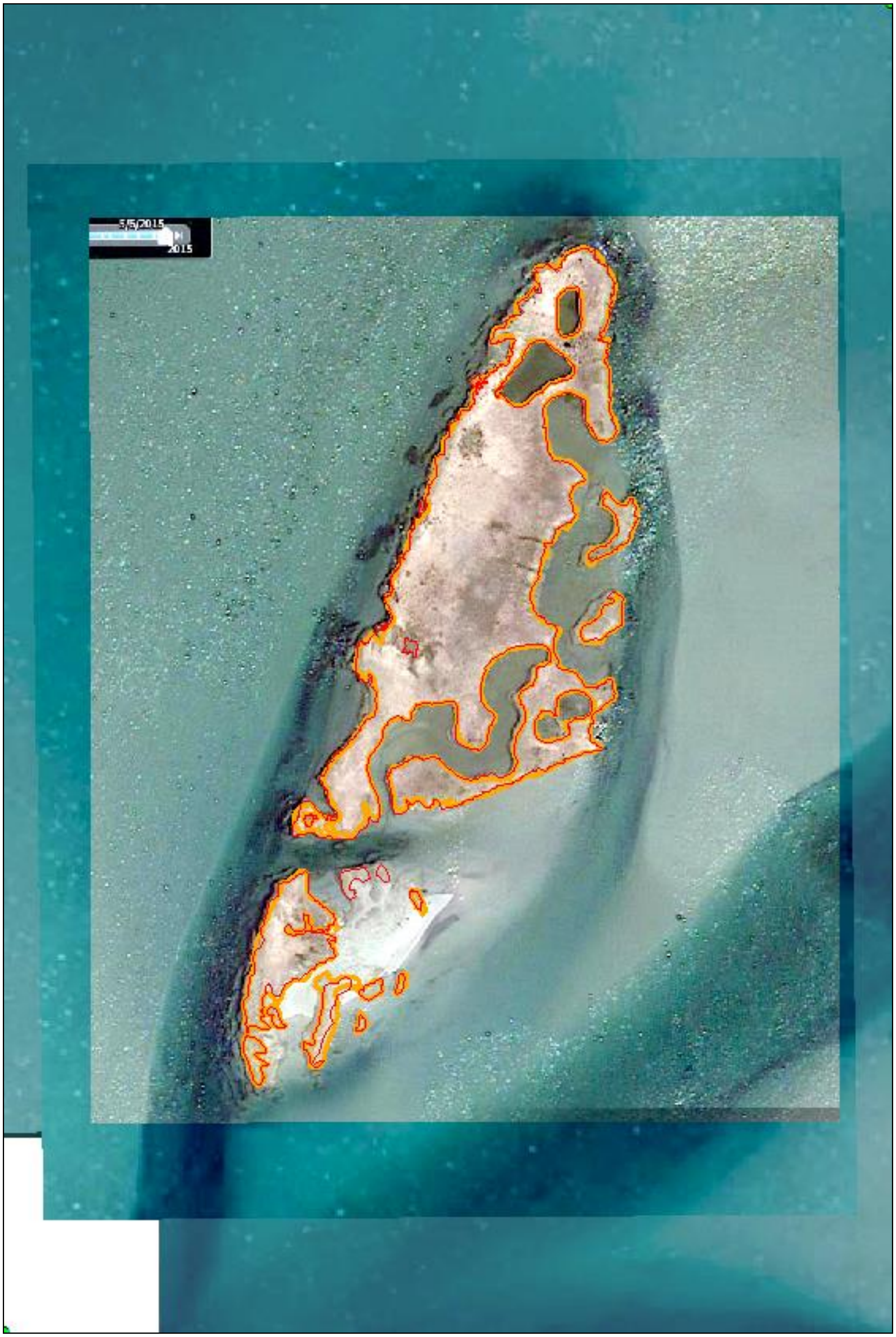

Fig. A25 Bailey Flat May 2015 boundaries (red) on source photograph; previous September 2014 boundaries in orange. Note the presumed apparent recovery of some small marsh areas on the sand overwashed area of the south island.

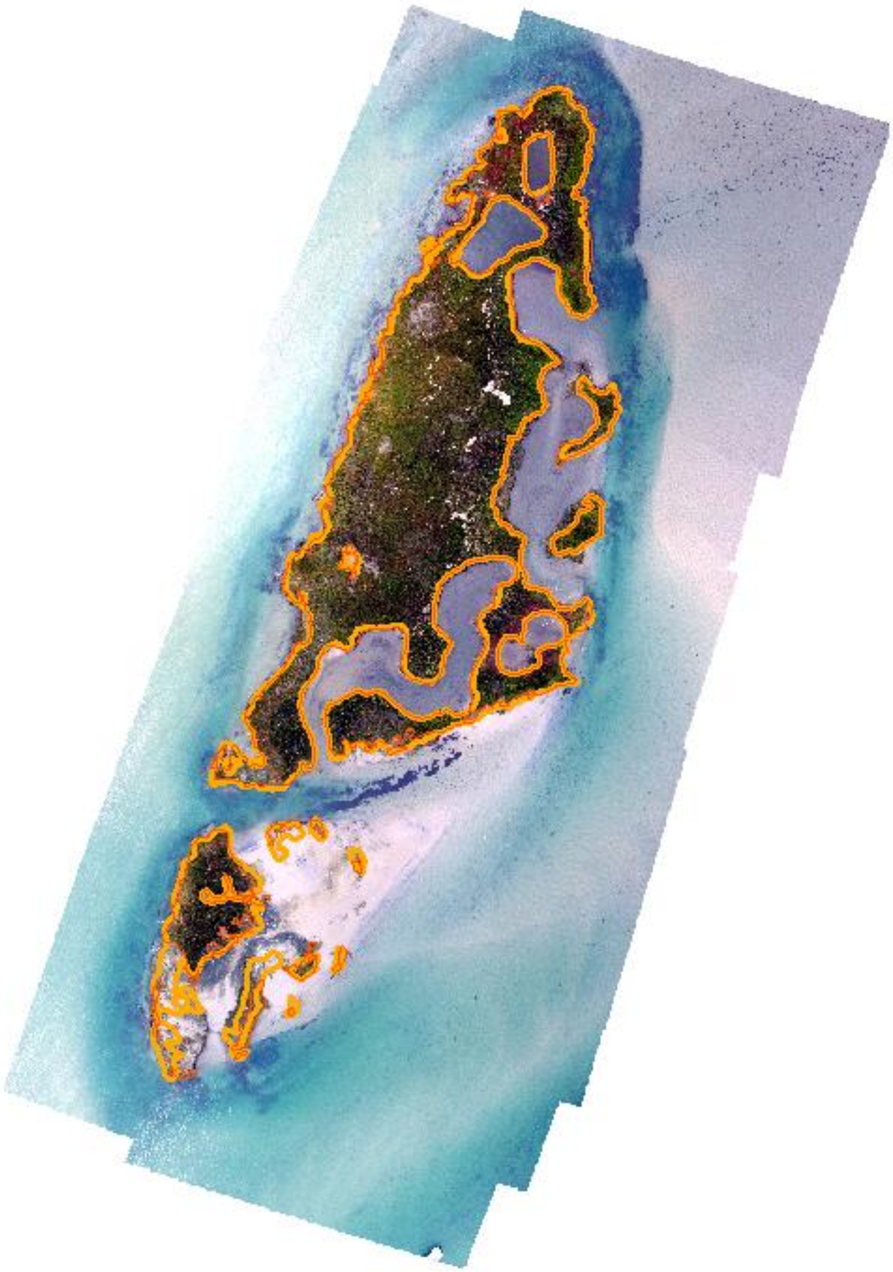

Fig. A26 Bailey Flat October 2016 boundaries (red) on source photograph; previous May 2015 boundaries in orange. Note the apparent large scale loss on the south island.

Whites Flat

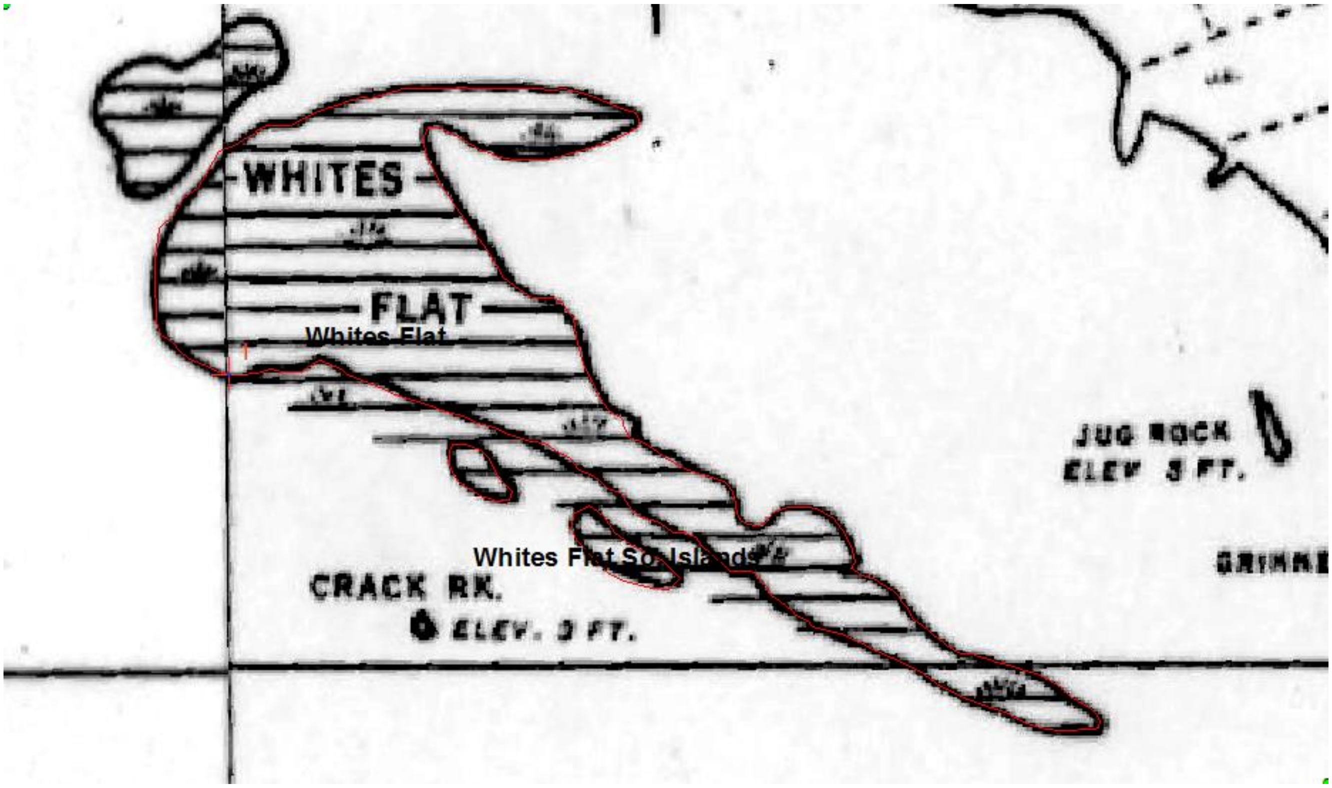

Fig. A27 Whites Flat 1936 Nautical T-sheet boundaries based on interpretation of November 1934 aerial photograph. Barrier flats on south side were missing in post 1934 photographs, and were not included in base area calculations

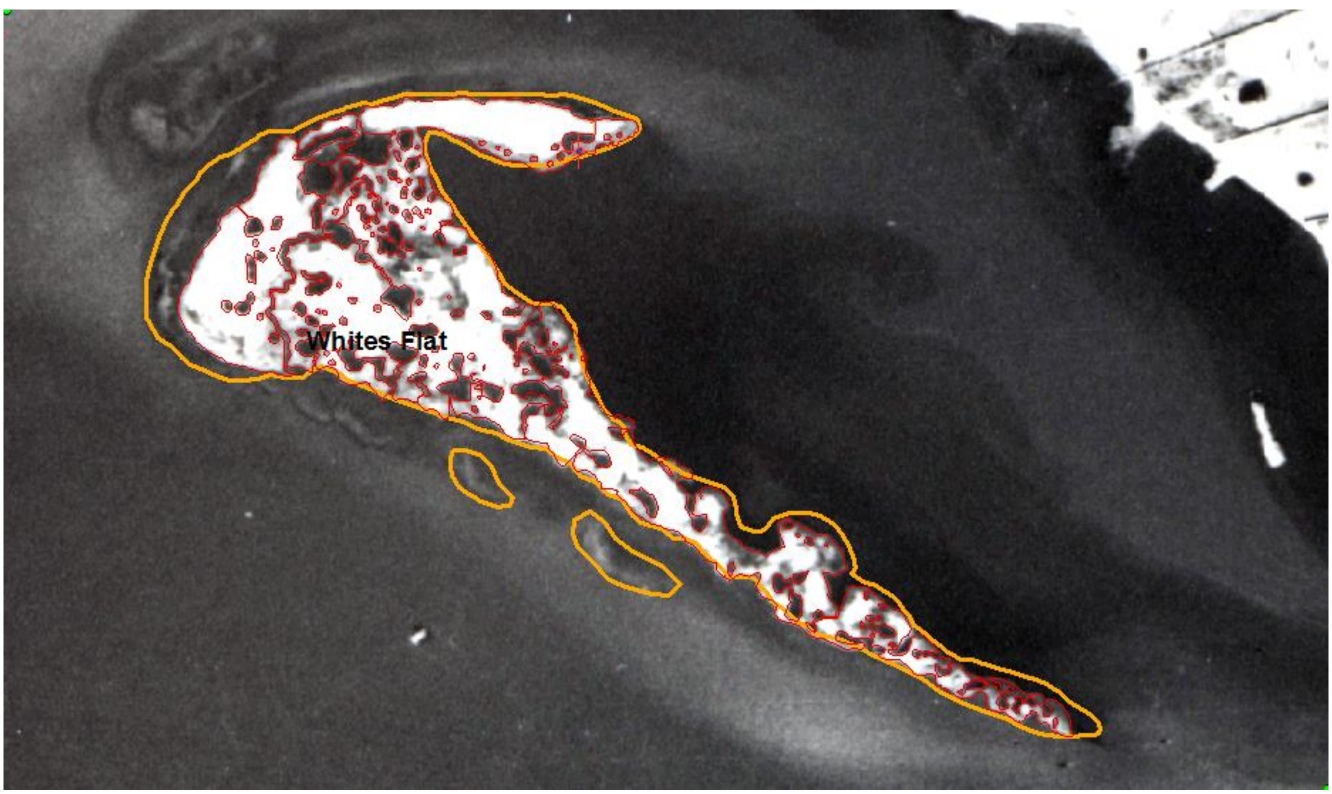

Fig. A28 Whites Flat with December 1938 boundaries (red) on source photograph, with previous T-sheet boundaries.

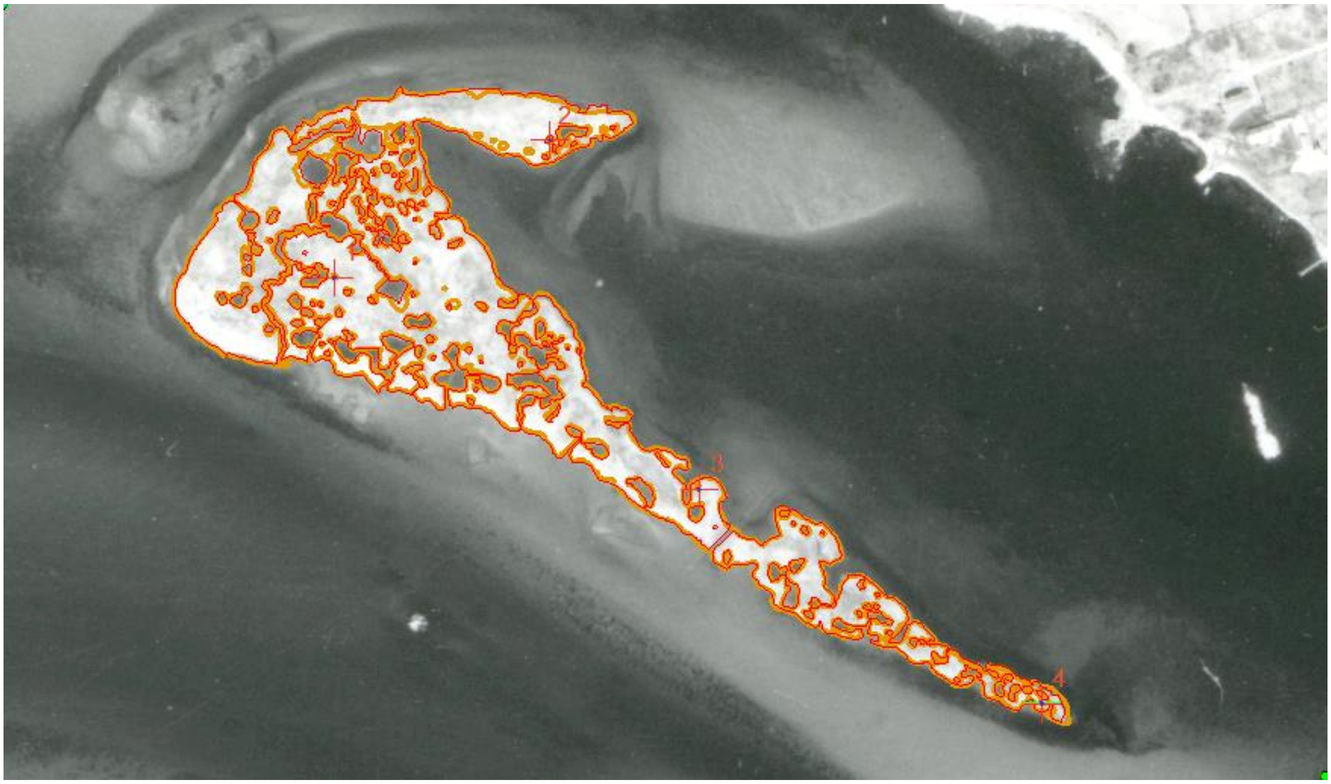

Fig. A29 Whites Flat with April 1954 boundaries (red) on source photograph; previous December 1938 boundaries (orange).

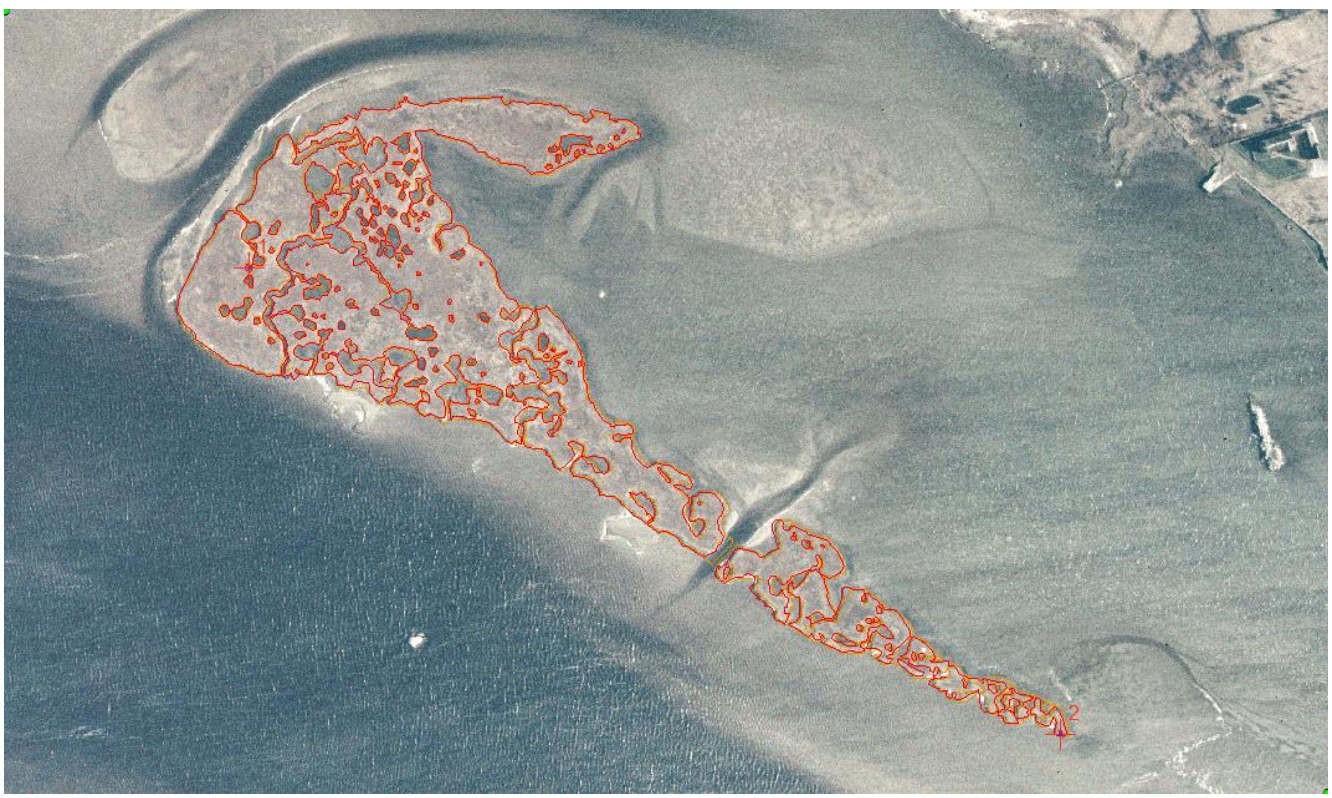

Fig. A30 Whites Flat with April 1962 boundaries (red) on source photograph with previous April 1954 boundaries (orange).

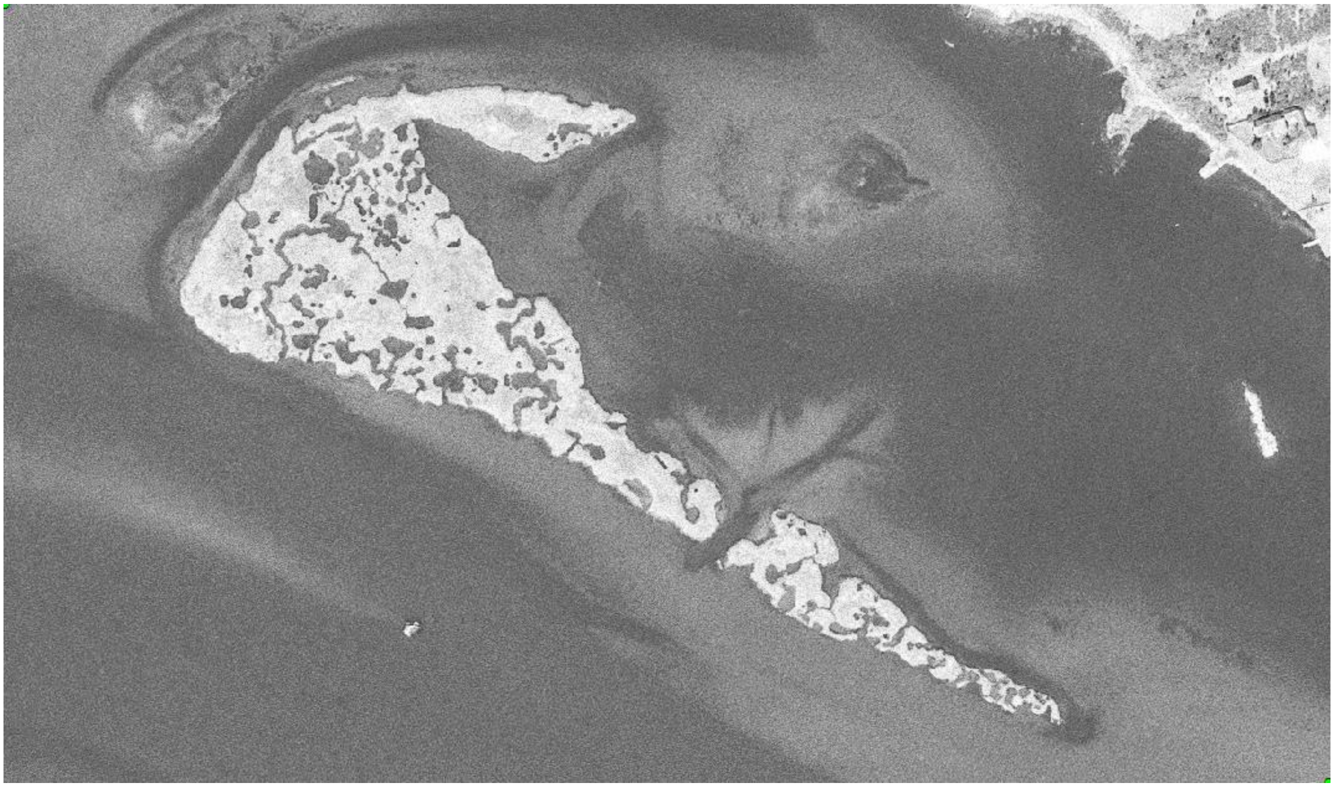

Fig. A31 April 1974 aerial image of Whites Flat (not interpreted).

Fig. A32 June 1982 aerial image of Whites Flat (not interpreted).

Fig. A33 March 1996 aerial image of Whites Flat (not interpreted; note that image was taken taken at low tide).

Fig. A34 Whites Flat with April 2001 boundaries (red) on source photograph, with previous April 1962 boundaries (orange).

Fig. A35 Whites Flat with April 2005 boundaries (red) on source photograph, with previous April 2001 boundaries (orange).

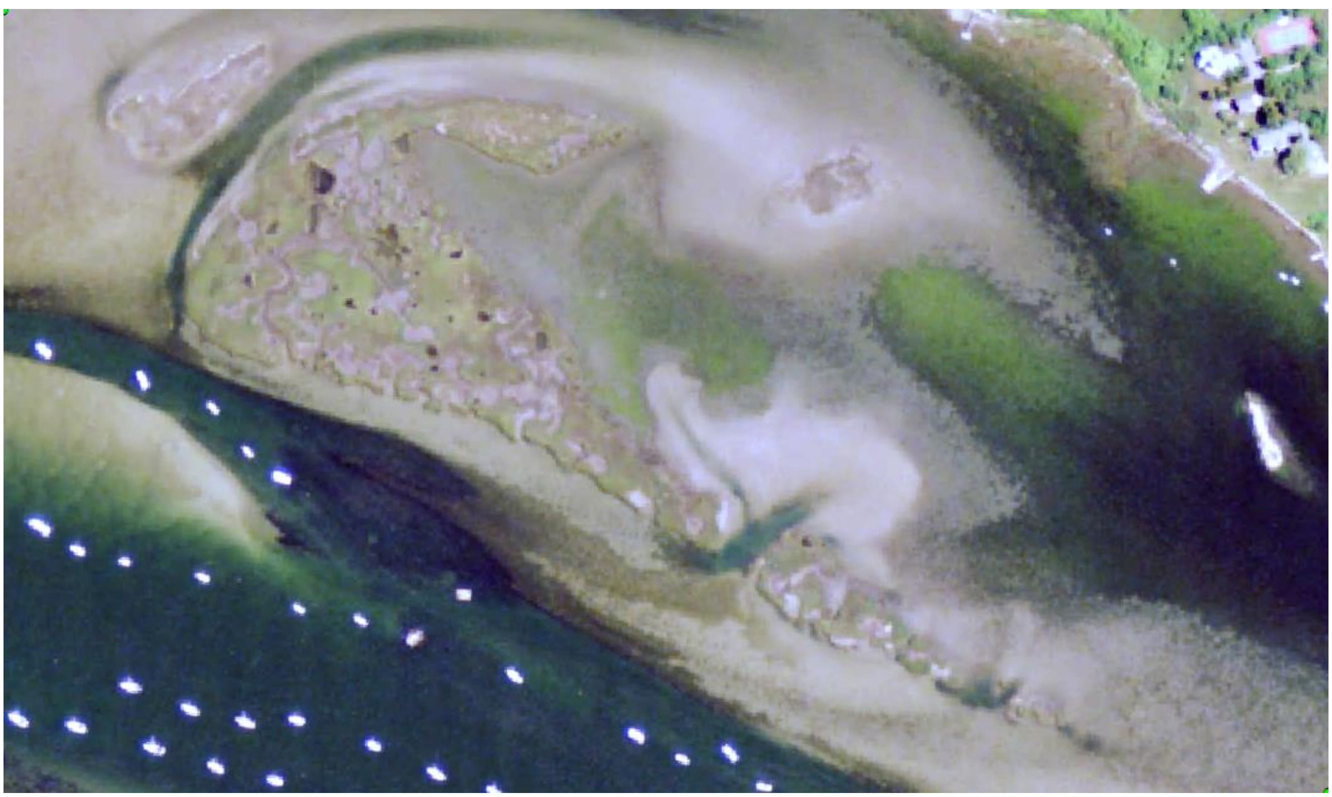

Fig. A36 September 2008 aerial image of Whites Flat (not interpreted).

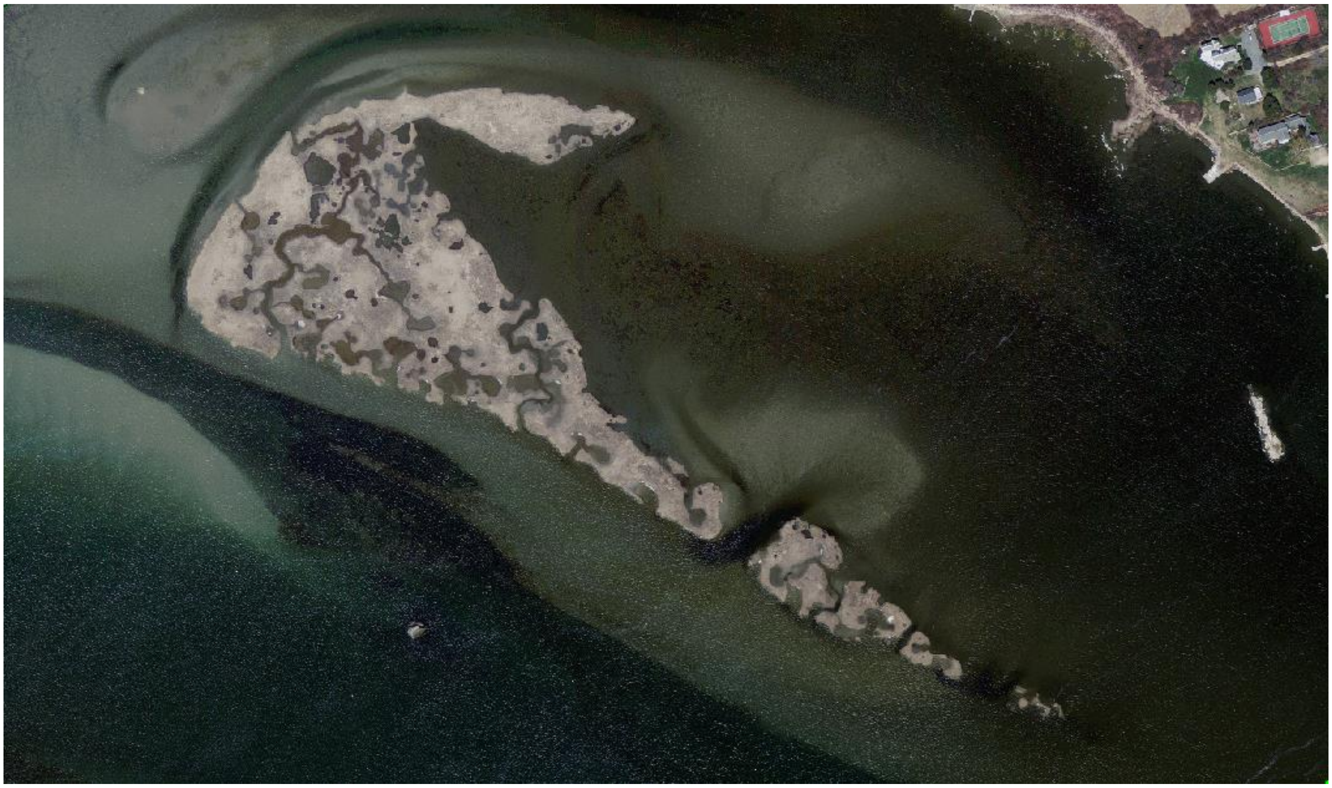

Fig. A37 April 2009 aerial image of Whites Flat (not interpreted).

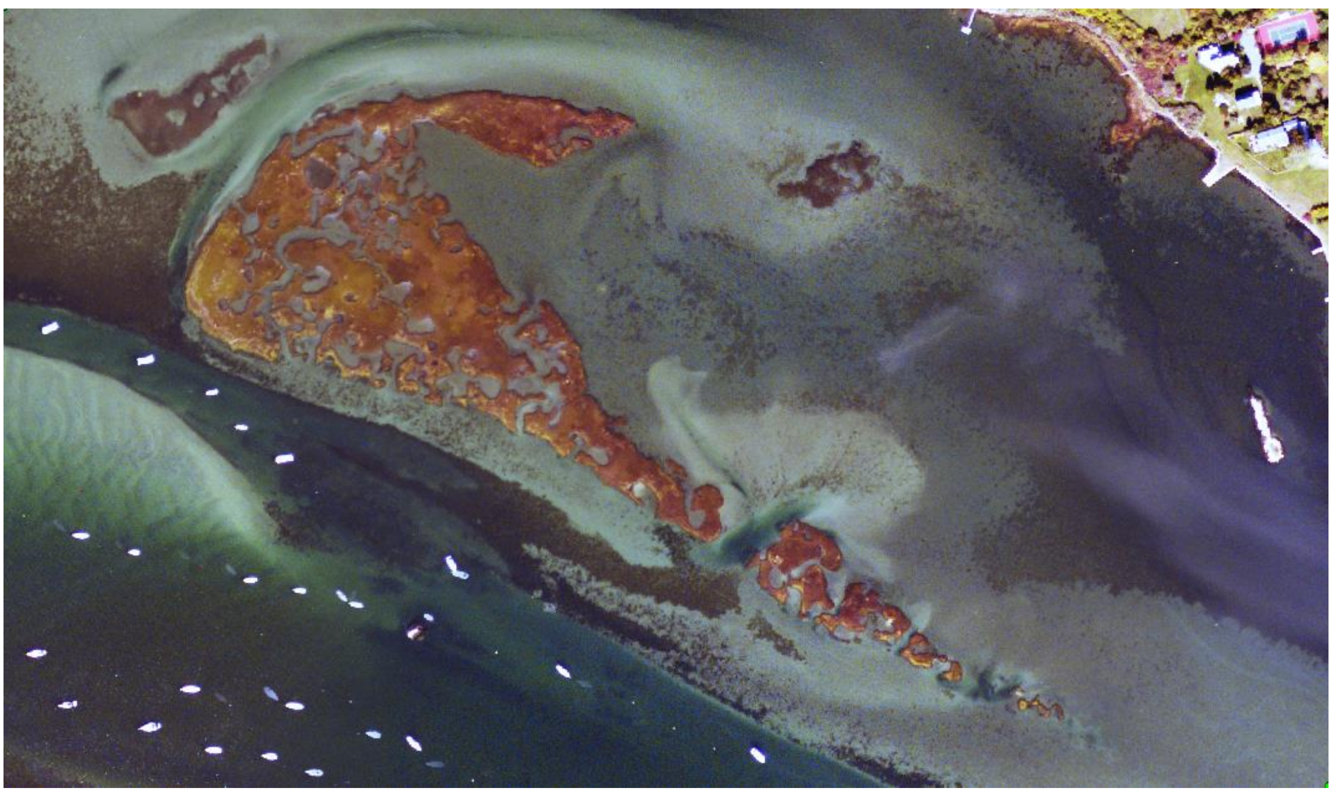

Fig. A38 September 2009 aerial image of Whites Flat (not interpreted).

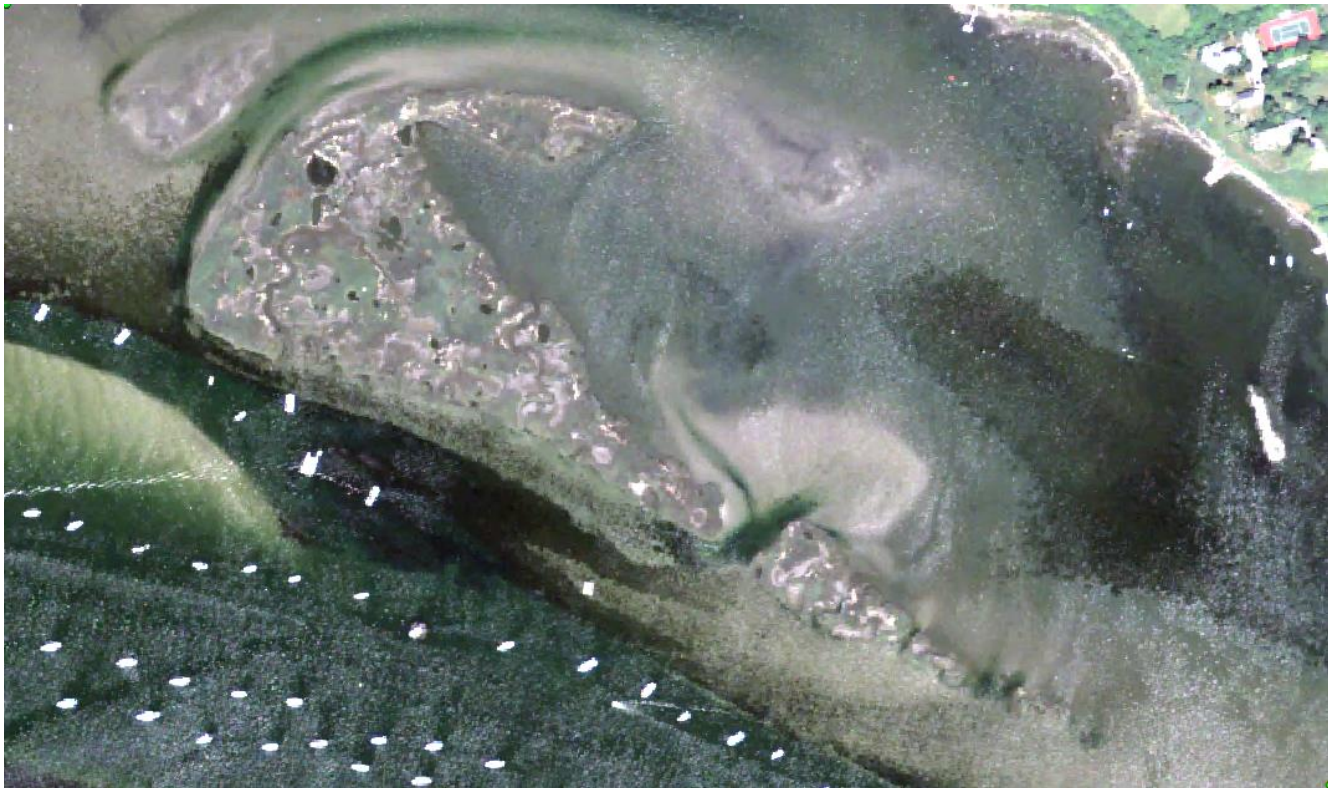

Fig. A39 August 2010 aerial image of Whites Flat (not interpreted).

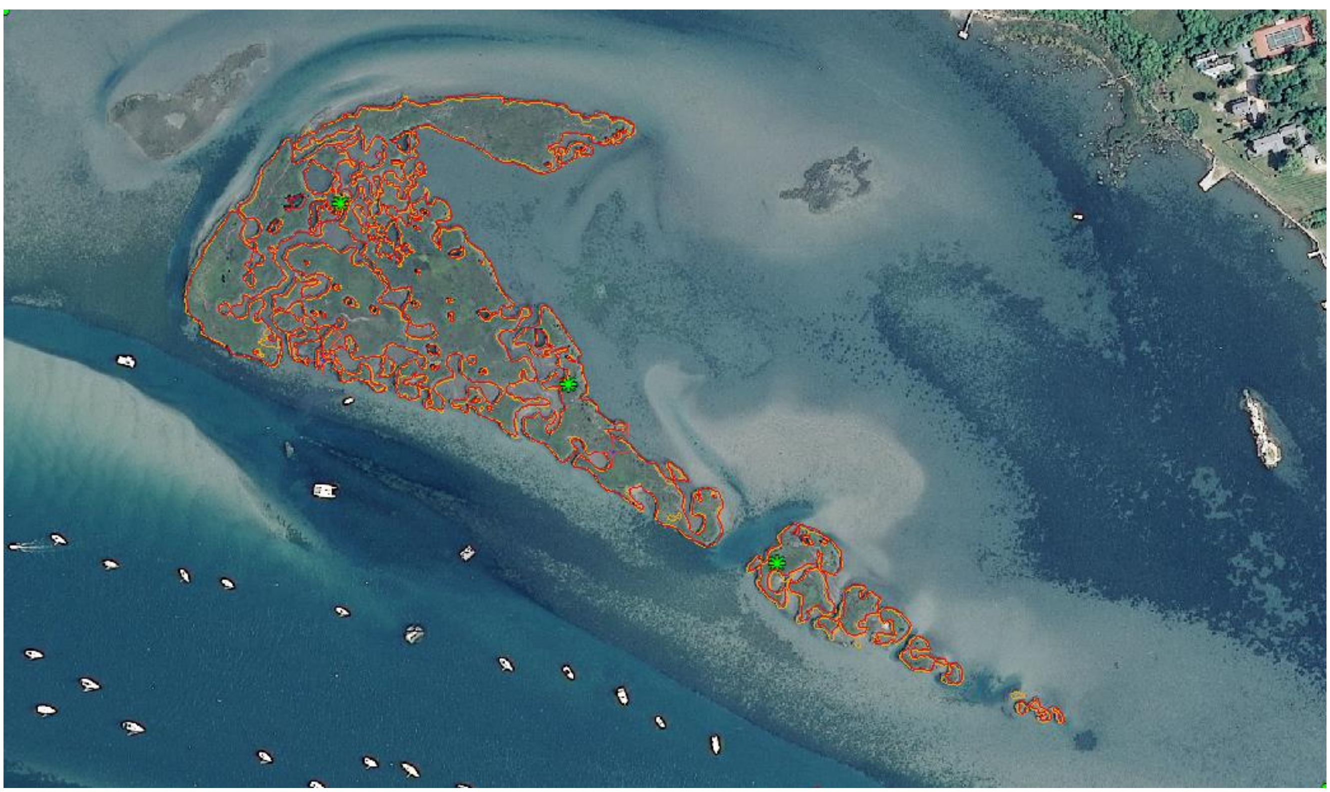

Fig. A40 Whites Flat with June 2012 boundaries (red) on source photograph, with previous April 2005 boundaries (orange).

Fig. A41 Whites Flat with September 2013 boundaries (red) on source photograph, with previous June 2012 boundaries (orange).

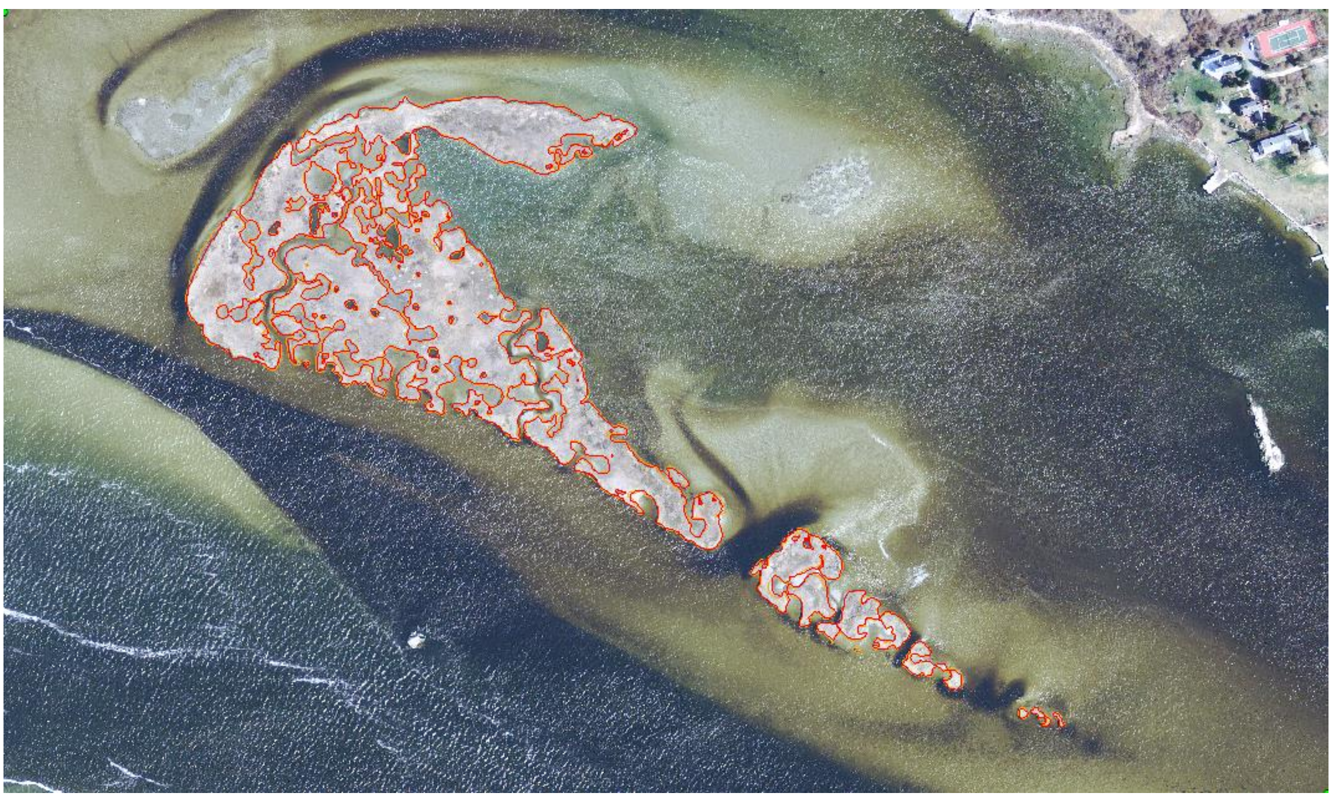

Fig. A42 Whites Flat with April 2014 boundaries (red) on source photograph with previous September 2013 boundaries.

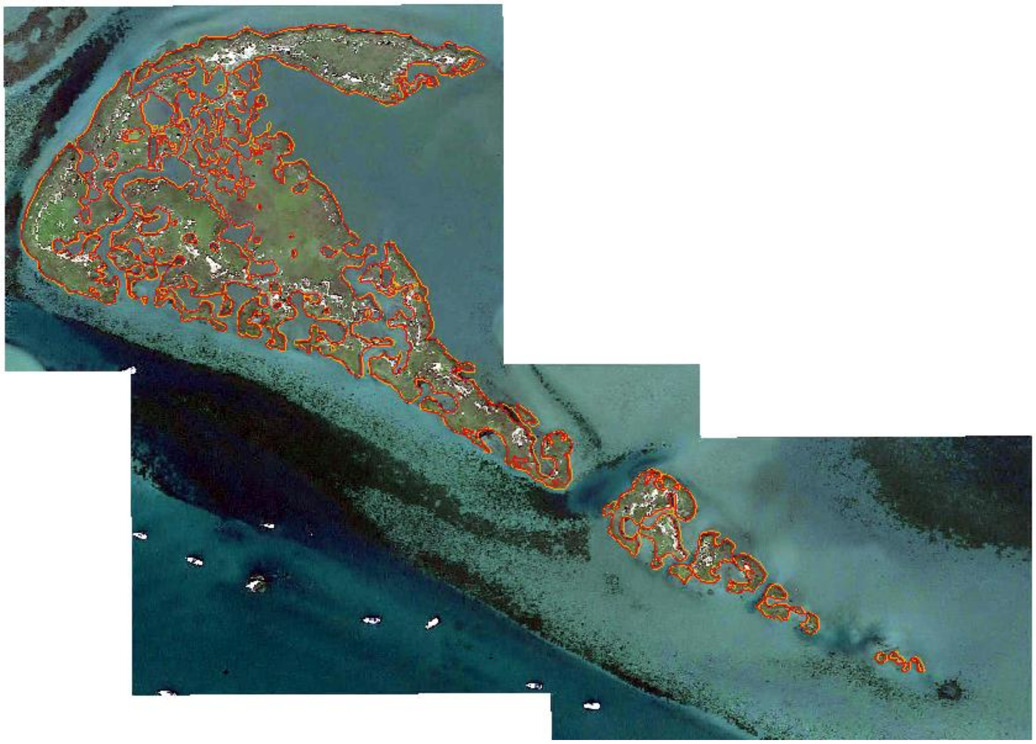

Fig. A43 Whites Flat with May 2015 boundaries (red) on source photograph (Google Earth), with previous April 2014 boundaries (orange).

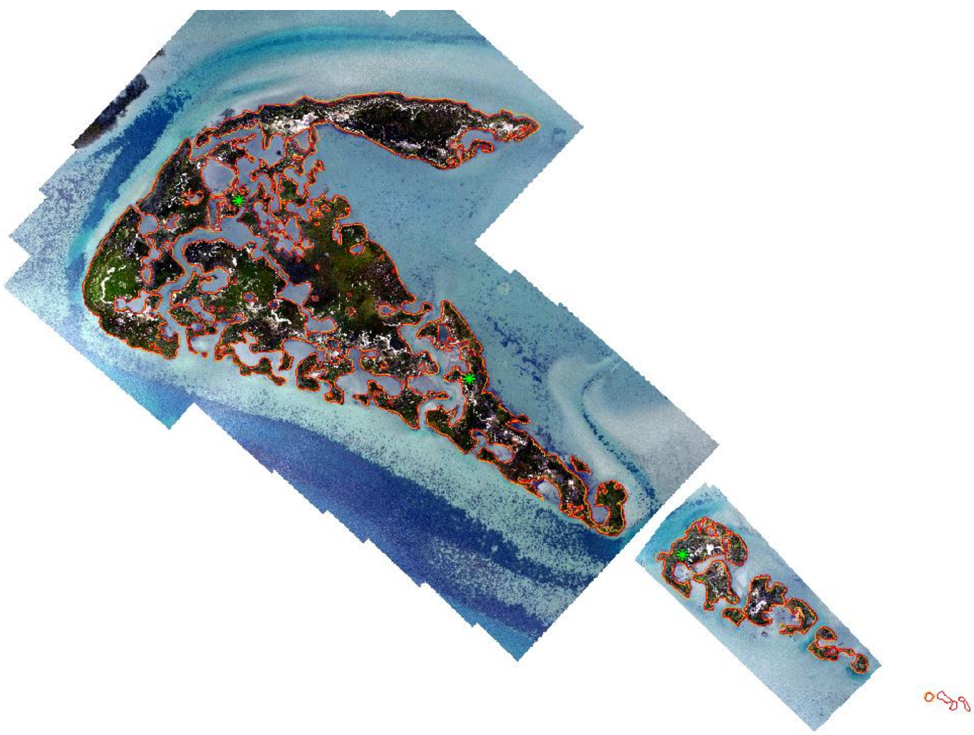

Fig. A44 Whites Flat with October 2016 boundaries (red) on source photograph with previous May 2015 boundaries.

Great Flat 1

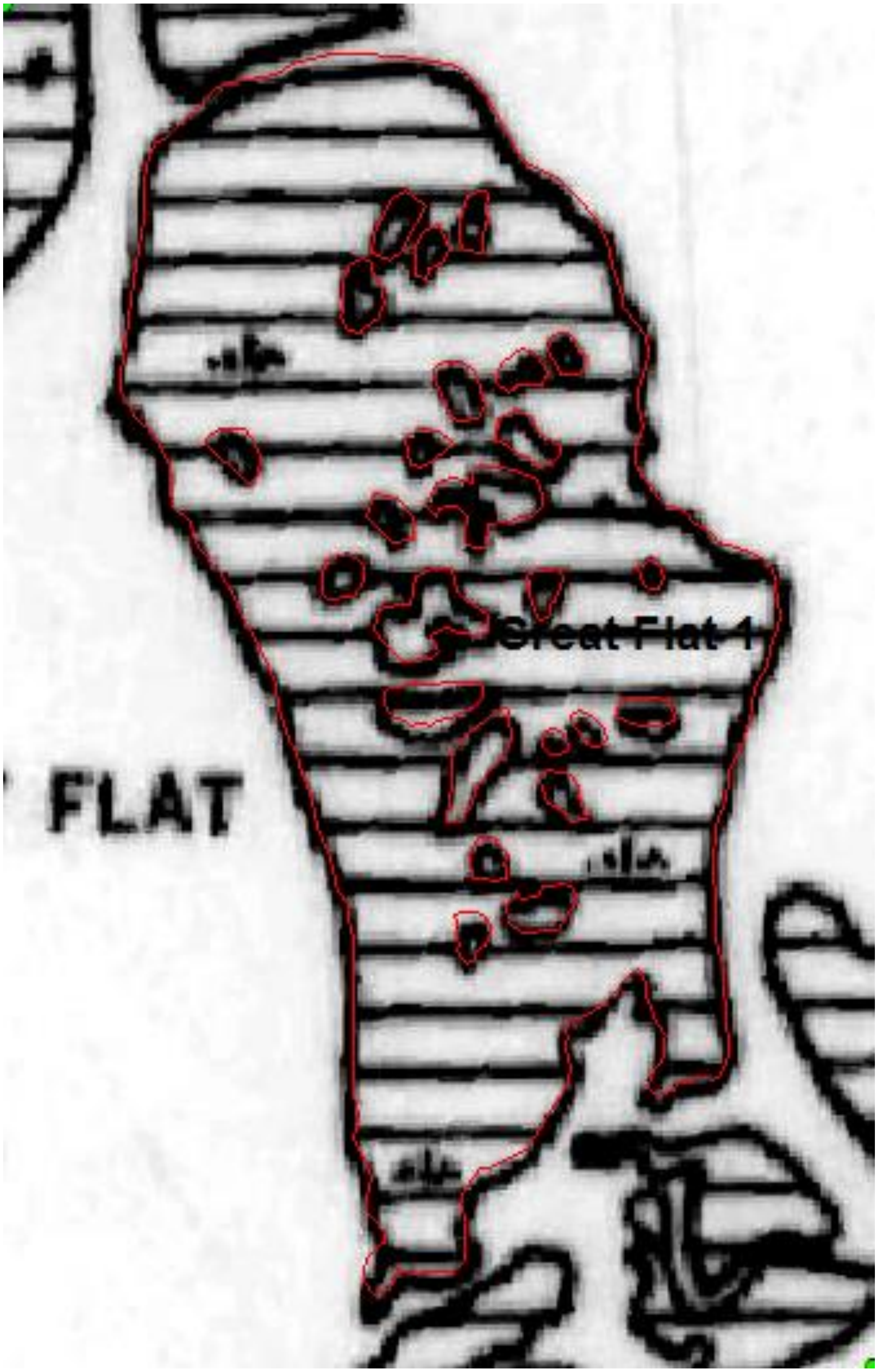

Fig. A45 Great Flat 1 on a 1936 Nautical T-sheet with boundaries based on interpretation of November 1934 aerial photograph.

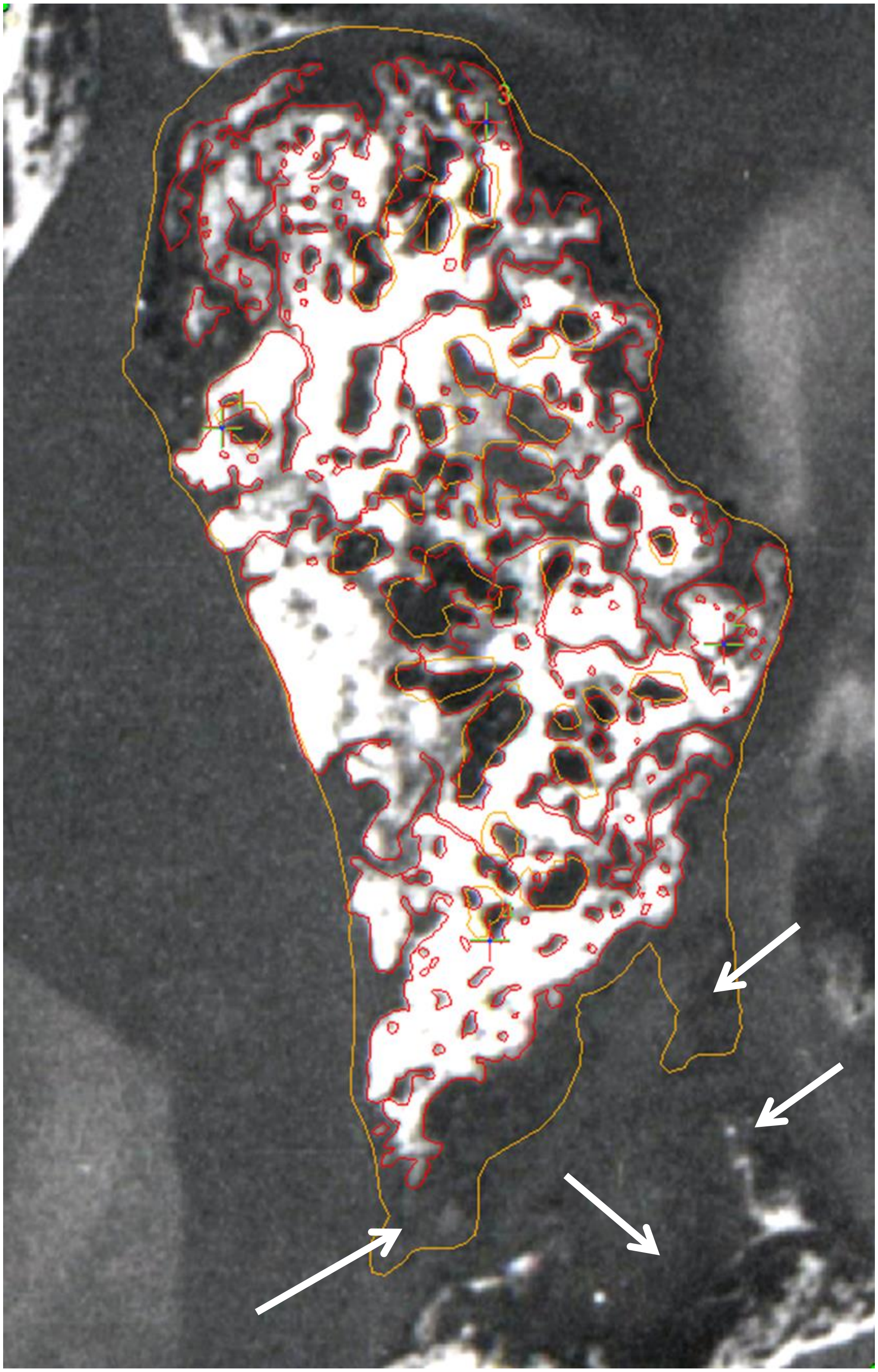

Fig. A46 Great Flat 1 with December 1938 boundaries (red) on source photograph, and nautical chart T-sheet boundaries (orange) based on November 1934 aerial photograph. Arrows indicate apparent major loss from Hurricane of 38.

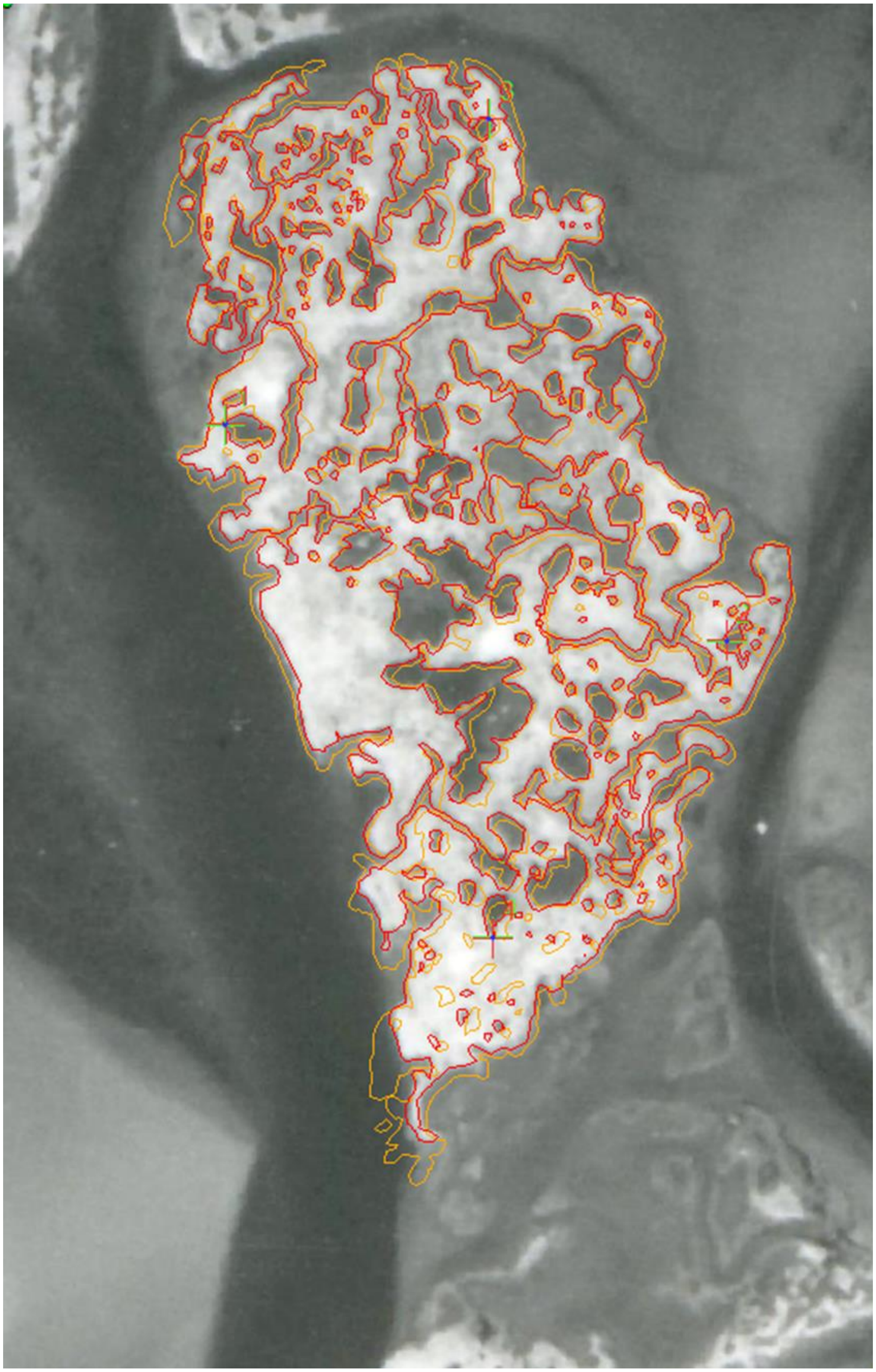

Fig. A47 Great Flat 1 with April 1954 boundaries (red) on source photograph with previous December 1938 boundaries (orange).

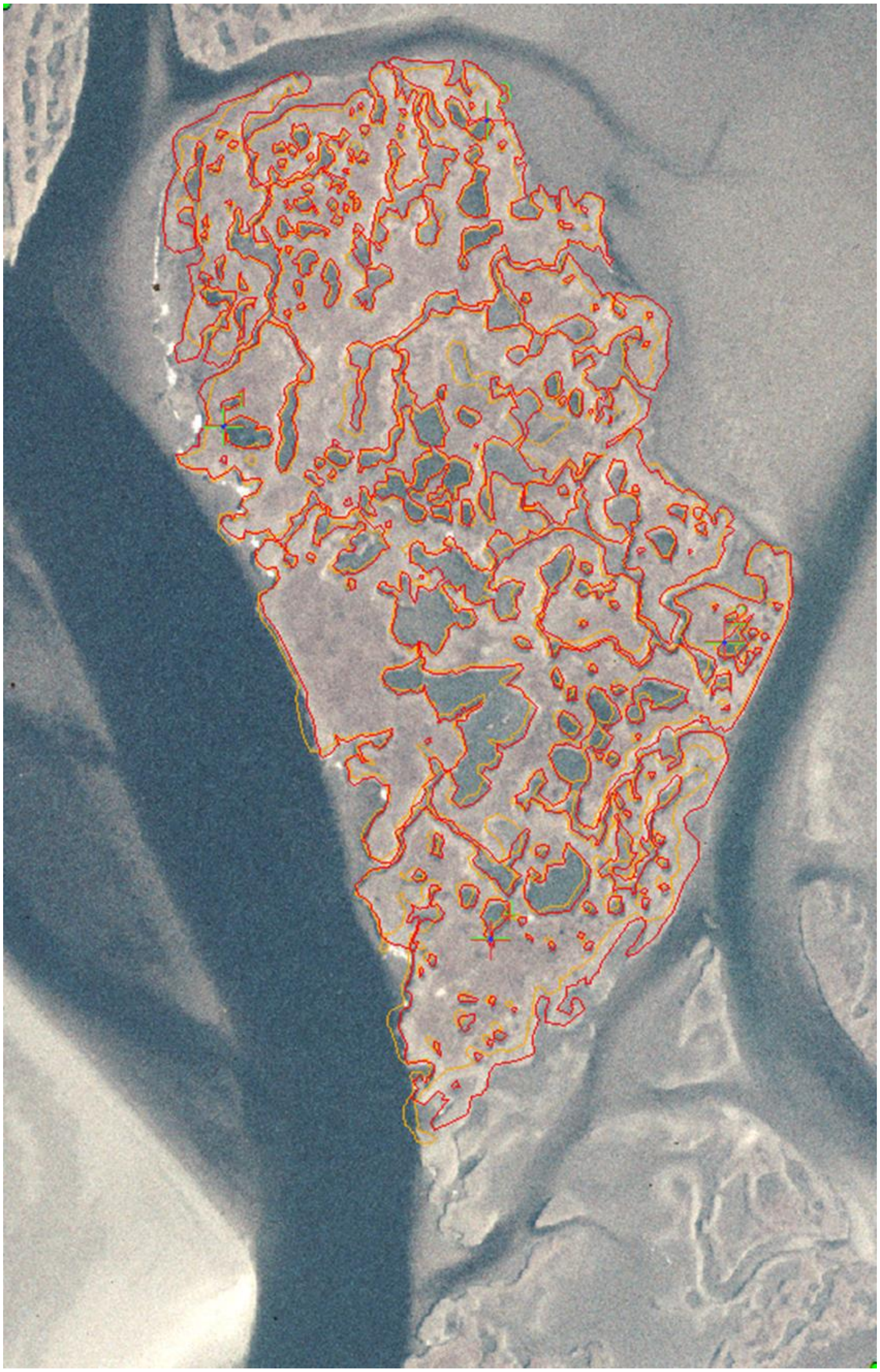

Fig. A48 Great Flat 1 with April 1962 boundaries (red) on source photograph with previous April 1954 boundaries (orange).

Fig. A49 Great Flat 1 with April 2001 boundaries (red) on source photograph with previous April 1962 boundaries (orange).

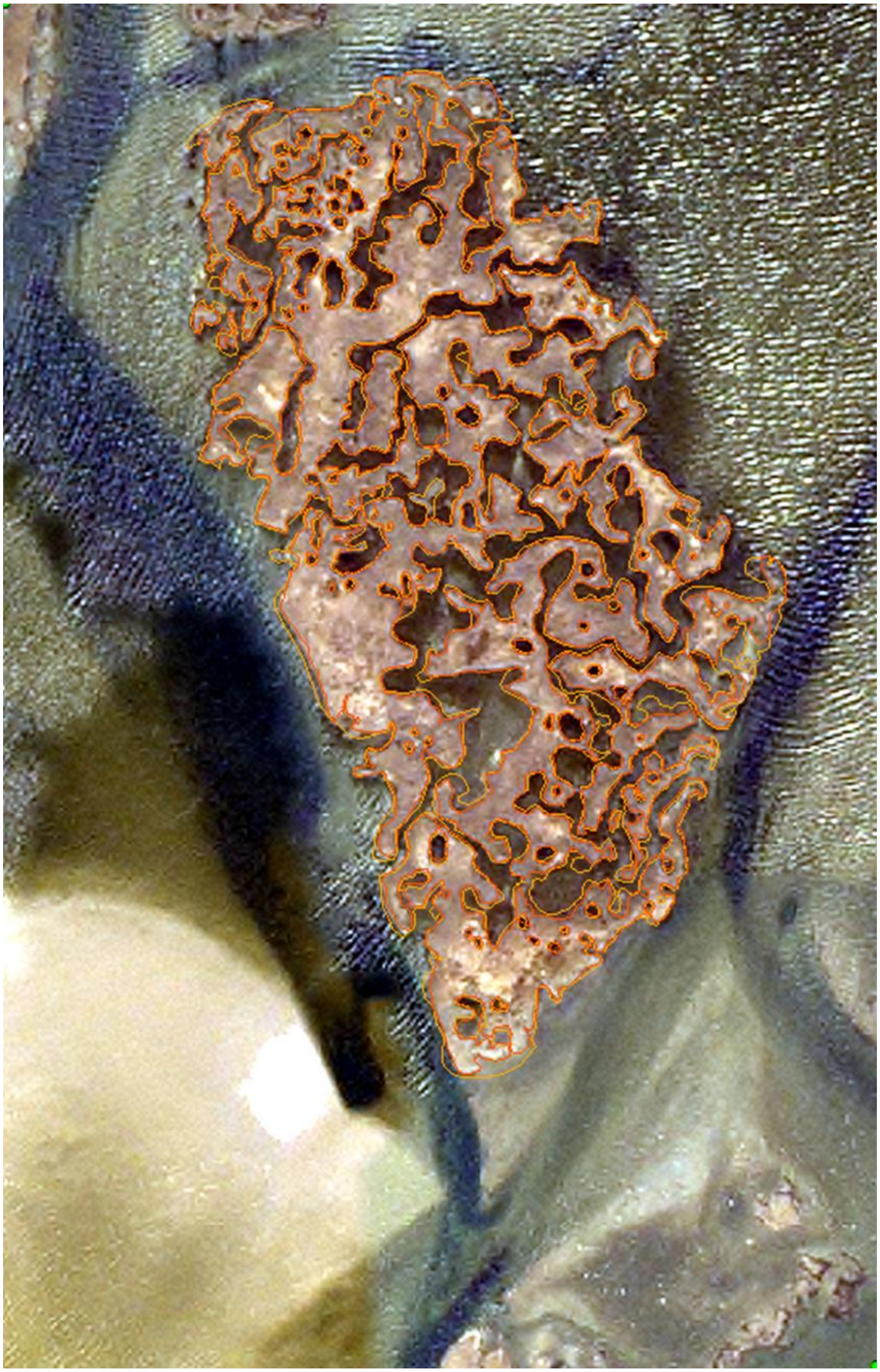

Fig. A50 Great Flat 1 with April 2005 boundaries (red) on source photograph with previous April 2001 boundaries (orange).

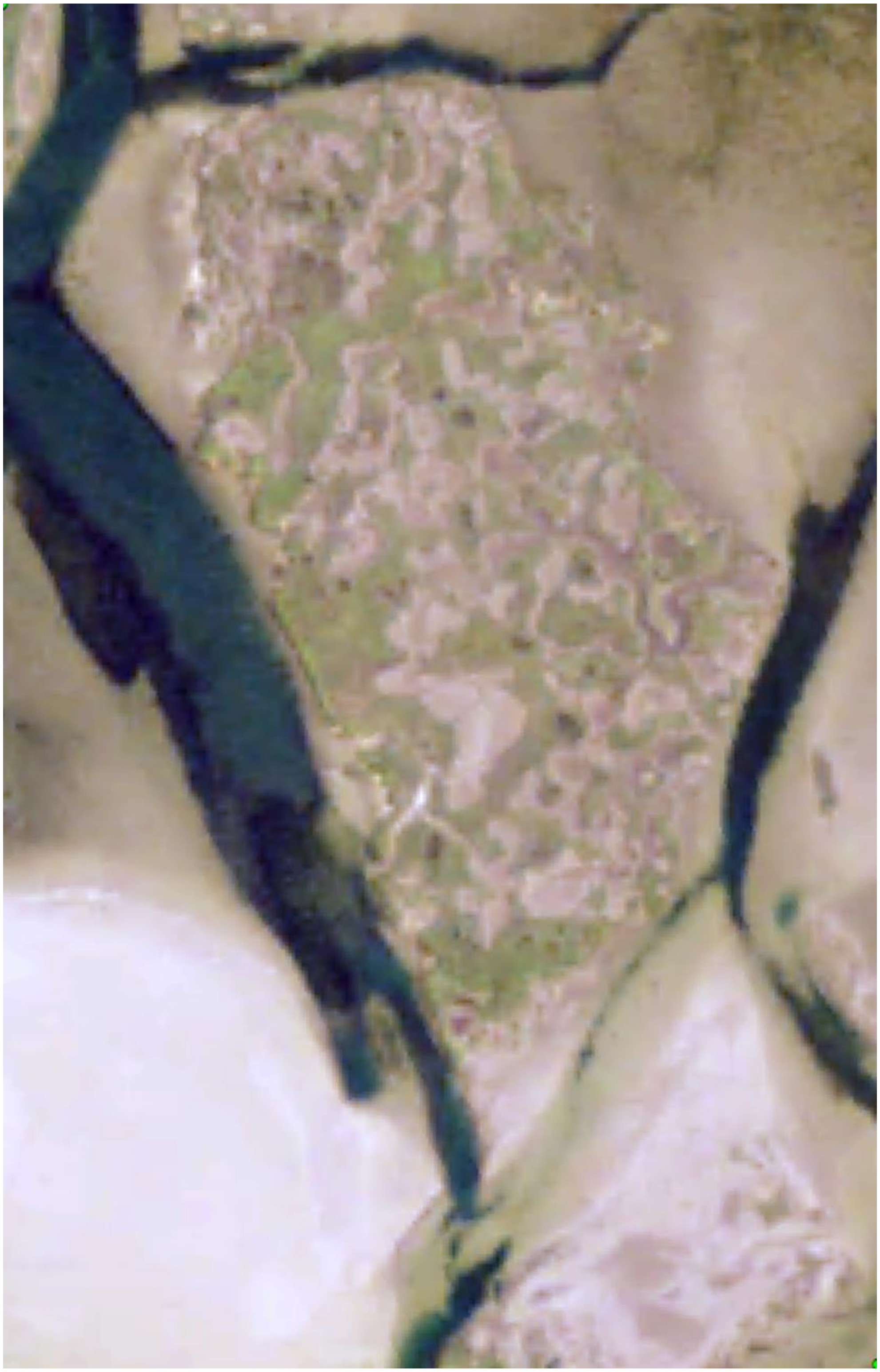

Fig. A51 September 2008 image of Great Flat 1 (not interpreted).

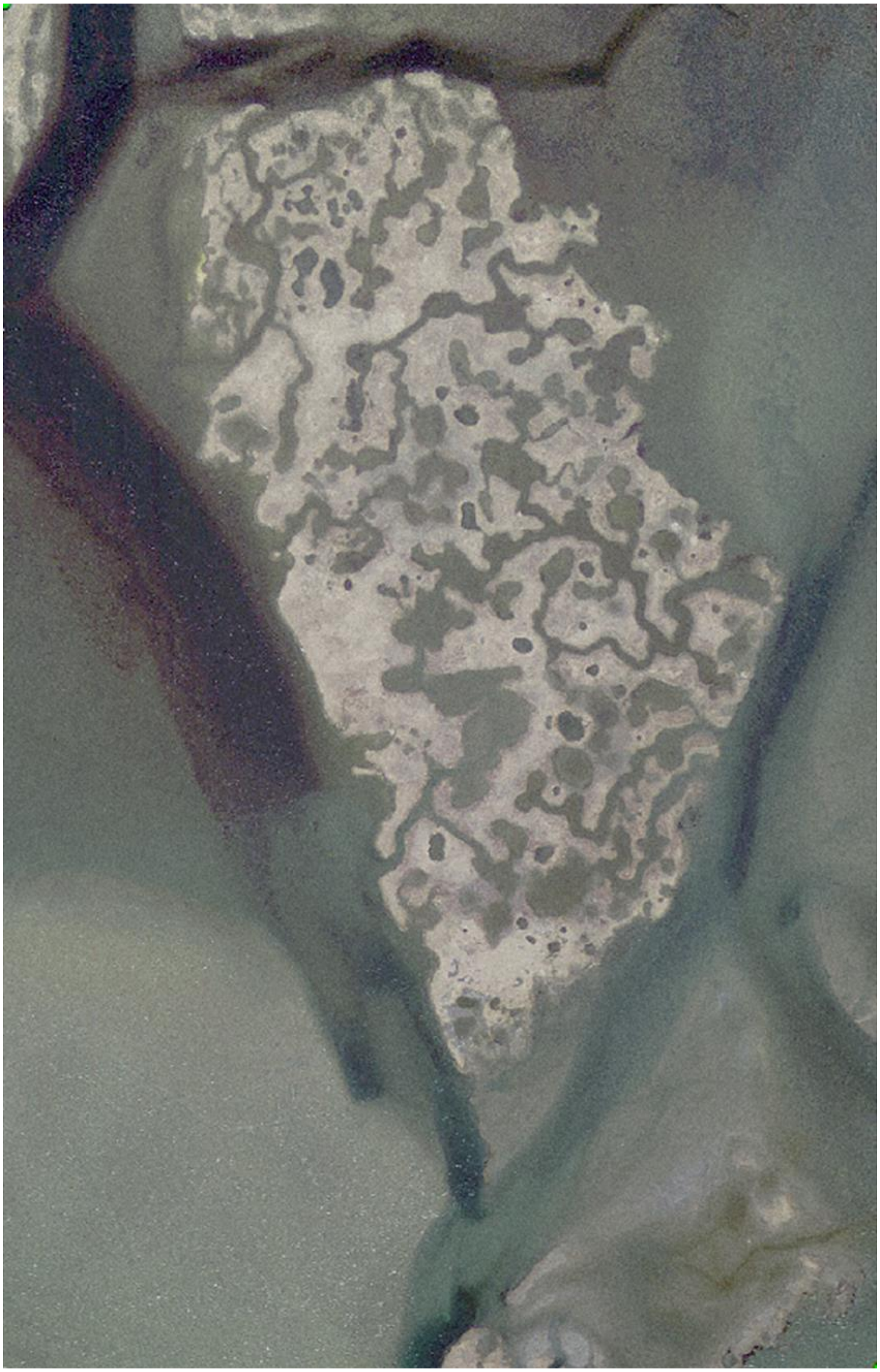

Fig. A52 April 2009 image of Great Flat 1 (not interpreted).

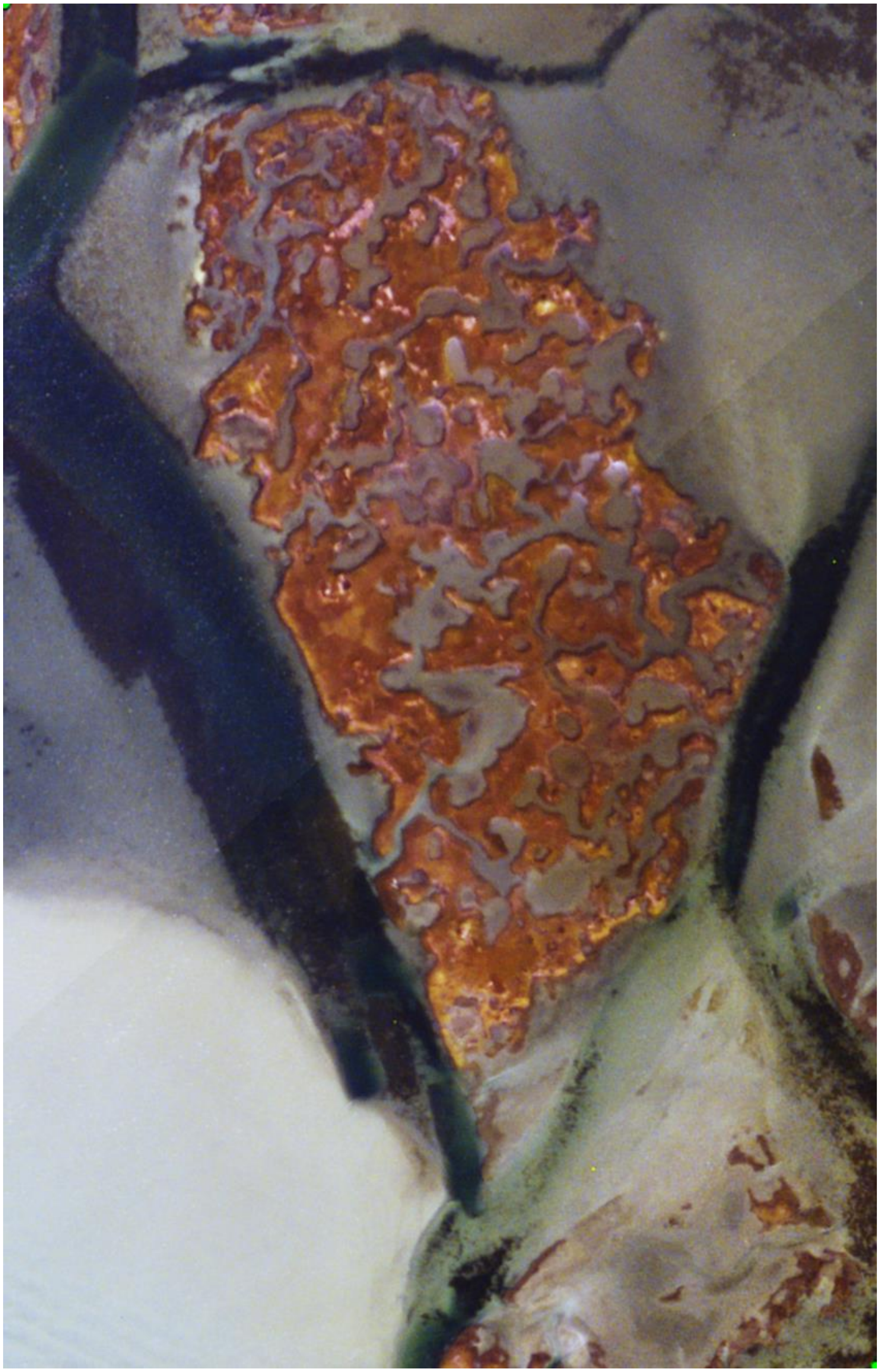

Fig. A53 September 2009 image of Great Flat 1 (not interpreted).

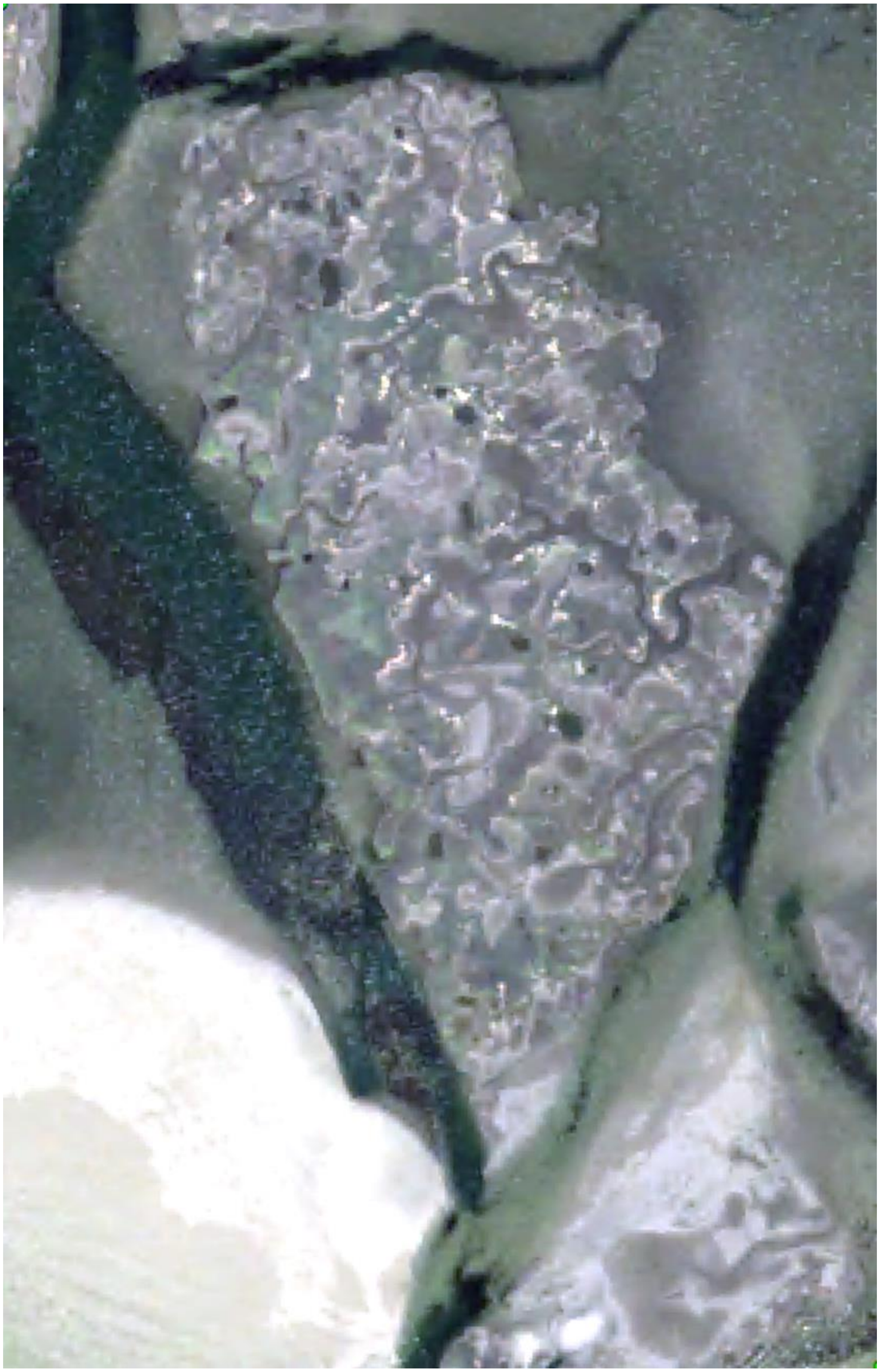

Fig. A54 August 2010 image of Great Flat 1 (not interpreted).

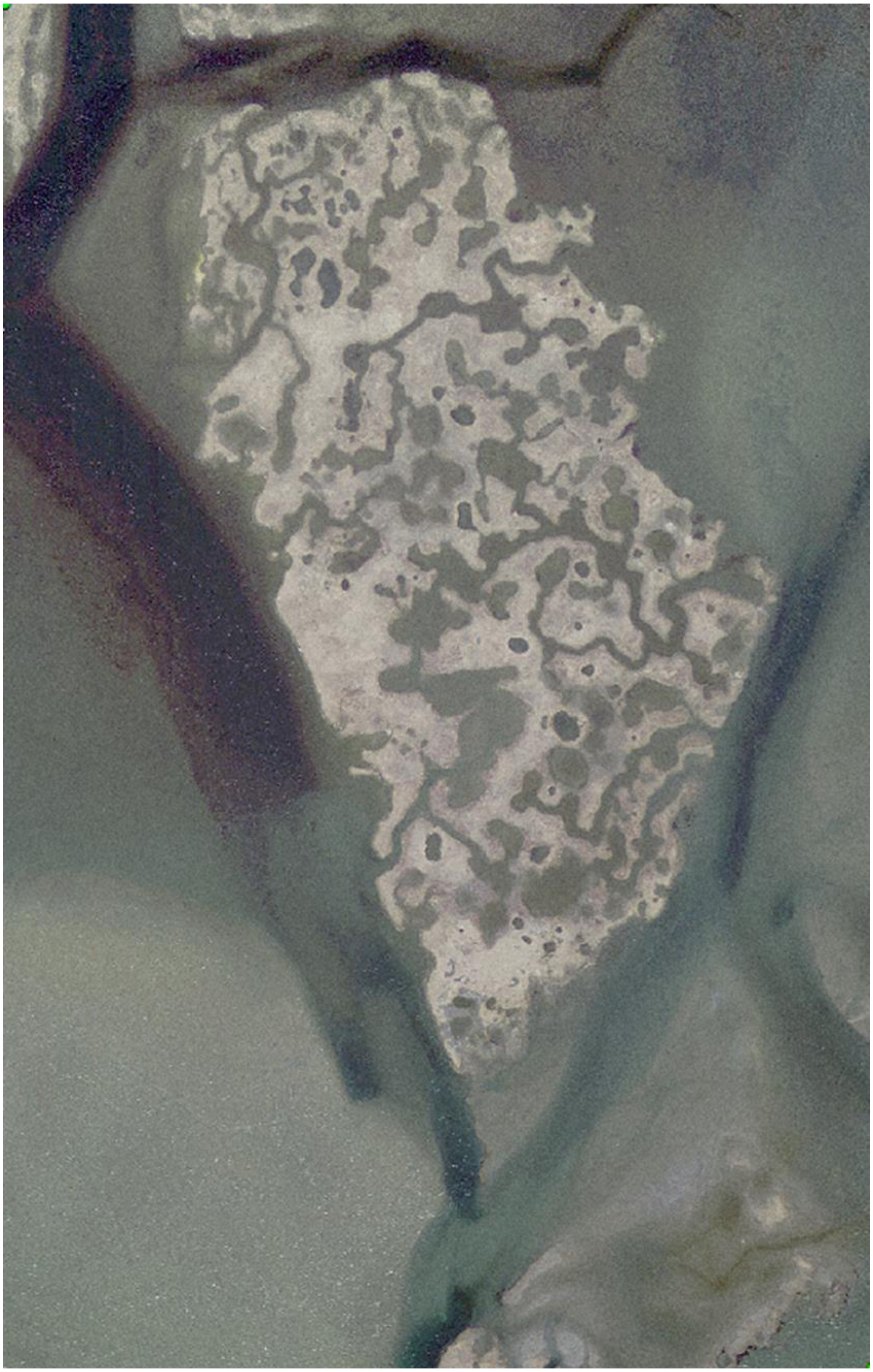

Fig. A55 April 2009 image of Great Flat 1 (not interpreted).

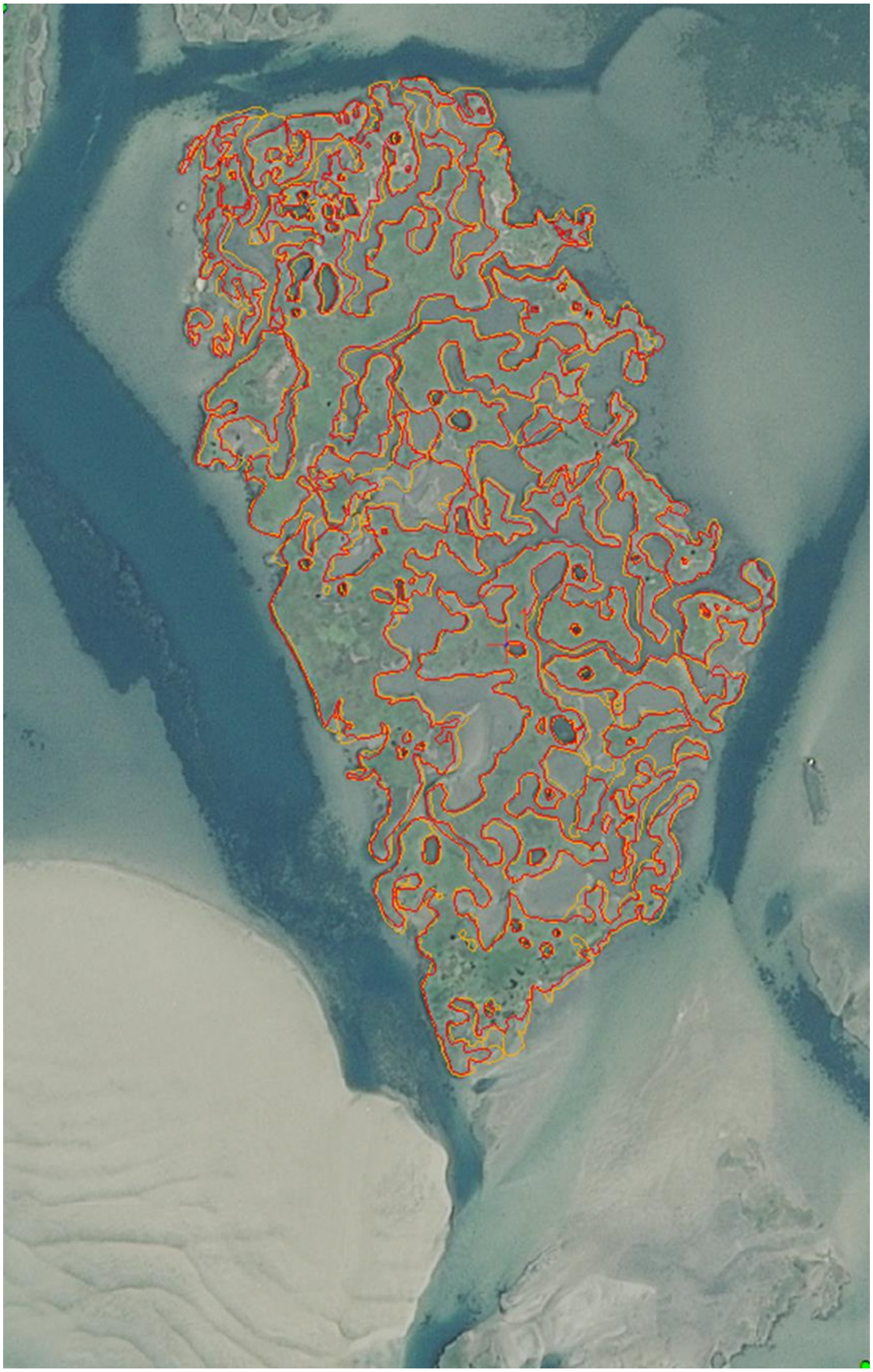

Fig. A56 Great Flat 1 with June 2012 boundaries (red) on source photograph with previous April 2005 boundaries (orange).

Fig. A57 Great Flat 1 with June 2013 boundaries (red) on source photograph with previous June 2012 boundaries (orange).

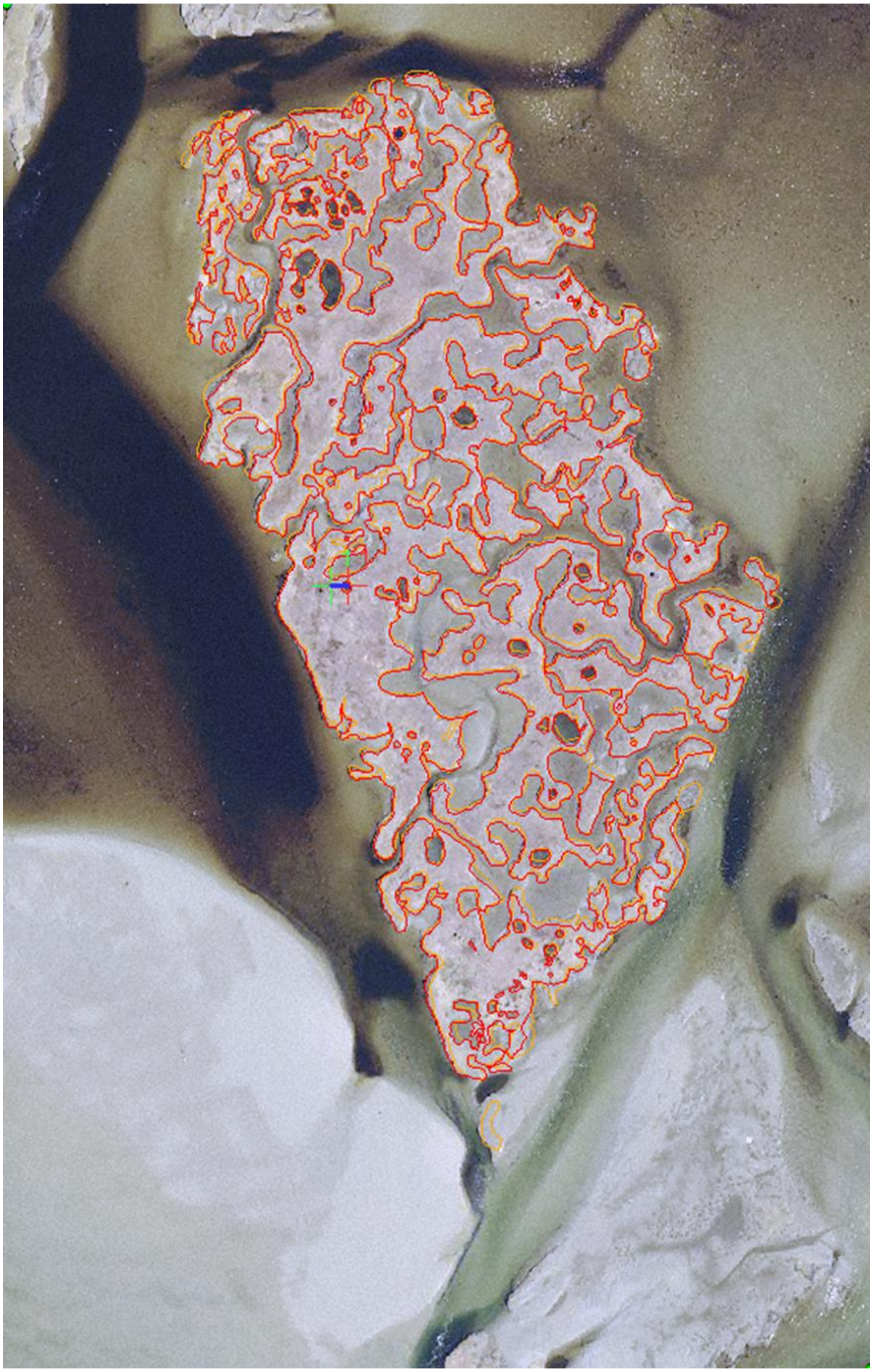

Fig. A58 Great Flat 1 with April 2014 boundaries (red) on source photograph with previous June 2013 boundaries (orange).

Fig. A59 Great Flat 1 with May 2015 boundaries (red) on source photograph with previous April 2014 boundaries (orange).

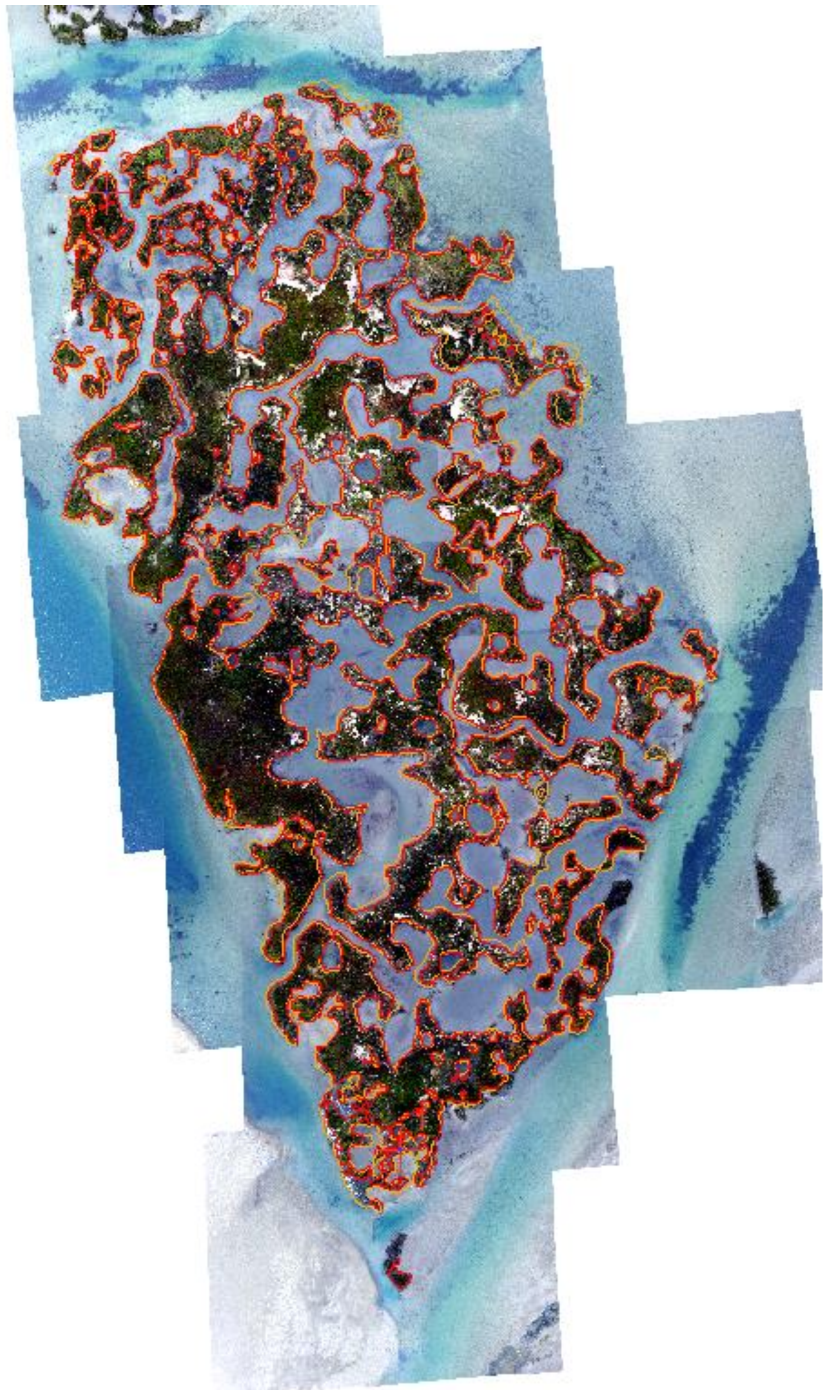

Fig. A60 Great Flat 1 with October 2016 boundaries (red) on source photograph with previous May 2015 boundaries (orange).

Sanford Flat

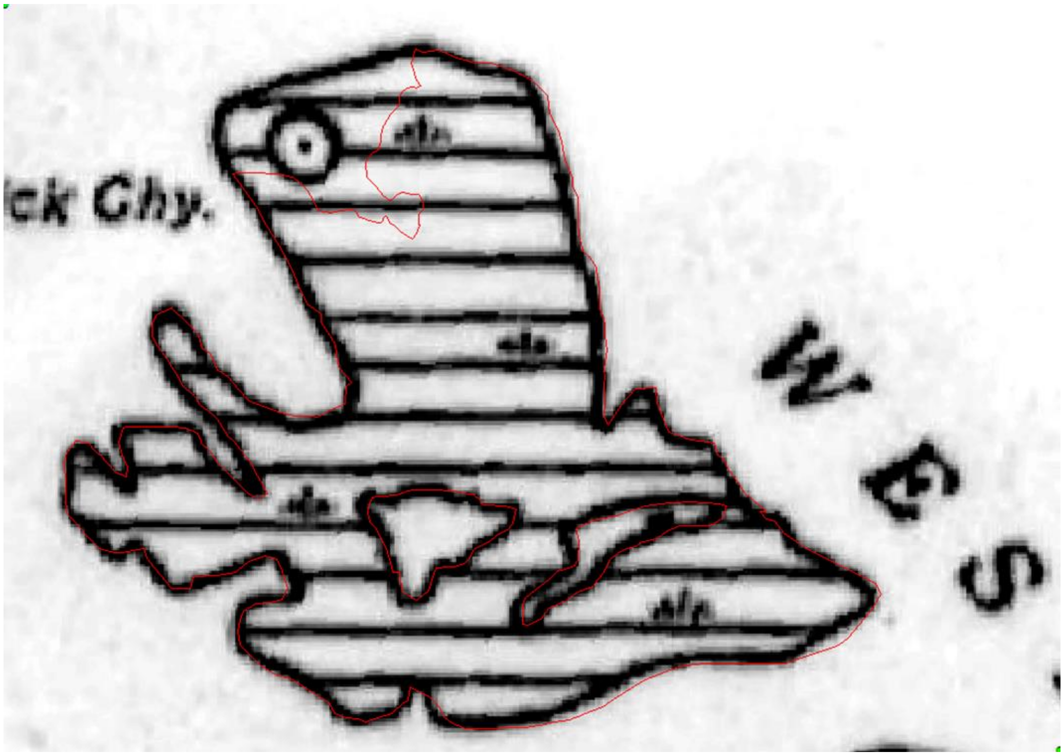

Fig. A61 Sanford Flat C on a 1936 Nautical T-sheet, whose boundaries (red) were based on a November 1934 aerial photograph.

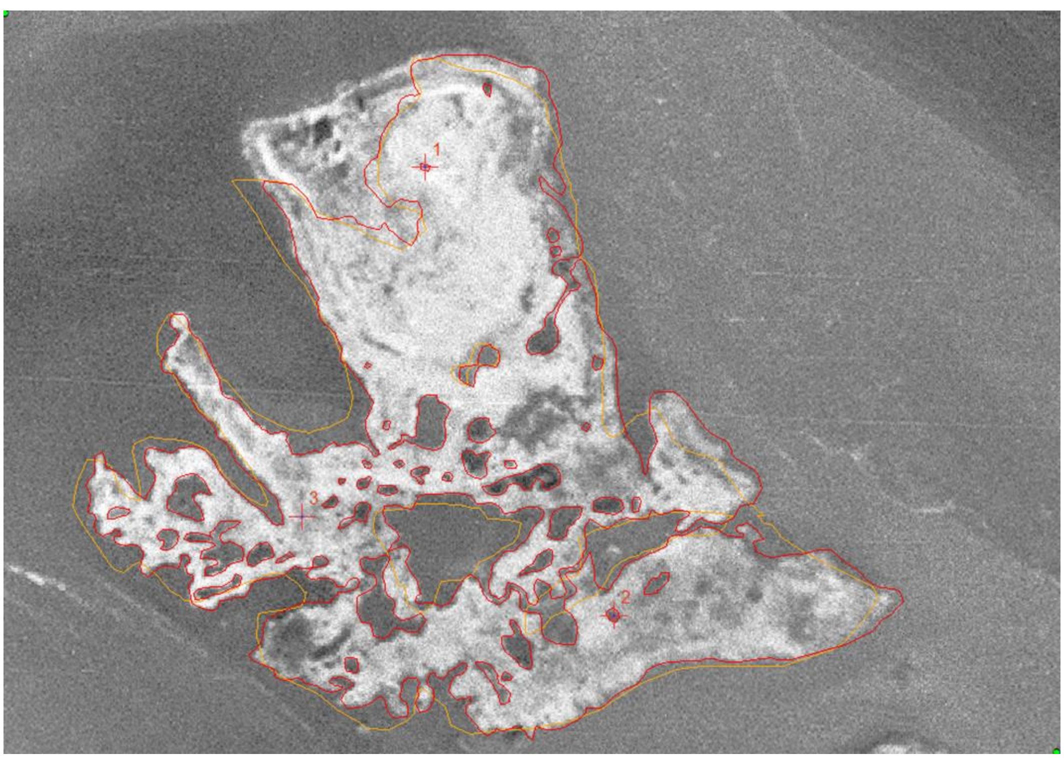

Fig. A62 Sanford Flat C with December 1938 boundaries (red) on source photograph, with previous 1934 era nautical chart T-sheet boundaries (orange).

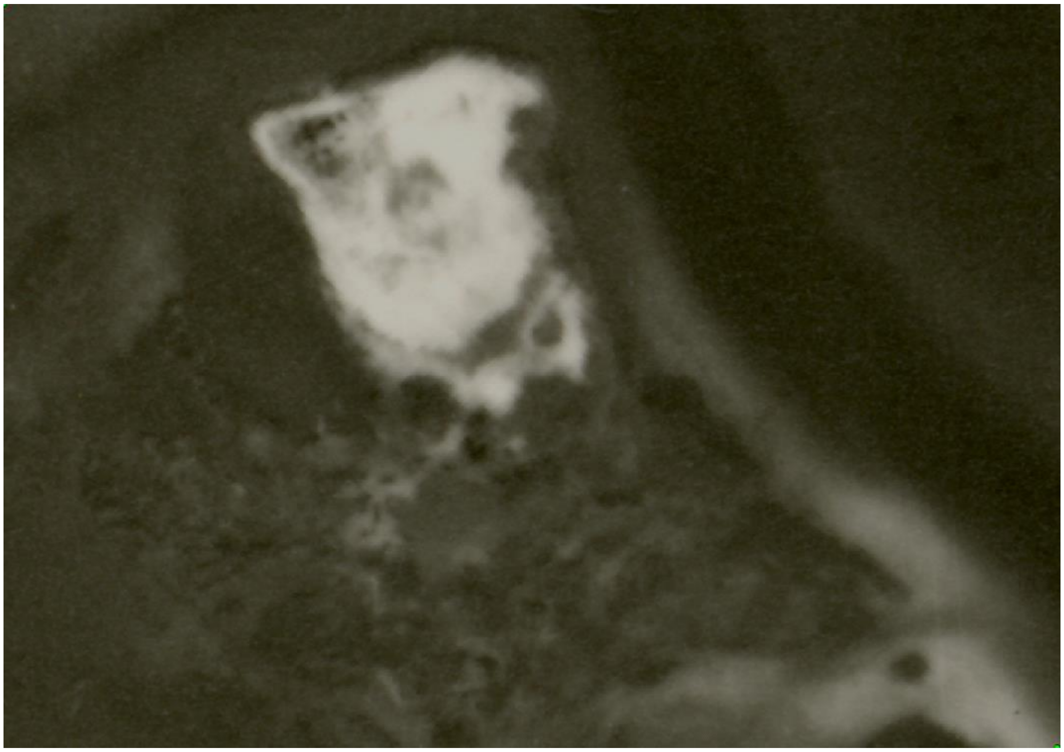

Fig. A63 June 1942 aerial image of Sanford Flat C (not interpreted).

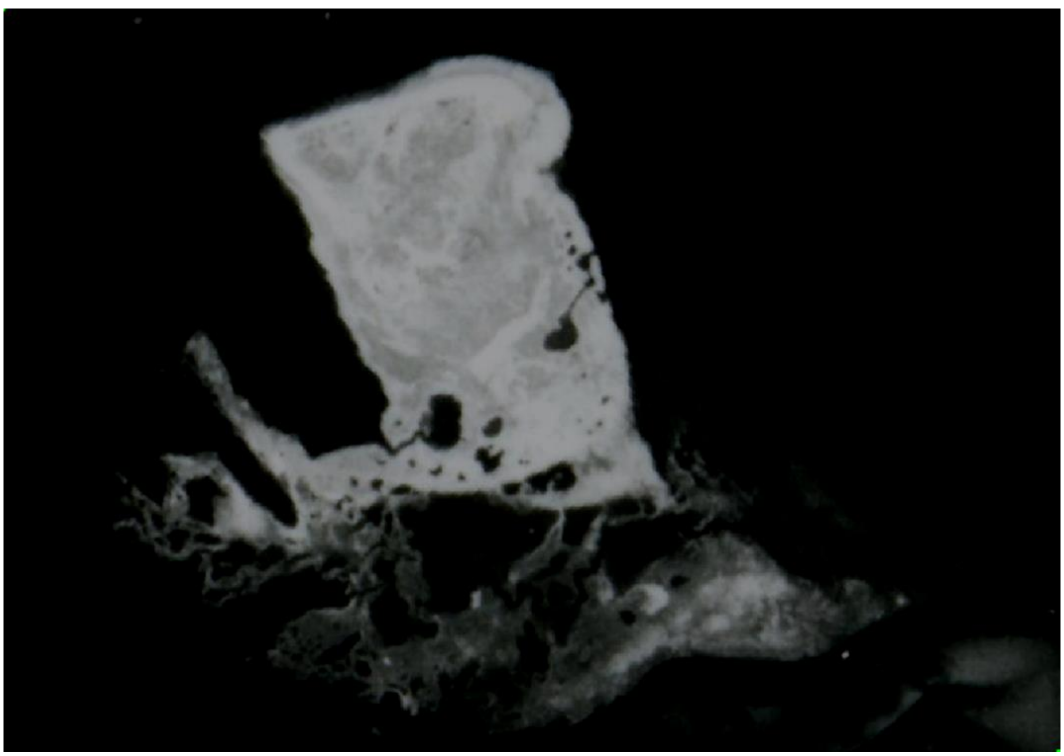

Fig. A64 April 1954 aerial image of Sanford Flat C (not interpreted).

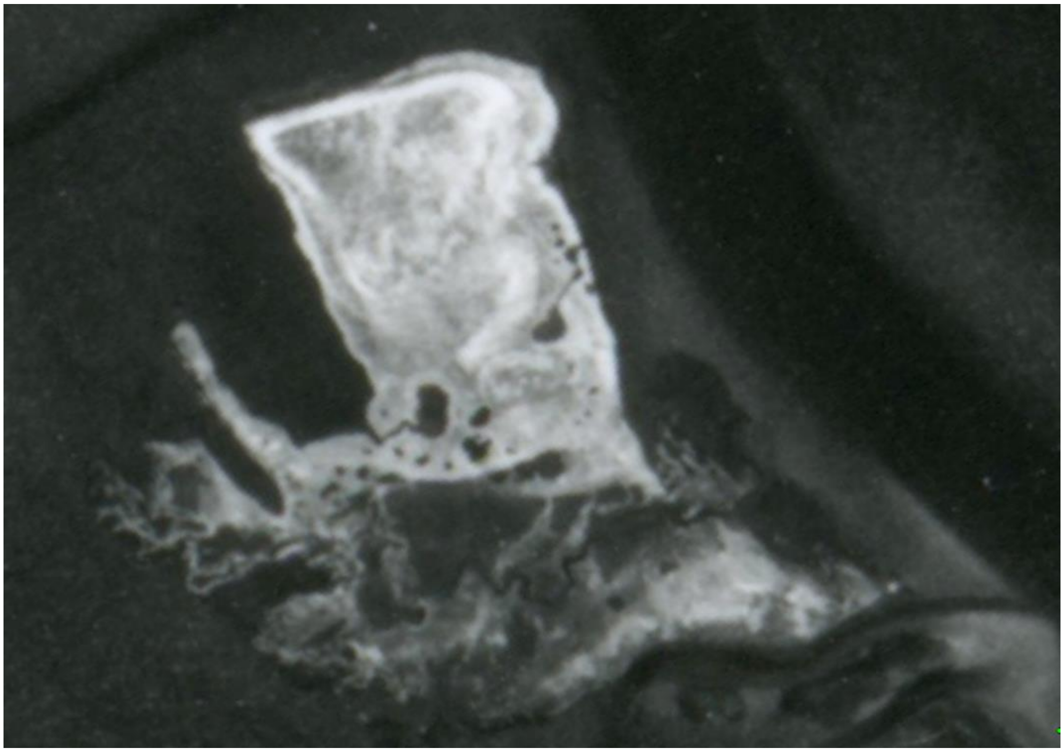

Fig. A65 May 1956 aerial image of Sanford Flat C (not interpreted)

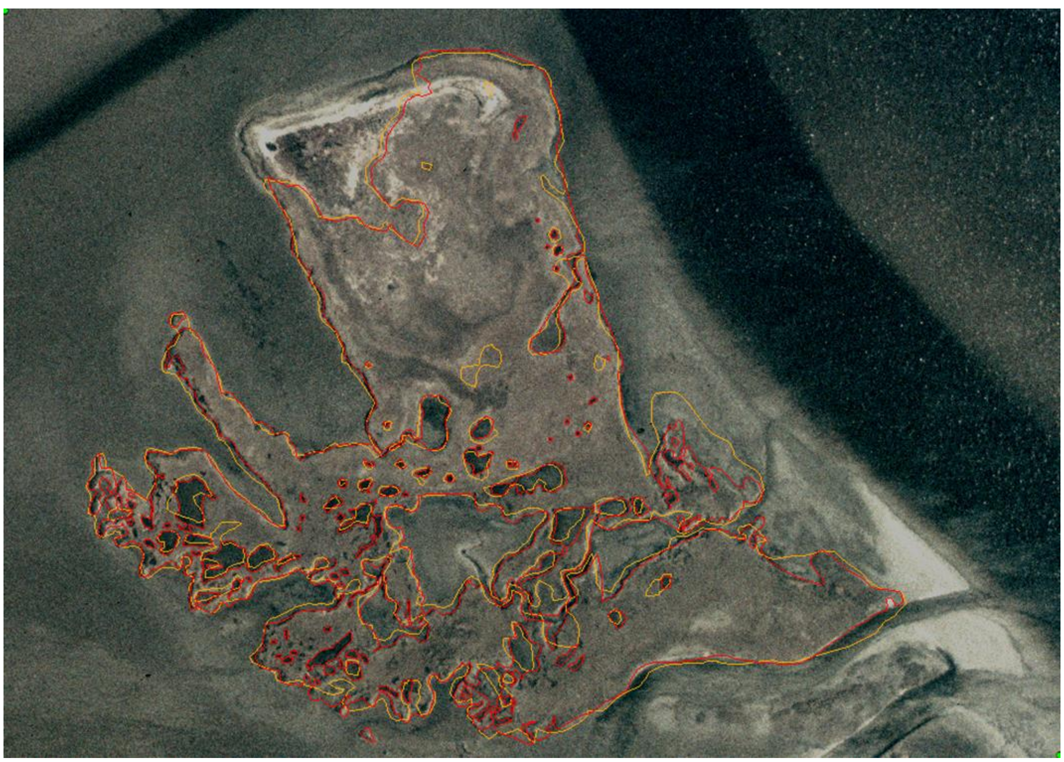

Fig. A66 Sanford Flat C with boundaries (red) on source photograph, with previous December 1938 boundaries (orange). Note the absence of large pans in the center of the island; compare to the 1996 image and post 2005 images).

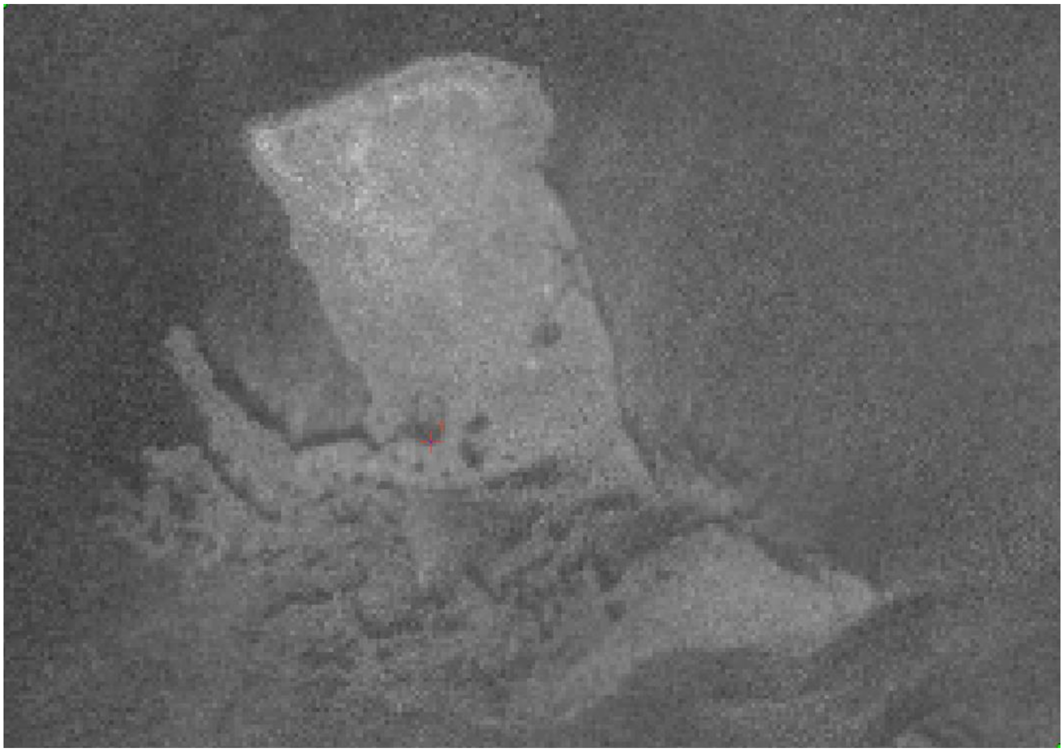

Fig. A67 April 1980 aerial image of Sanford Flat C (not interpreted).

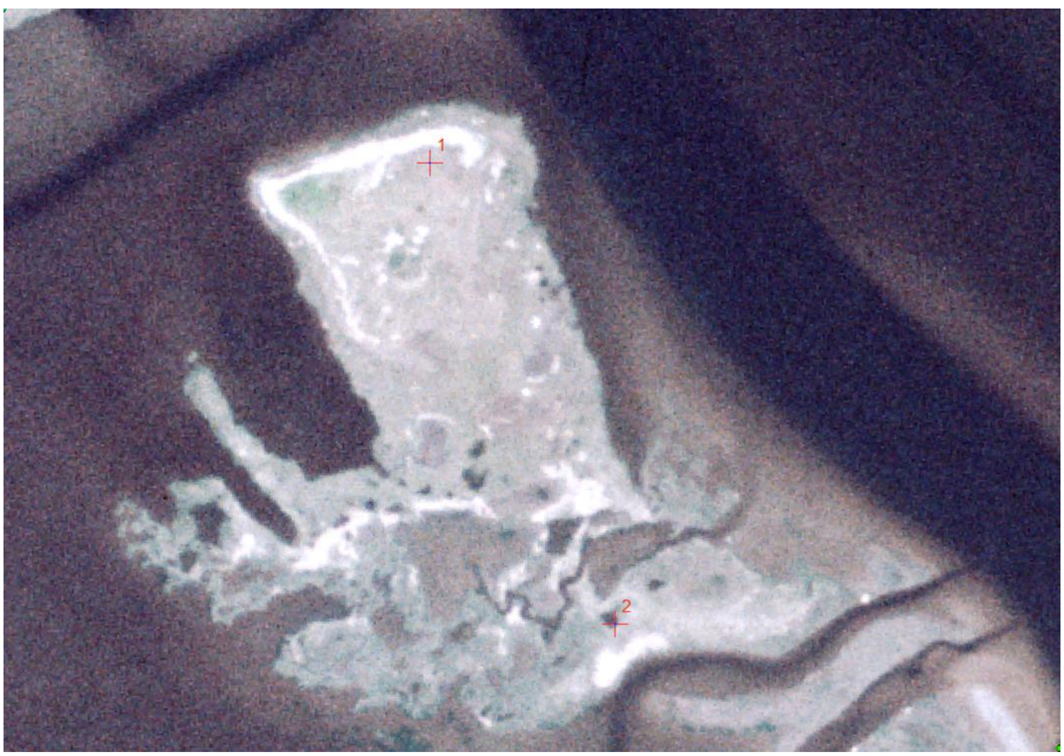

Fig. A68 June 1982 aerial image of Sanford Flat C (not interpreted).

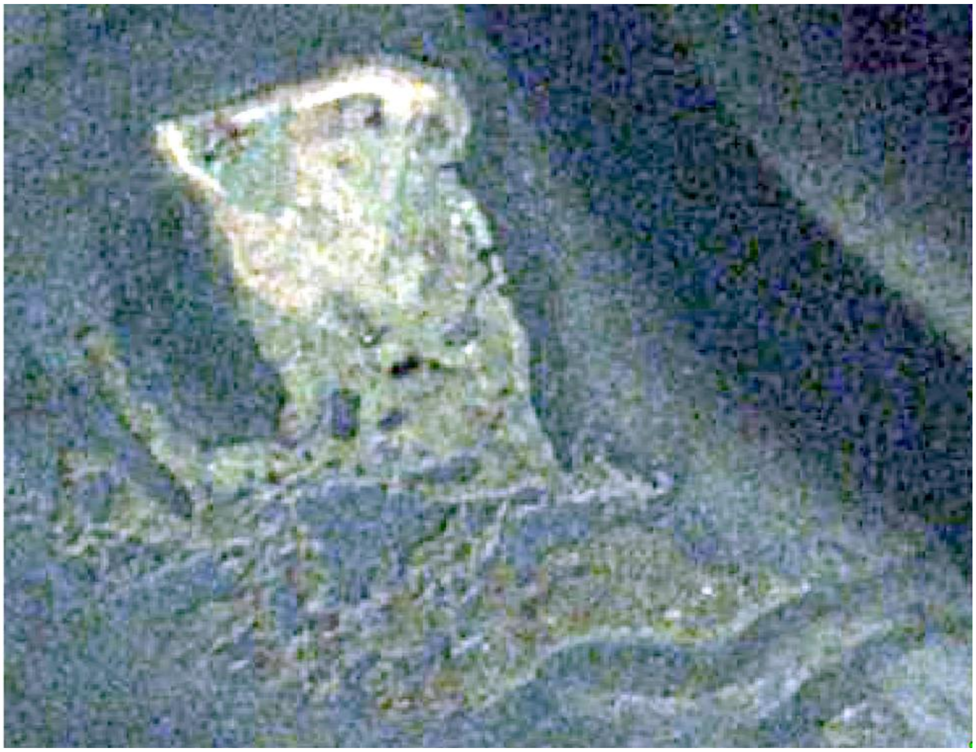

Fig. A69 June 1994 aerial image of Sanford Flat C (not interpreted; note the clear absence of large pans in the center of the island; compare to the 1996 image and post 2005 images).

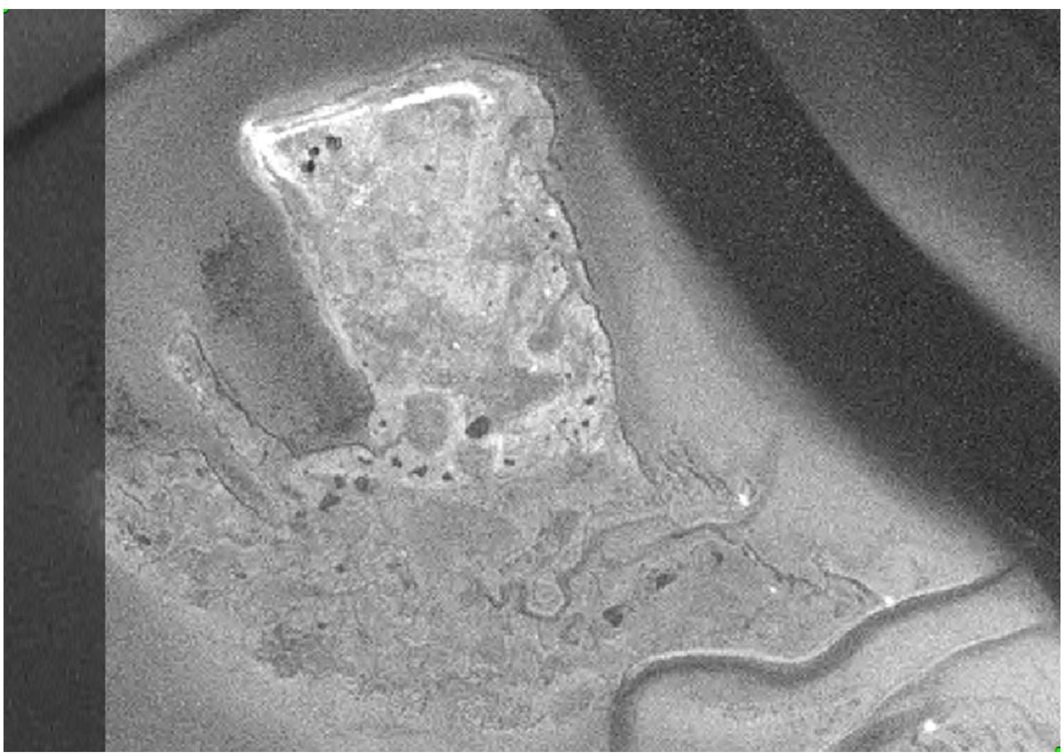

Fig. A70 March 1996 aerial image of Sanford Flat C (not interpreted).

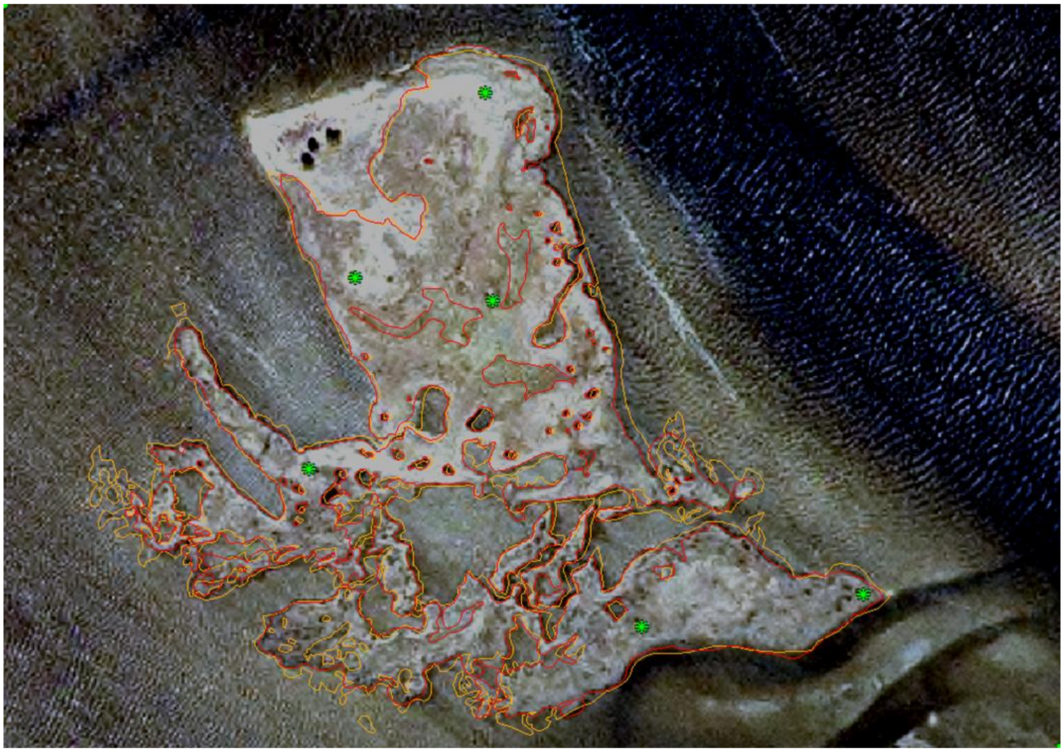

Fig. A71 Sanford Flat C with April 2001 boundaries (red) on source photograph with previous April 1962 boundaries (orange).

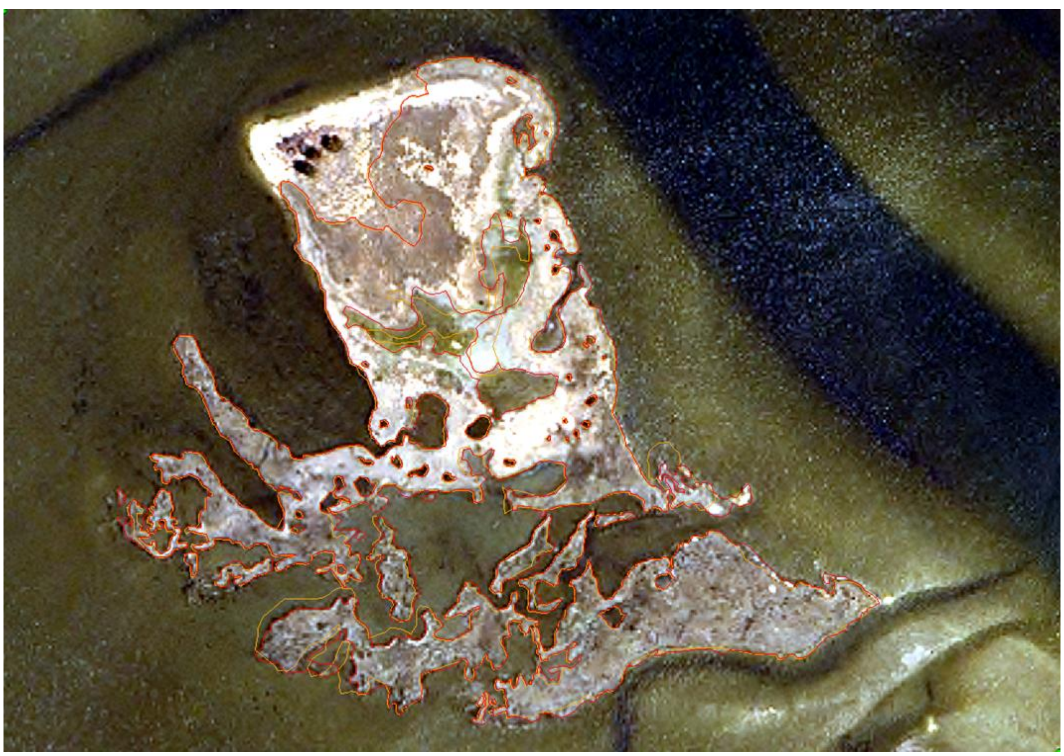

Fig. A72 Sanford Flat C with April 2005 boundaries (red) on source photograph with previous April 2001 boundaries (orange).

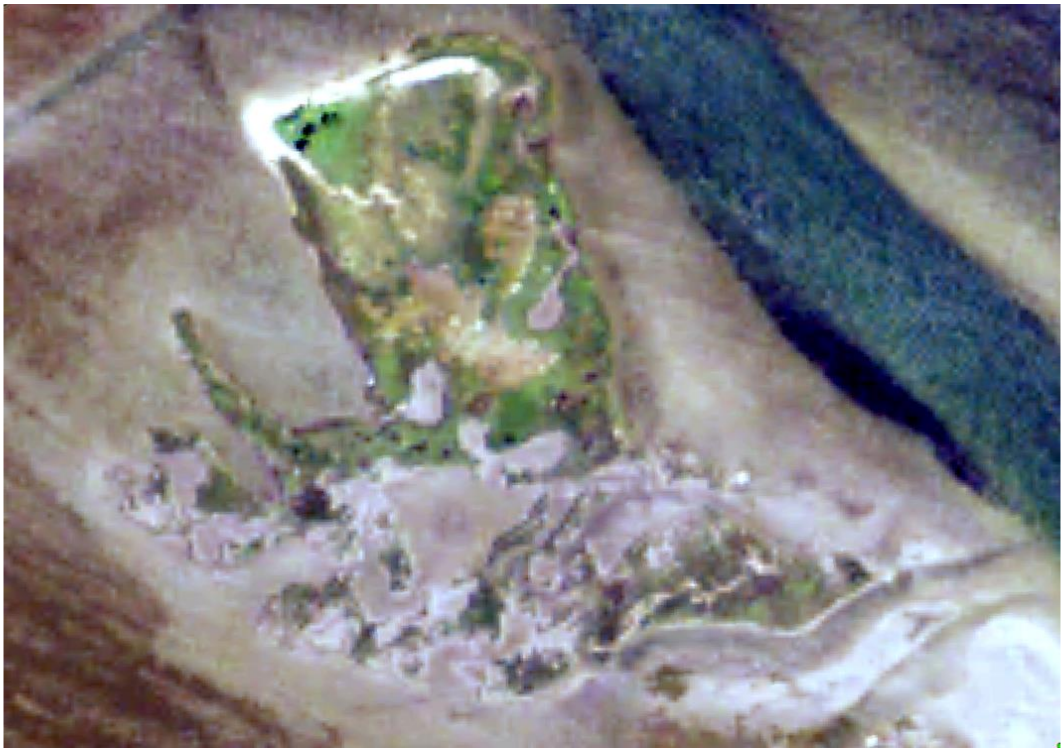

Fig. A73 September 2008 aerial image of Sanford Flat C (not interpreted)

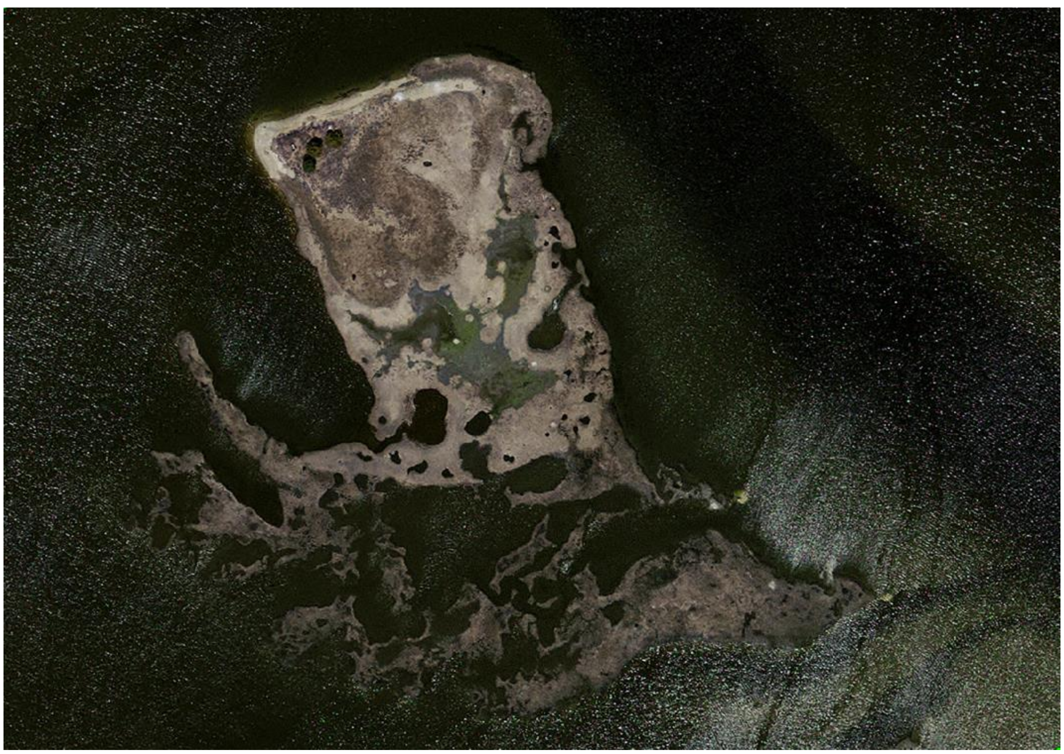

Fig. A74 April 2009 aerial image of Sanford Flat C (not interpreted)

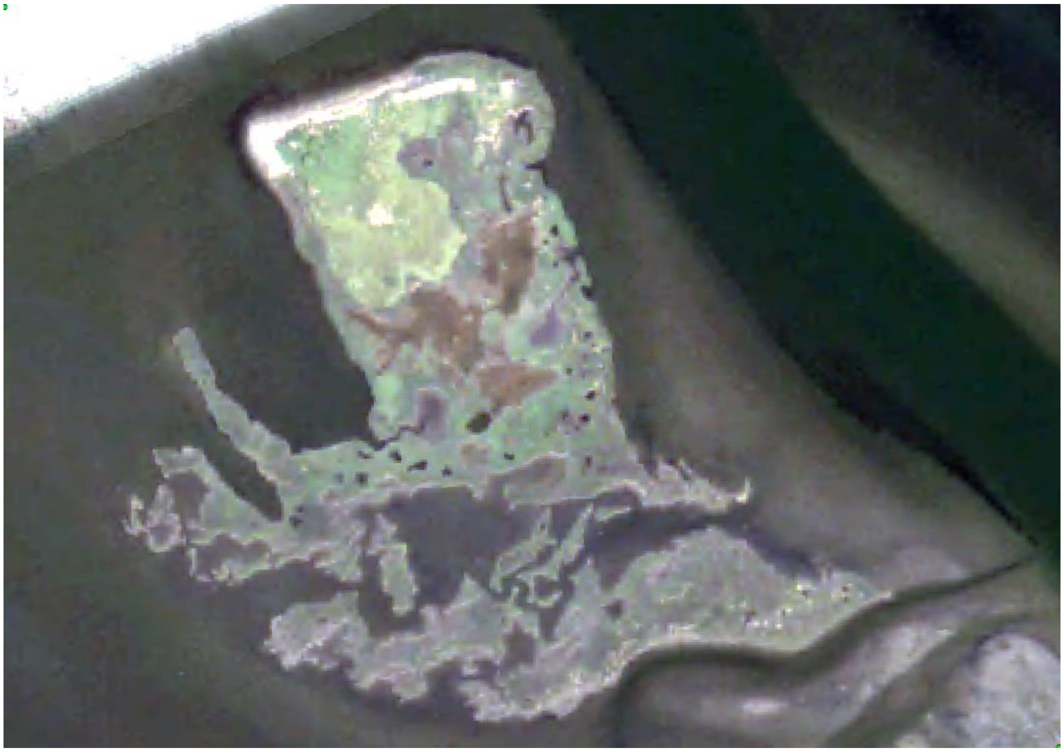

Fig. A75 August 2010 aerial image of Sanford Flat C (not interpreted)

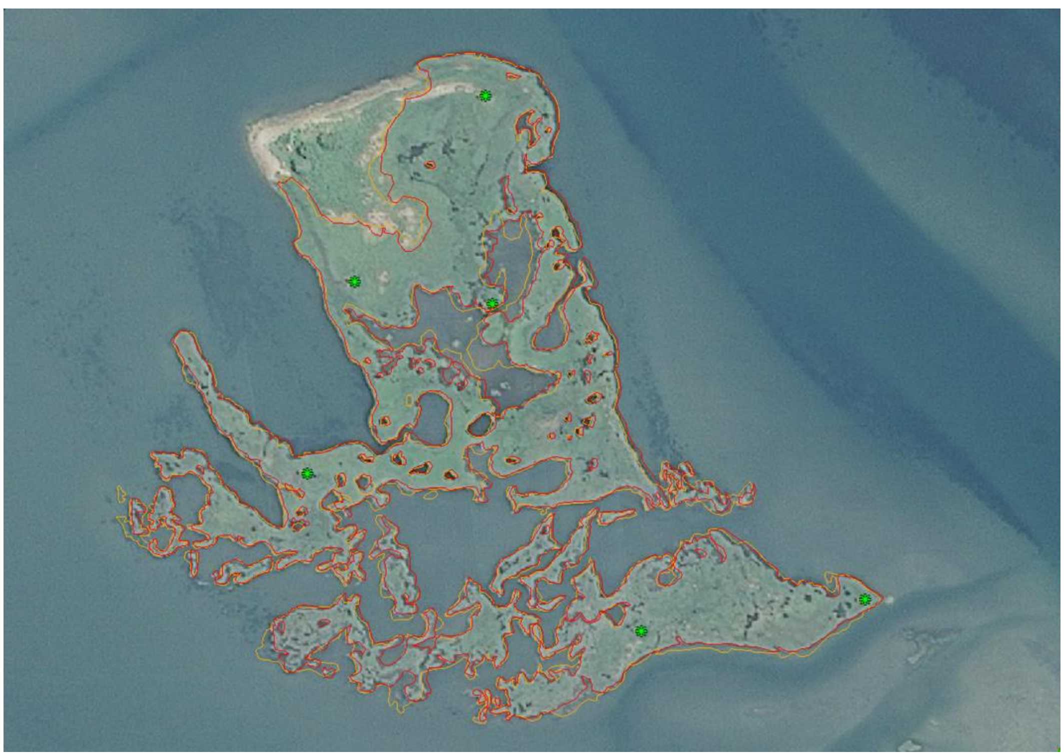

Fig. A76 Sanford Flat C with June 2012 boundaries (red) on source photograph with previous April 2005 boundaries (orange).

Fig. A77 Sanford Flat C with June 2013 boundaries on source photograph with previous June 2012 boundaries (orange).

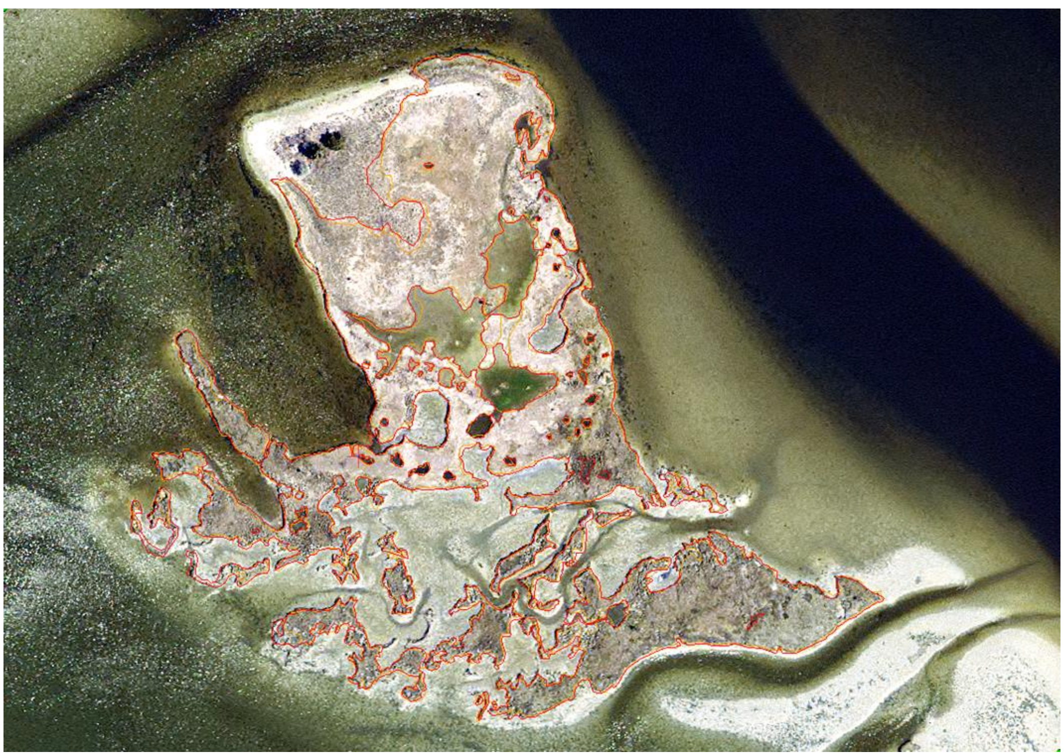

Fig. A78 Sanford Flat C with April 2014 boundaries (red) on source photograph with previous June 2013 boundaries (orange).

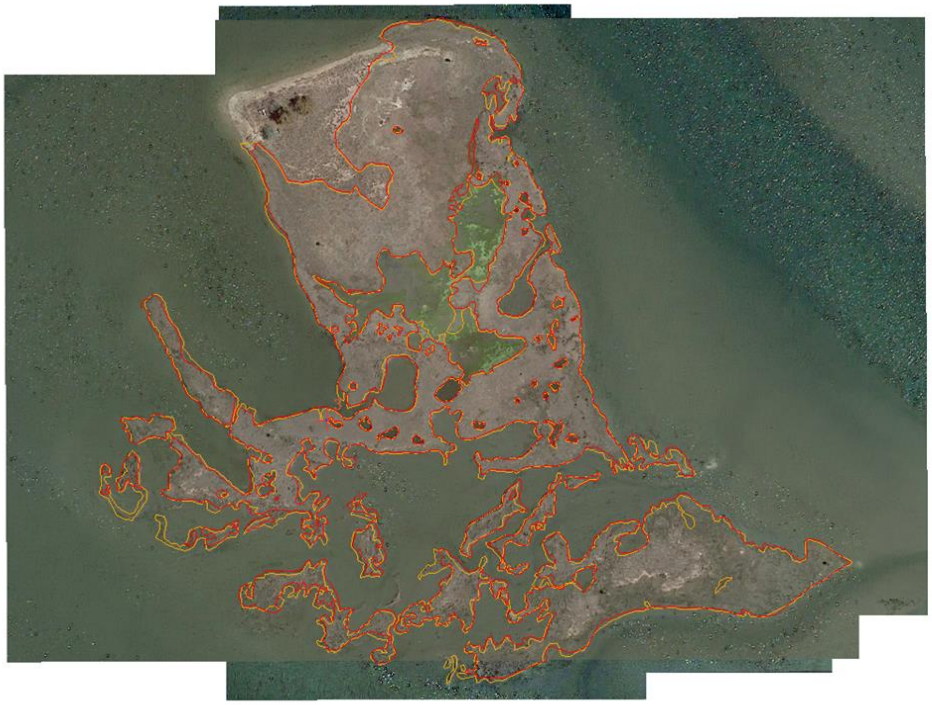

Fig. A79 Sanford Flat C with May 2015 boundaries (red, Google Earth) on source photograph with previous April 2014 boundaries (orange).

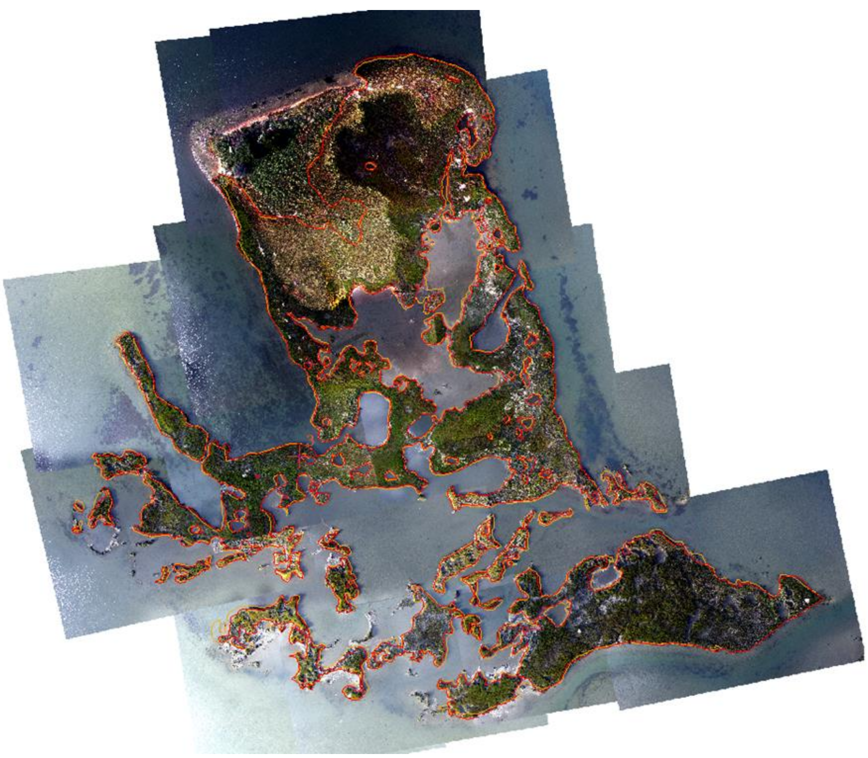

Fig. A80 Sanford Flat C with October 2016 (UAV) boundaries (red) on source photograph with previous May 2015 boundaries (orange).

Great Flat 12

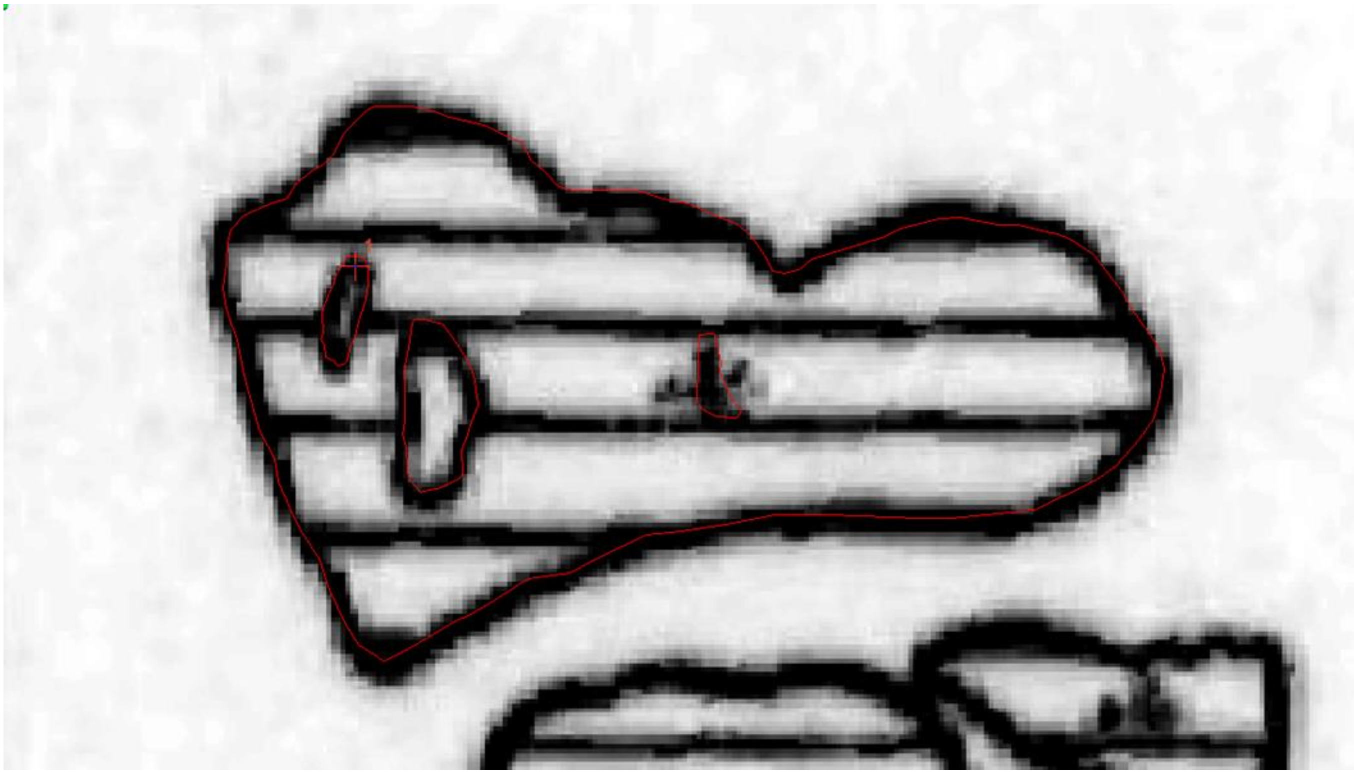

Fig. A81 Great Flat 12 on a 1936 Nautical T-sheet with boundaries based on interpretation of November 1934 aerial photograph. Barrier flats on south side were missing in post 1934 photograph, and were not included in base area calculations

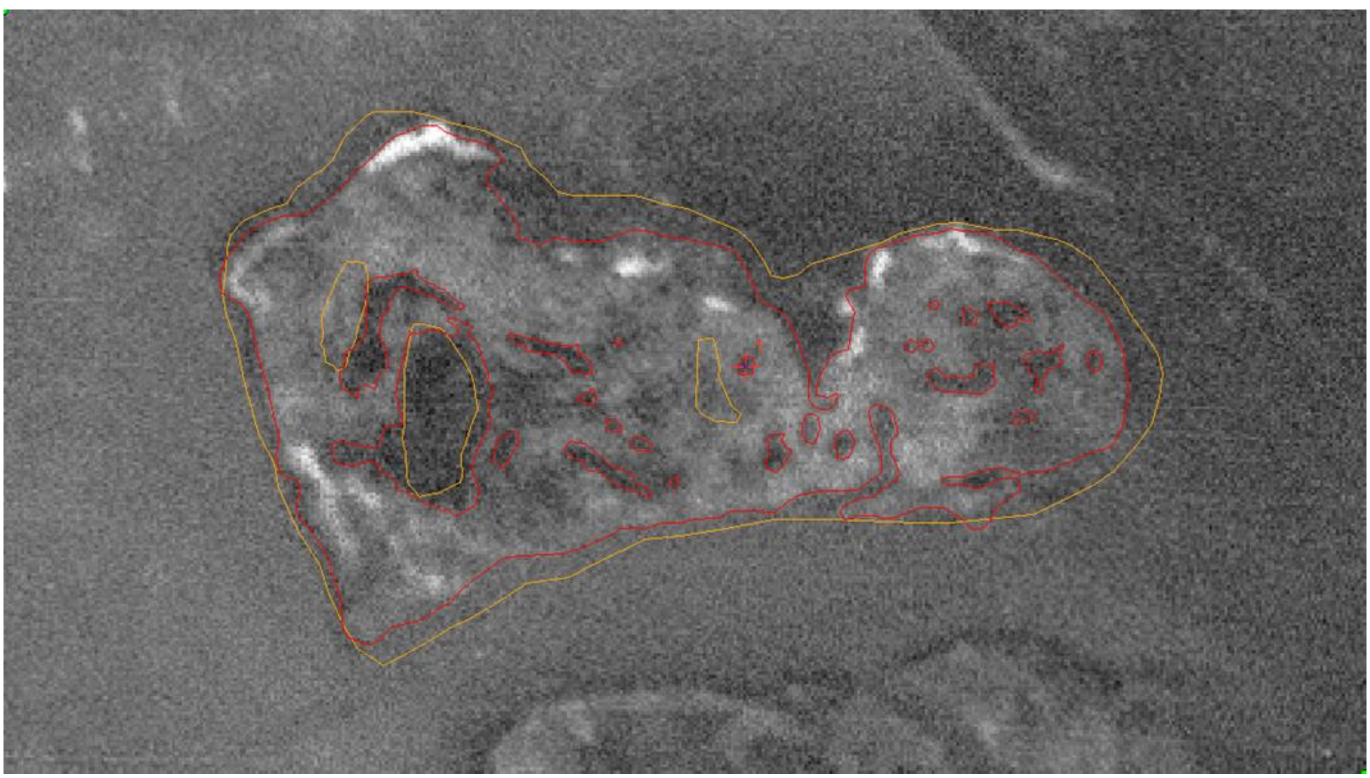

Fig. A82 Great Flat 12 with December 1938 boundaries (red) on source photograph, and chart T-sheet boundaries (orange) based on November 1934 aerial photograph.

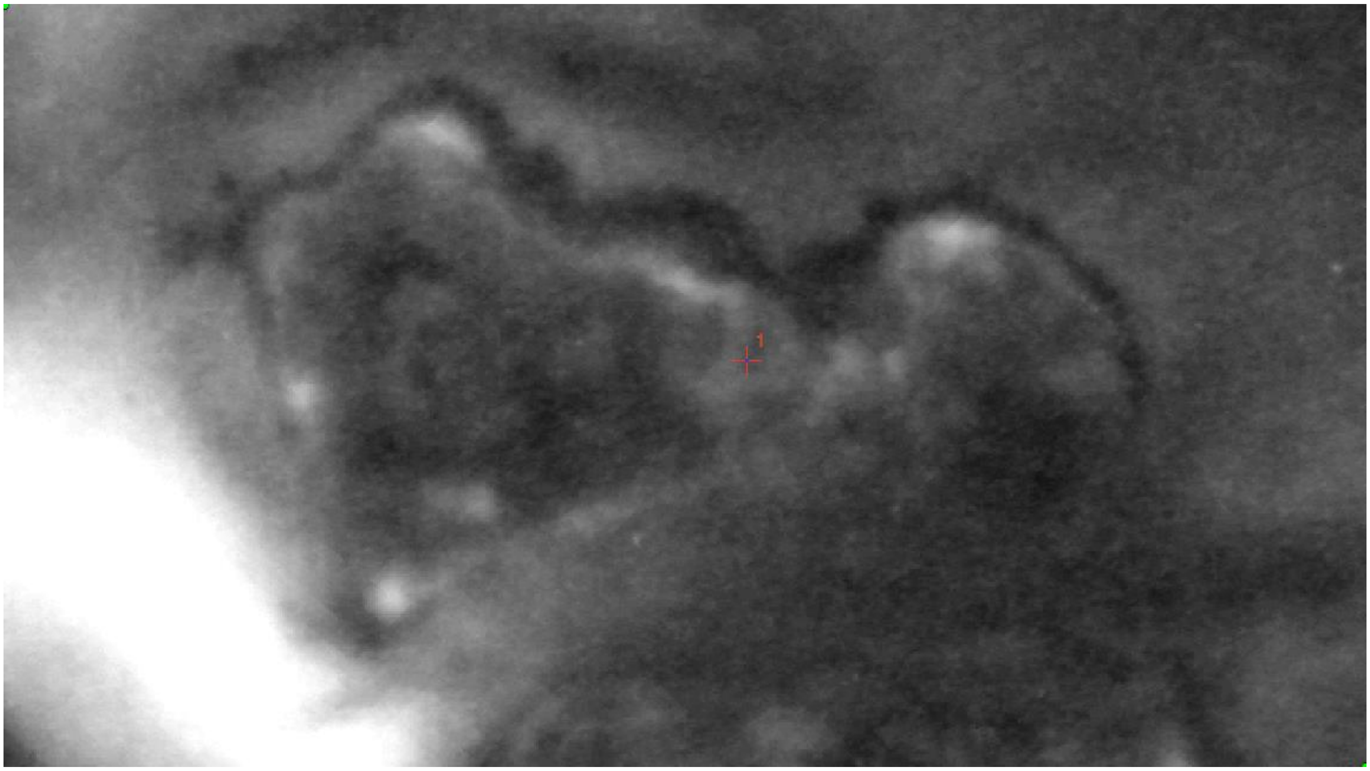

Fig. A83 June 1942 aerial image of Great Flat 12 (not interpreted).

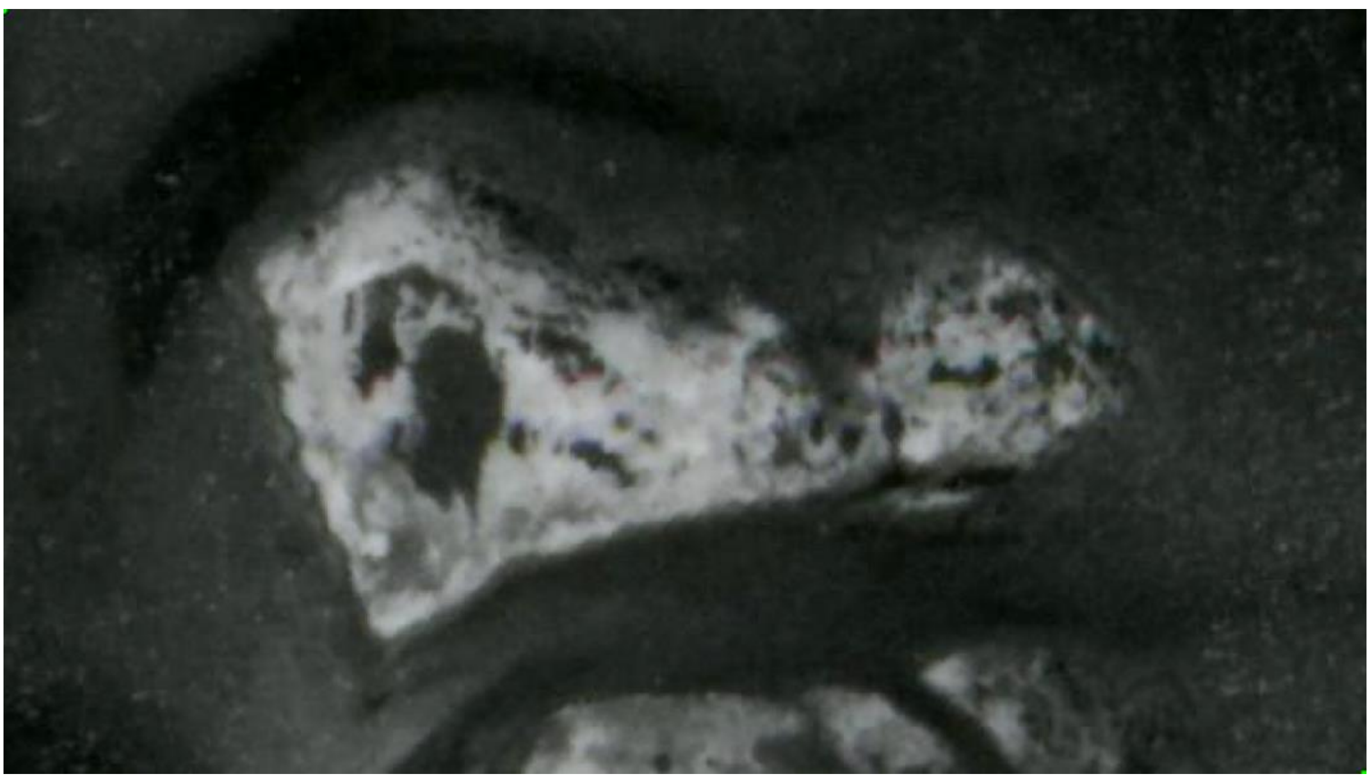

Fig. A84 April 1954 aerial image of Great Flat 12 (not interpreted).

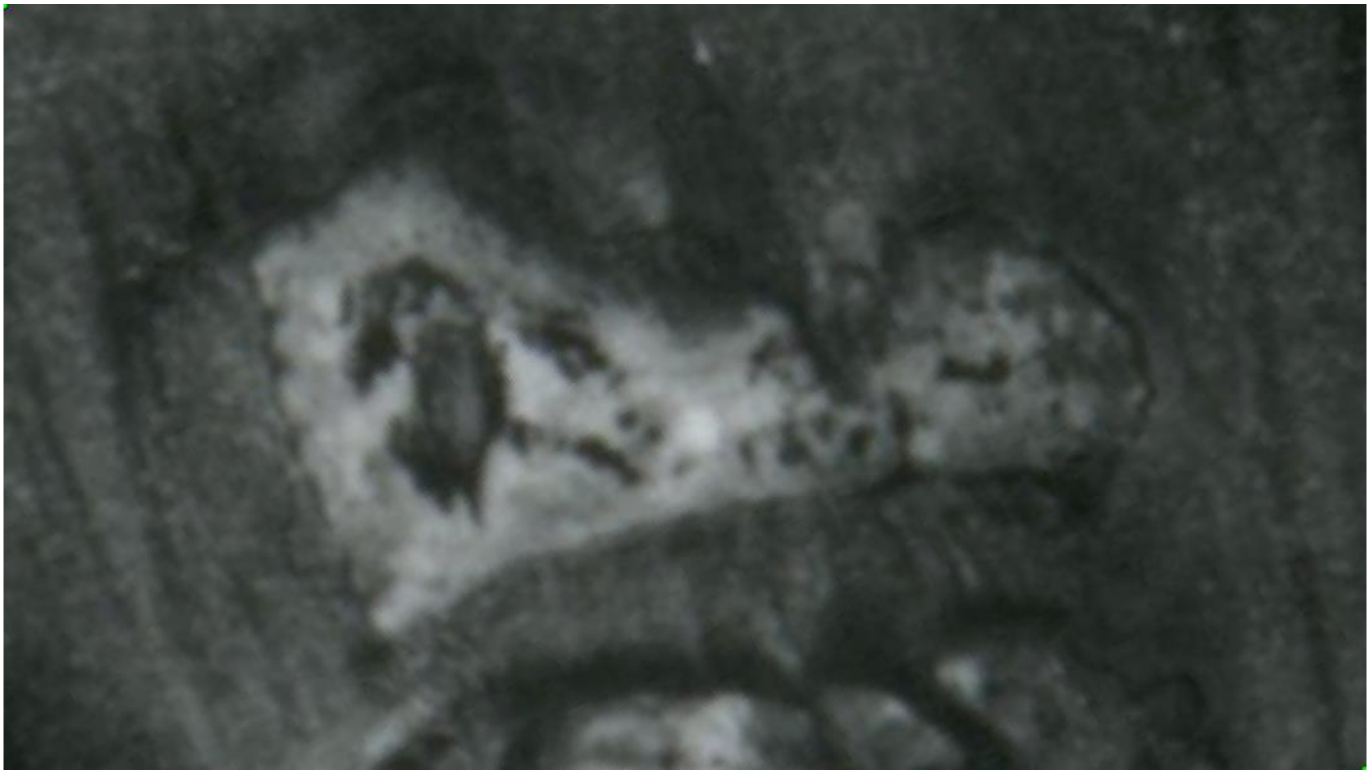

Fig. A85 May 1956 aerial image of Great Flat 12 (not interpreted).

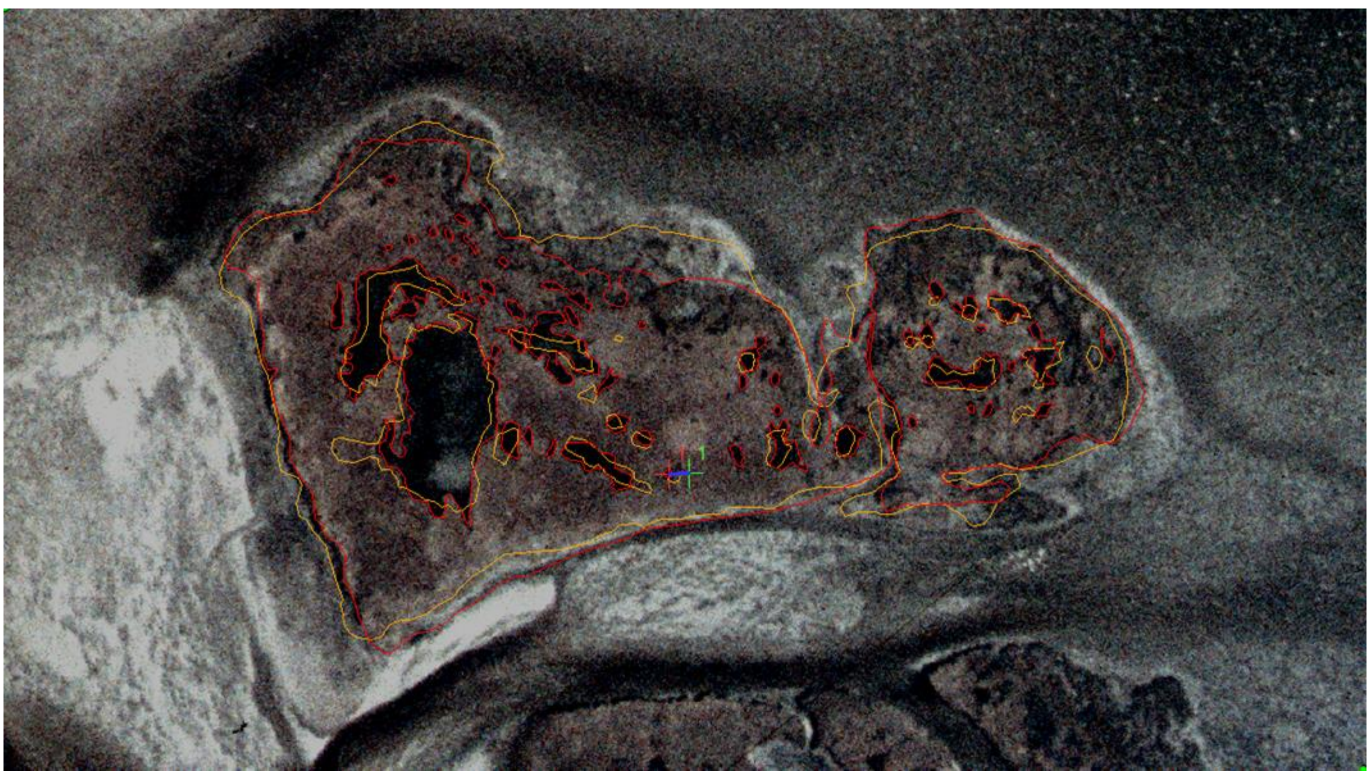

Fig. A86 Great Flat 12 with April 1962 boundaries (red) on source photograph, with previous December 1938 boundaries (orange).

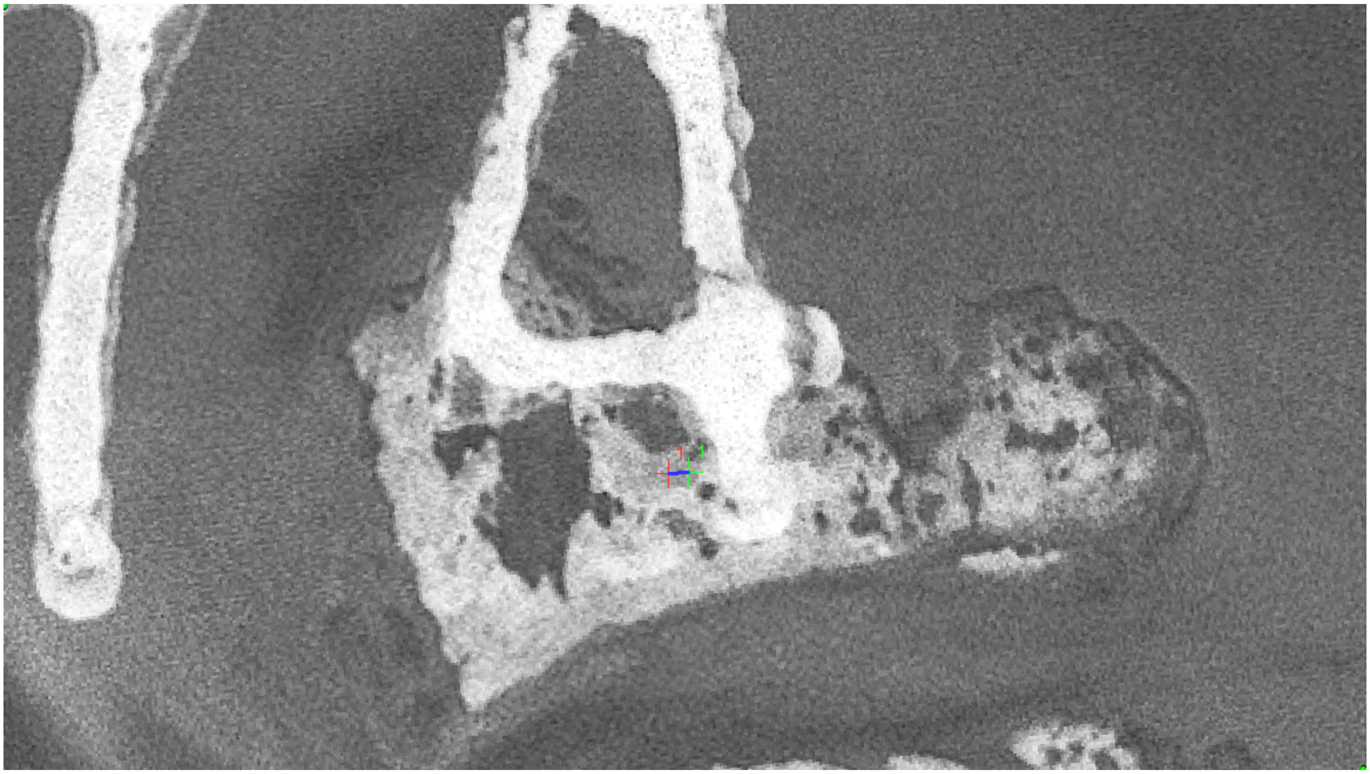

Fig. A87 April1974 aerial image of Great Flat 12 (not interpreted, and partially obscured by lettering on photograph).

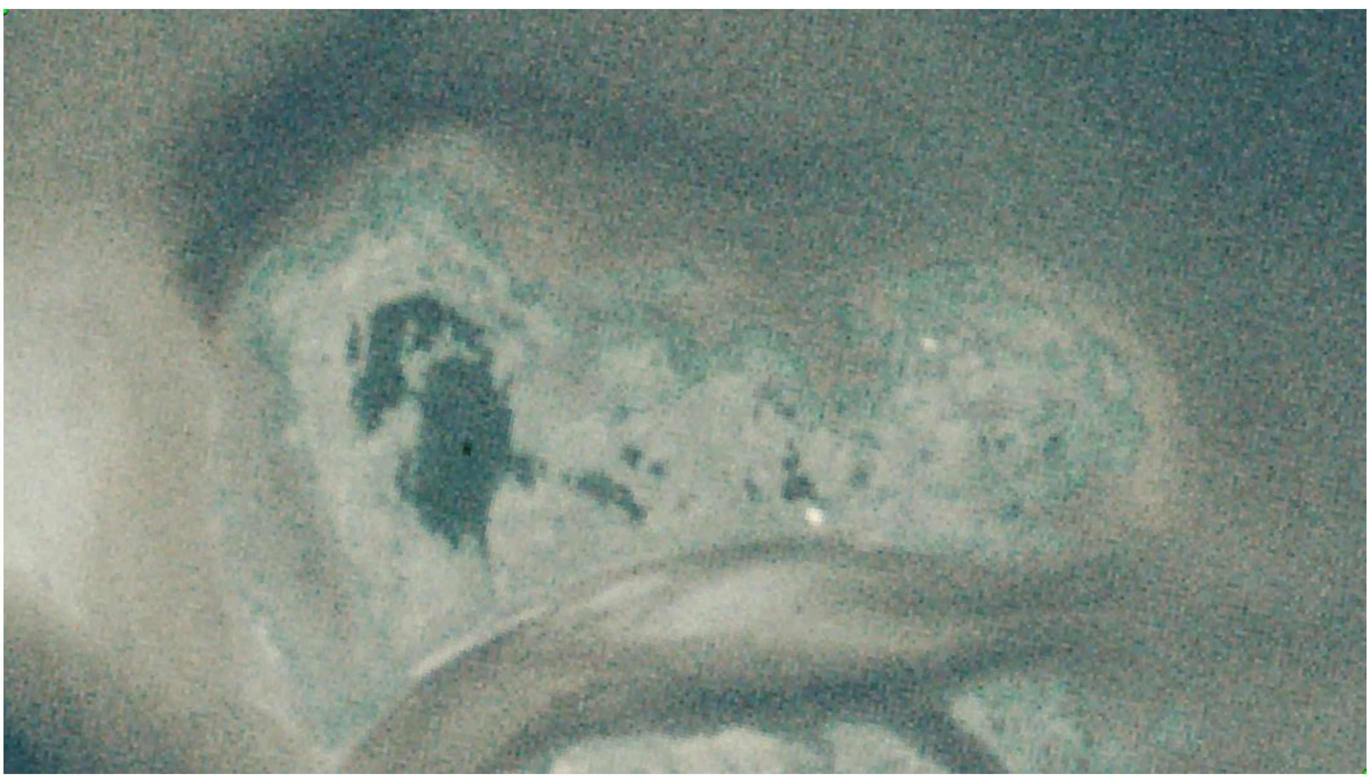

Fig. A88 June 1982 aerial image of Great Flat 12 (not interpreted).

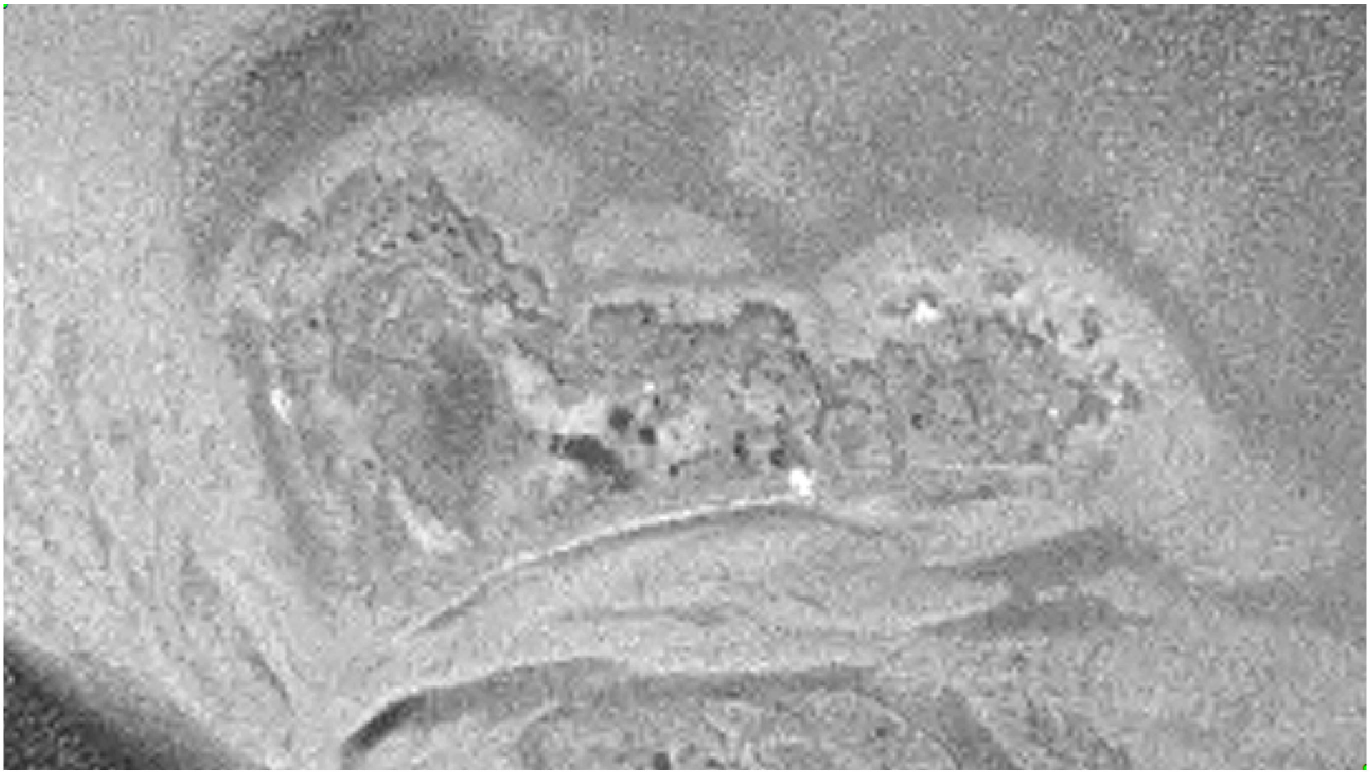

Fig. A89 March 1996 aerial image of Great Flat 12 (not interpreted.

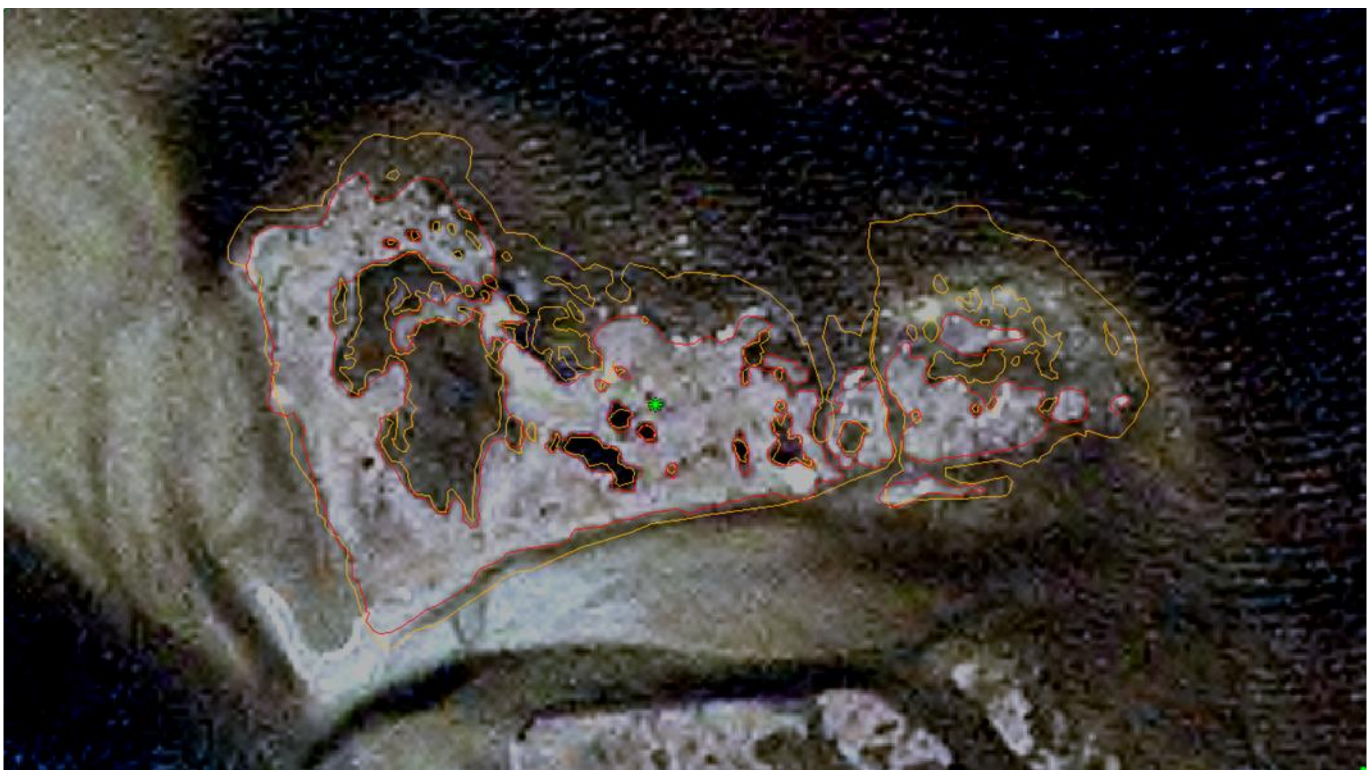

Fig. A90 Great Flat 12 with April 2001 boundaries (red) on source photograph, with previous April 1962 boundaries (orange).

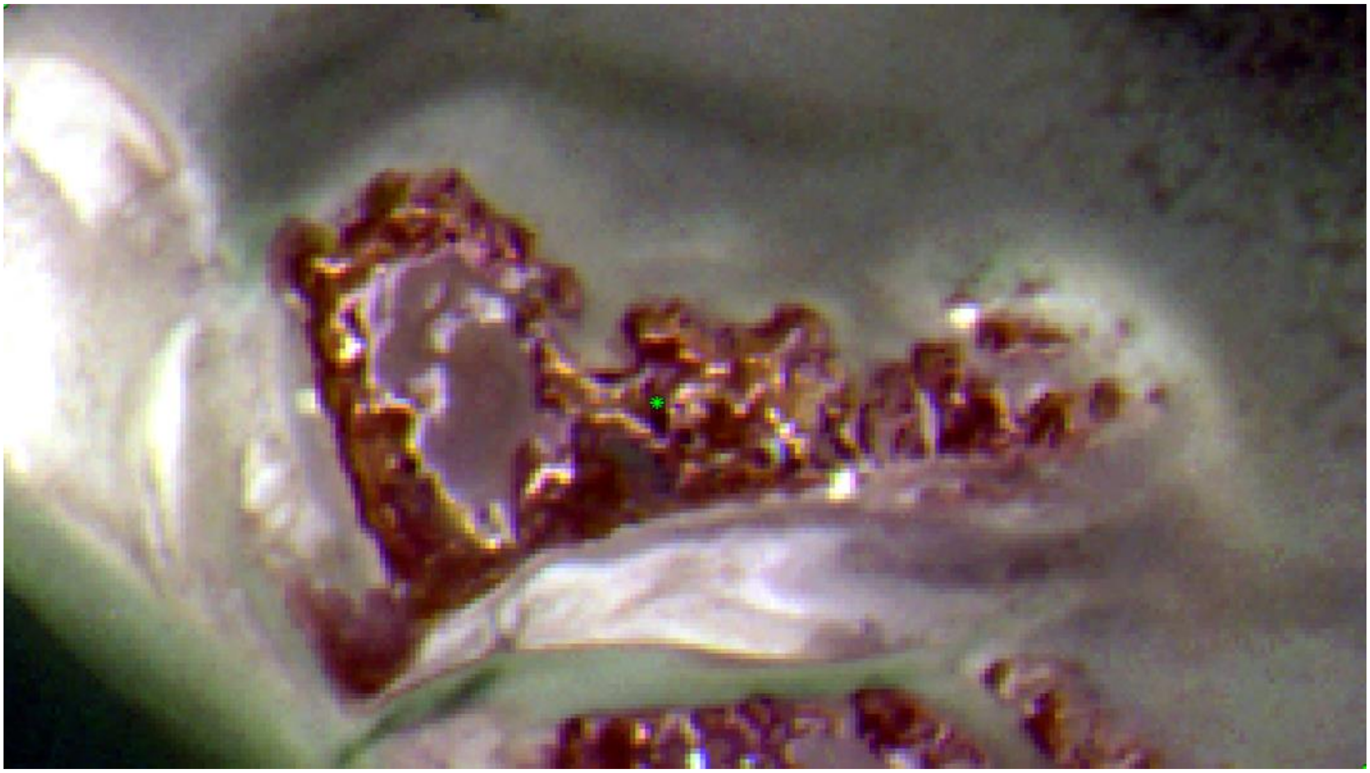

Fig. A91 June 2001 aerial image of Great Flat 12 (not interpreted).

Fig. A92 Great Flat 12 with April 2005 boundaries (red) on source photograph, with previous April 2001 boundaries (orange).

Fig. A93 September 2008 aerial image of Great Flat 12 (not interpreted).

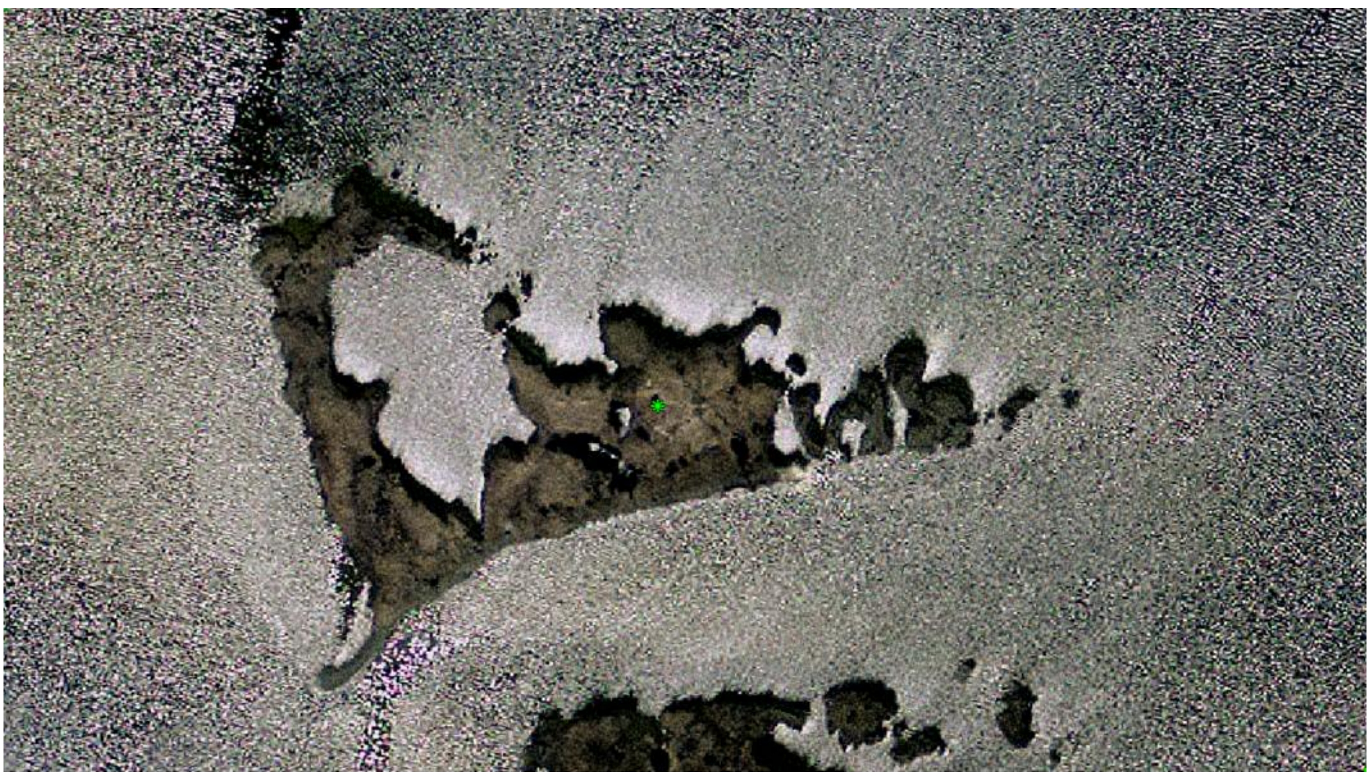

Fig. A94 April 2009 aerial image of Great Flat 12 (not interpreted).

Fig. A95 August 2010 aerial image of Great Flat 12 (not interpreted).

Fig. A96 Great Flat 12 with June 2012 boundaries (red) on source photograph, with previous April 2005 boundaries (orange).

Fig. A97 Great Flat 12 with September 2013 boundaries (red) on source photograph, with previous June 2012 boundaries (orange).

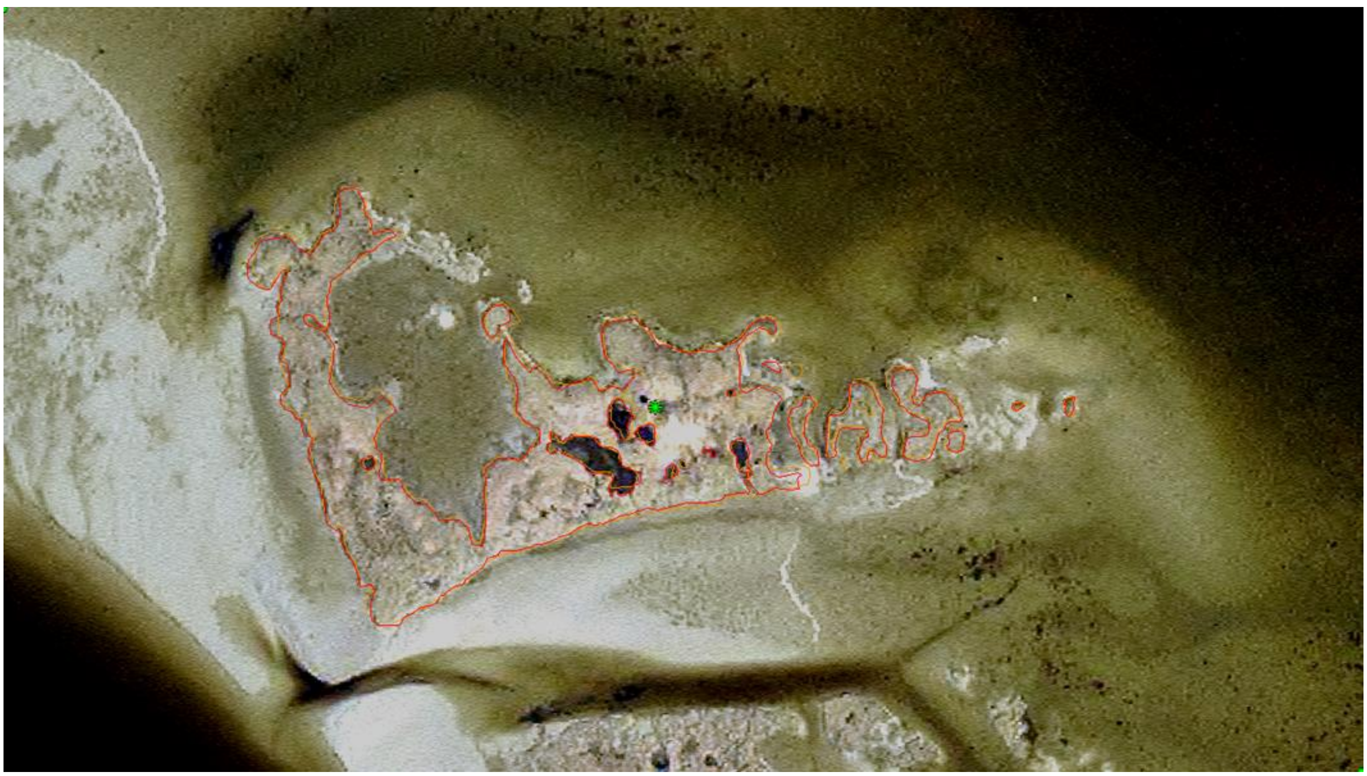

Fig. A98 Great Flat 12 with April 2014 boundaries (red) on source photograph, with previous September 2013 boundaries (orange).

Fig. A99 Great Flat 12 with May 2015 boundaries (red) on source photograph, with previous April 2014 boundaries (orange).

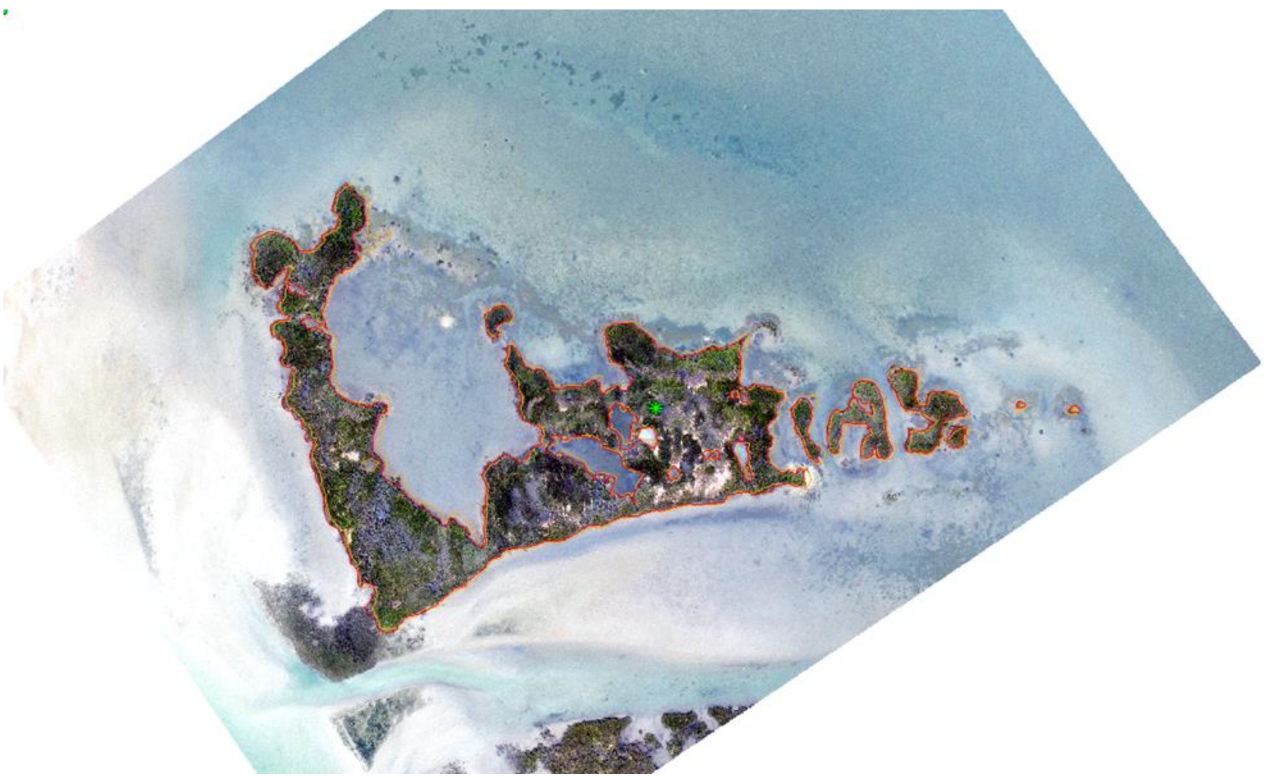

Fig. A100 Great Flat 12 with October 2016 boundaries (red; image from UAV) on source photograph, with previous May 2015 boundaries (orange).

North of Sanford 3

Fig. A101 North of Sanford 3 as delineated on a 1936 Nautical T-sheet, with boundaries based on interpretation of November 1934 aerial photograph.

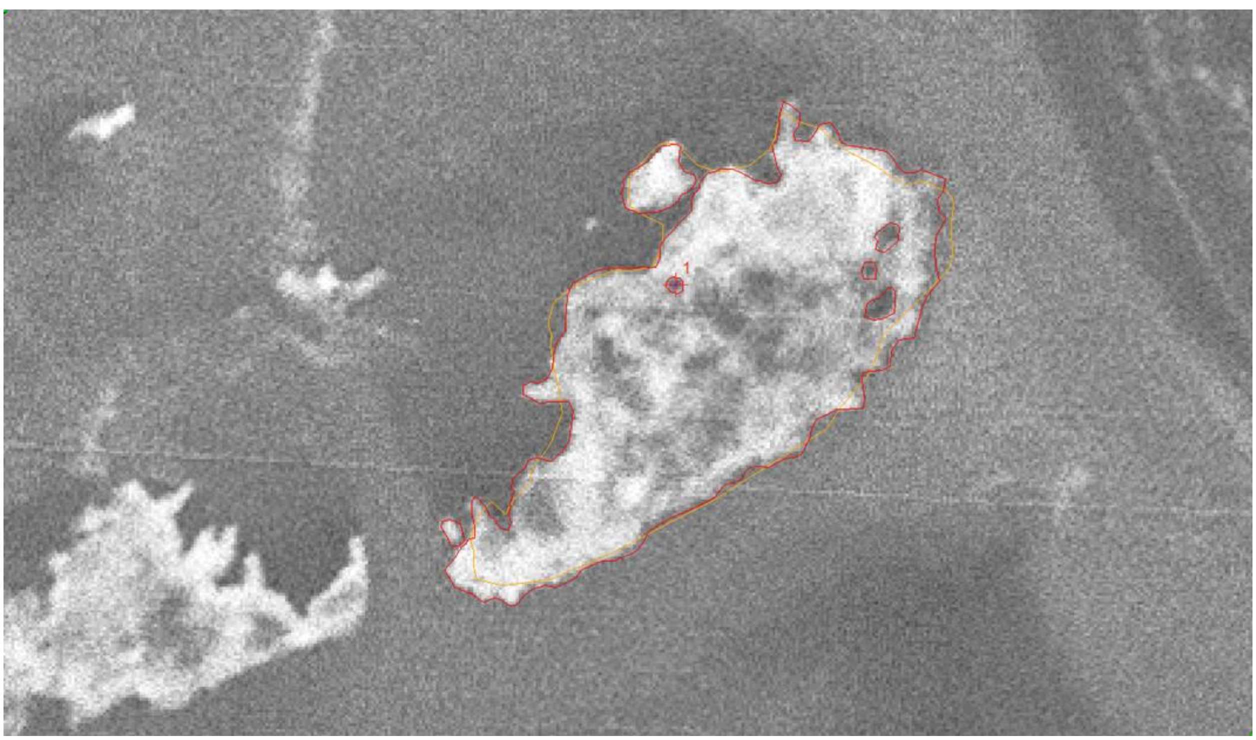

Fig. A102 North of Sanford 3 with December 1938 boundaries (red) on source photograph, and chart T-sheet boundaries (orange) based on November 1934 aerial photograph.

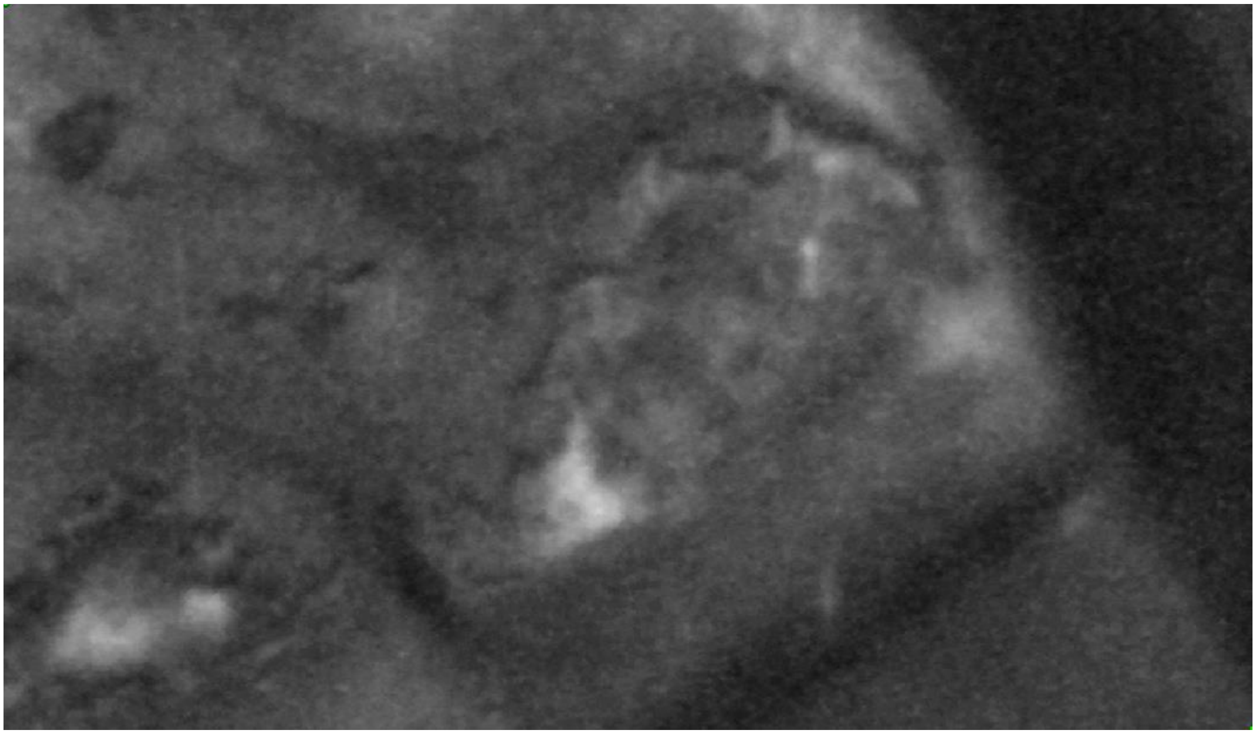

Fig. A103 June 1942 aerial image of North of Sanford 3 (not interpreted).

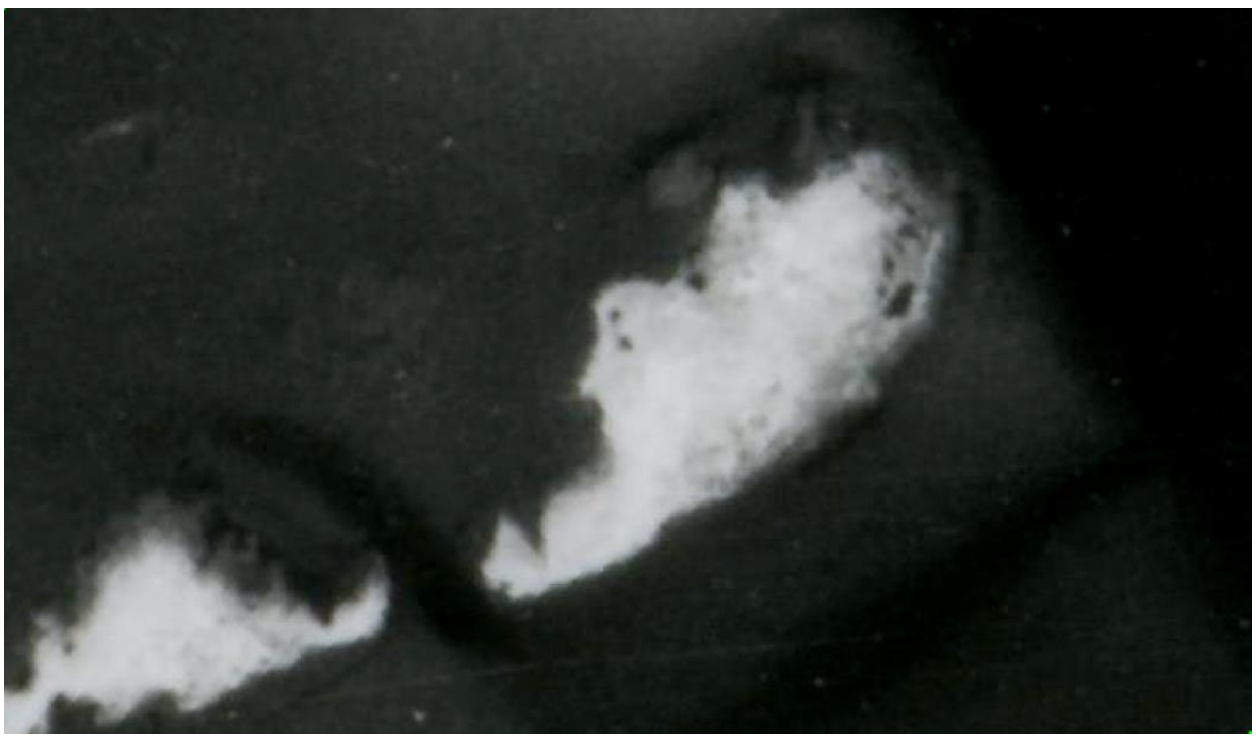

Fig. A104 April 1954 aerial image of North of Sanford 3 (not interpreted).

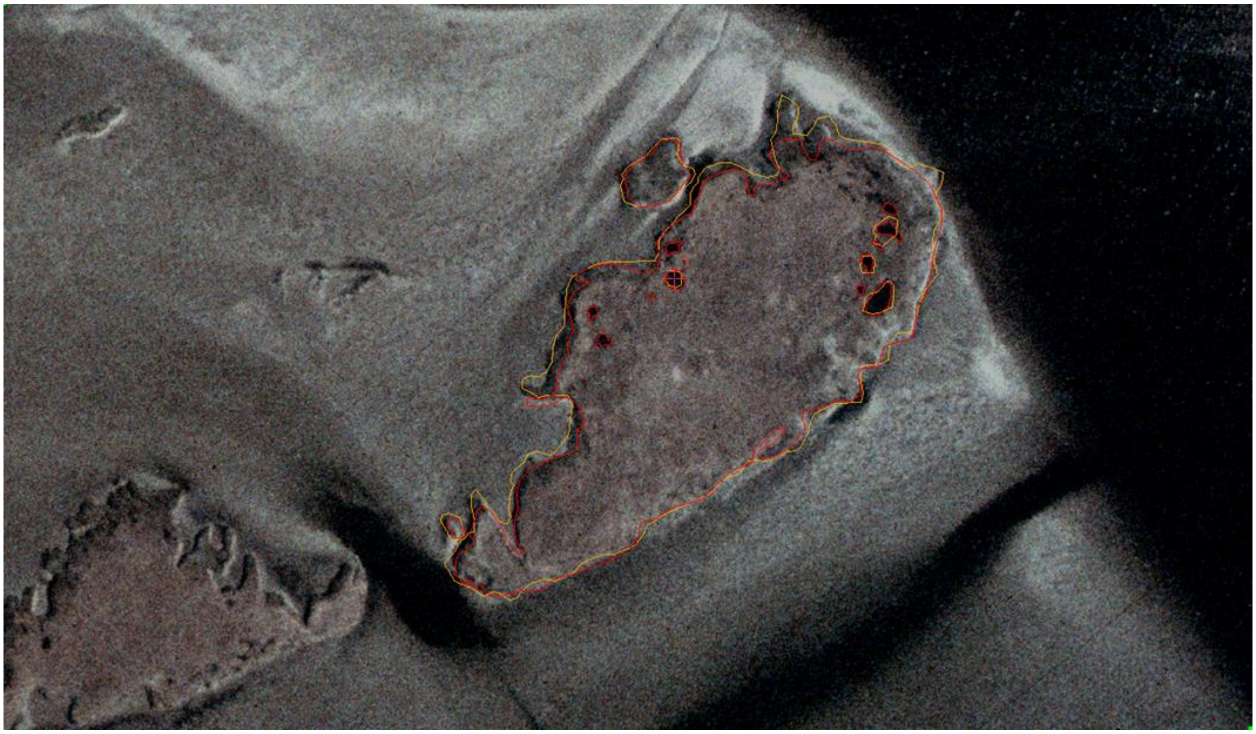

Fig. A105 North of Sanford 3 with April 1962 boundaries (red) on source photograph, with previous December 1938 boundaries (orange).

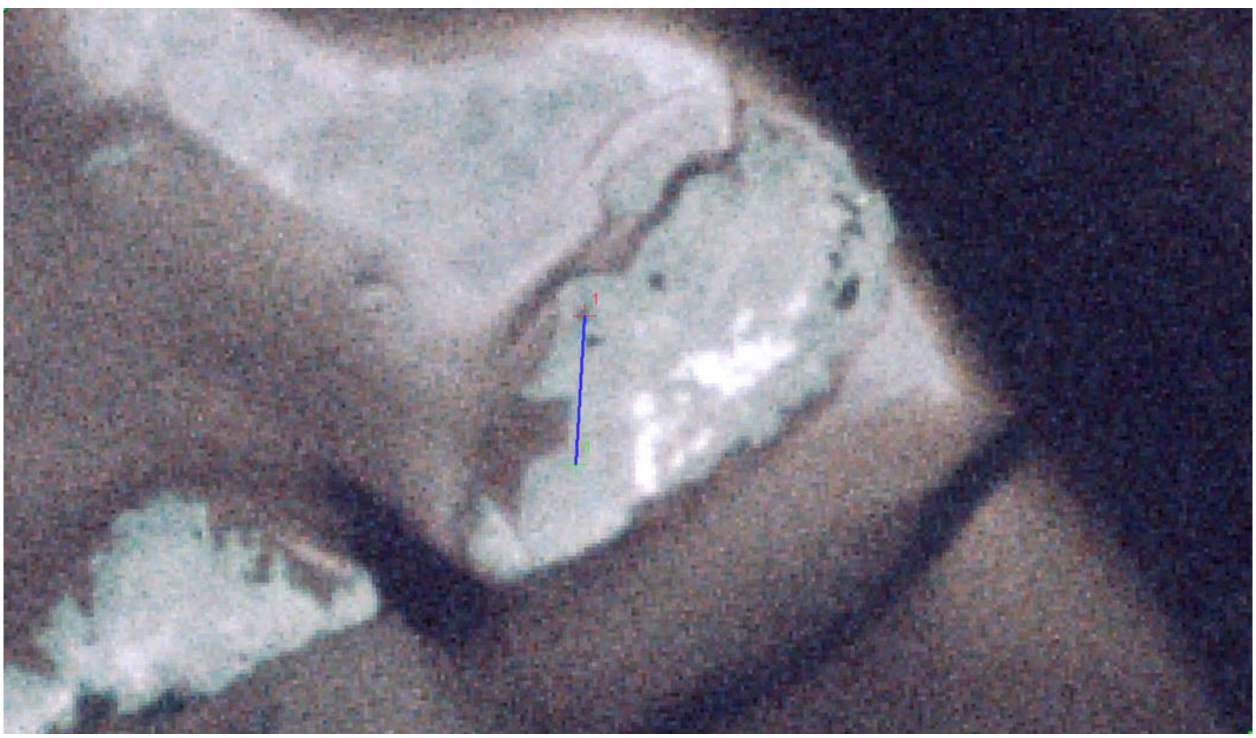

Fig. A106 June 1982 aerial image of North of Sanford 3 (not interpreted).

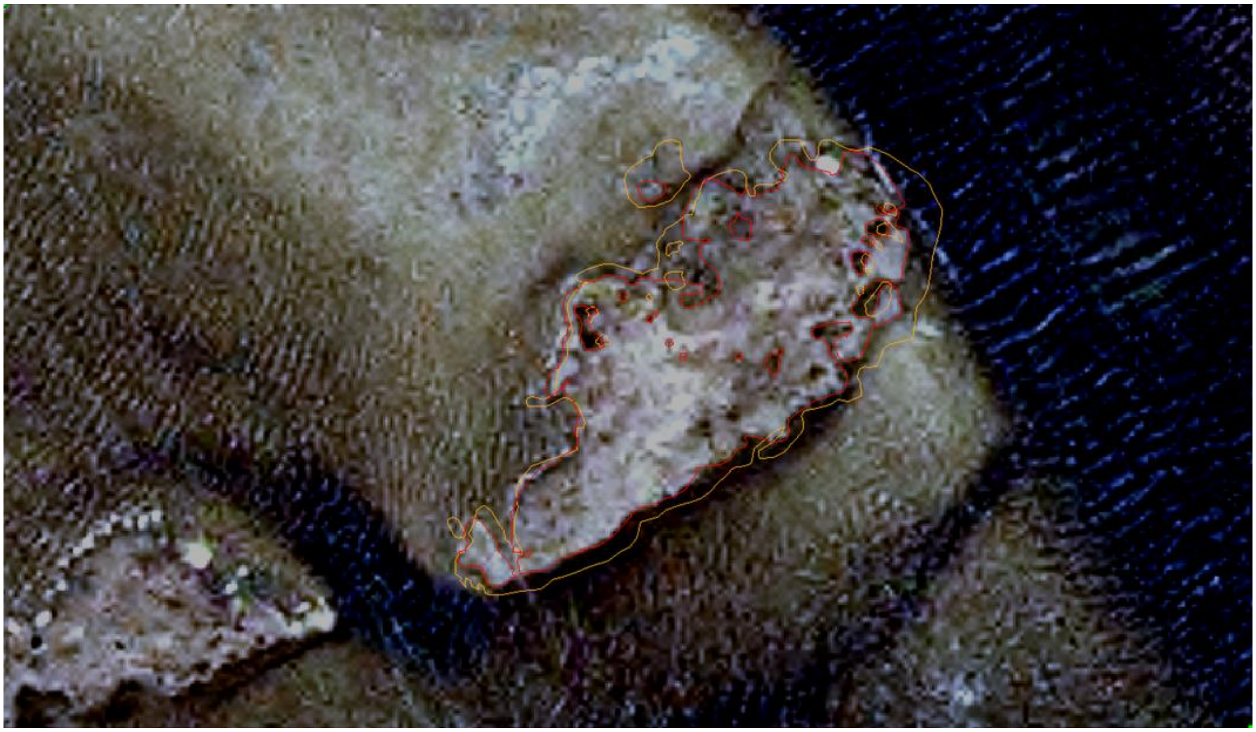

Fig. A107 North of Sanford 3 with April 2001 boundaries (red) on source photograph with previous April 1962 boundaries (orange).

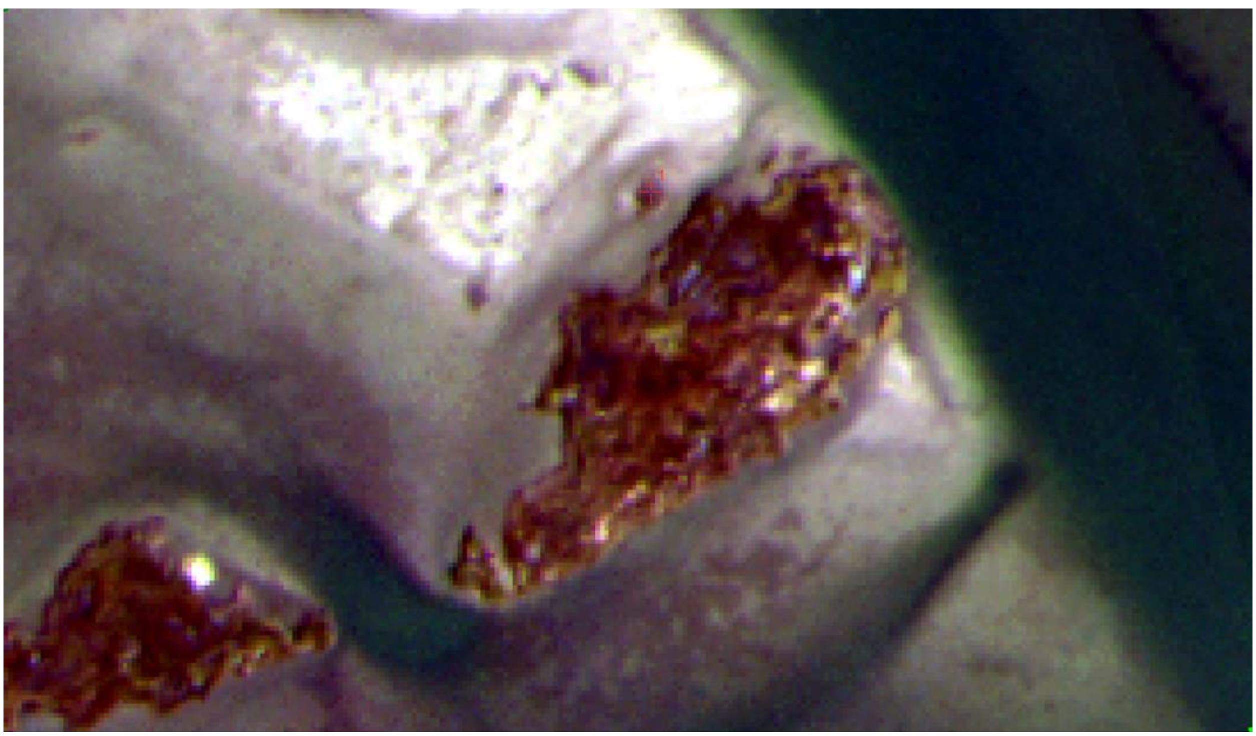

Fig. A108 June 2001 aerial image of North of Sanford 3 (not interpreted).

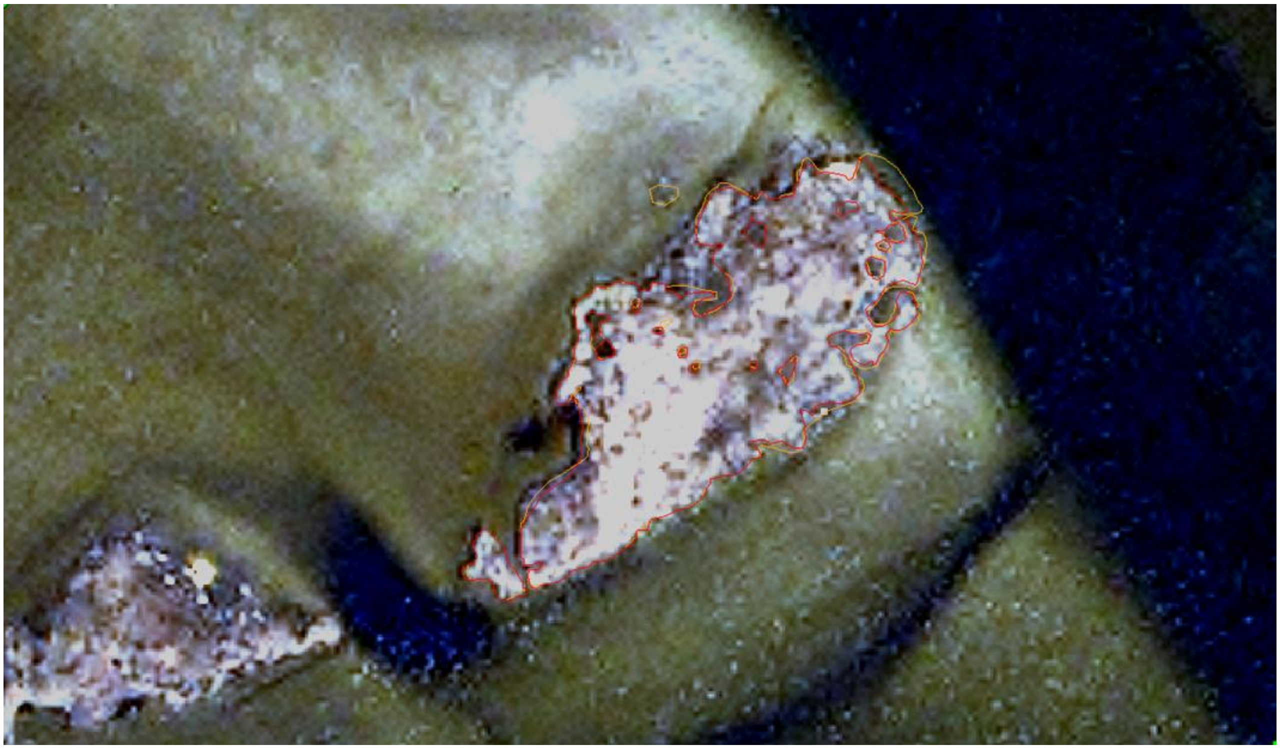

Fig. A109 North of Sanford 3 with April 2005 boundaries (red) on source photograph with previous April 2001 boundaries (orange).

Fig. A110 September 2008 aerial image of North of Sanford 3 (not interpreted).

Fig. A111 April 2009 aerial image of North of Sanford 3 (not interpreted).

Fig. A112 North of Sanford 3 with June 2012 boundaries (red) on source photograph with previous April 2005 boundaries (orange)

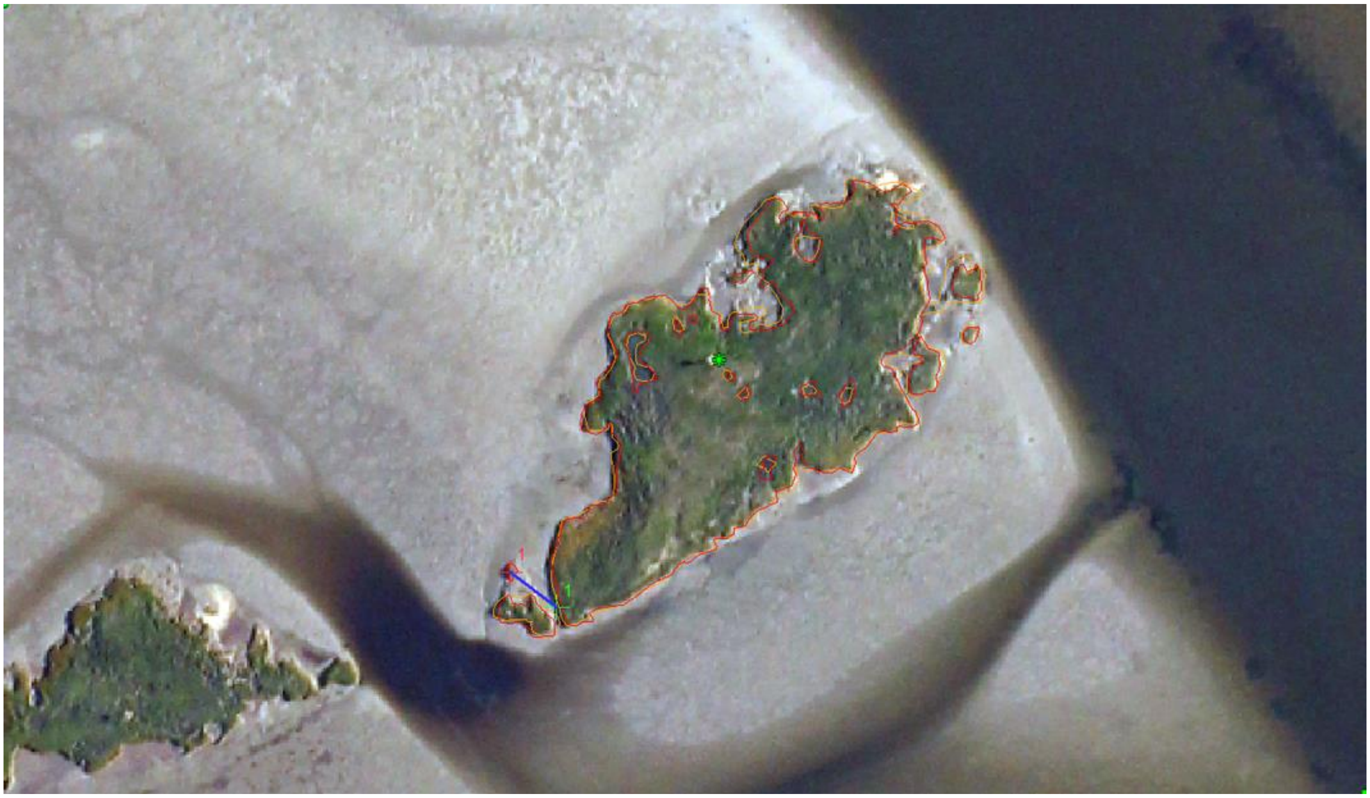

Fig. A113 North of Sanford 3 with September 2013 boundaries (red) on source photograph with previous June 2012 boundaries (orange).

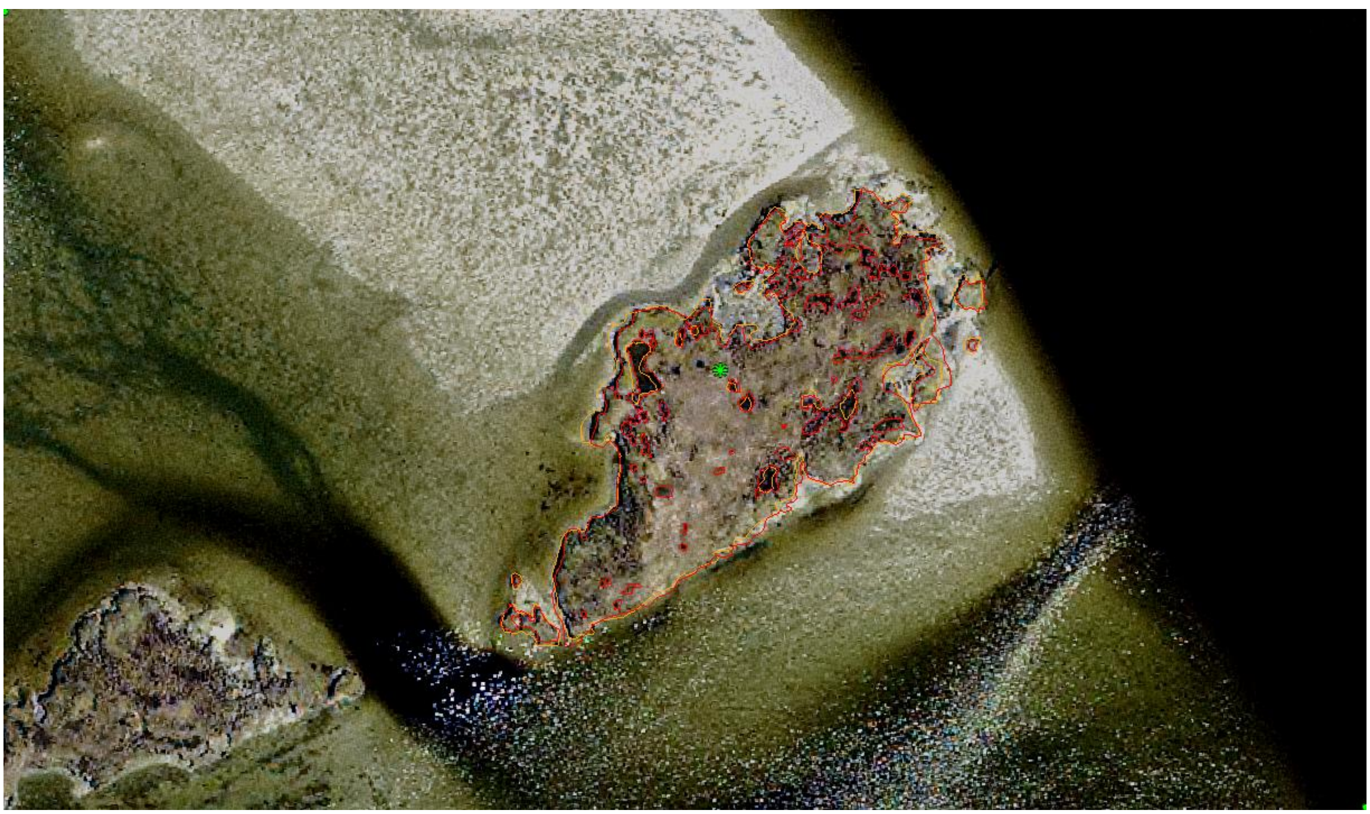

Fig. A114 North of Sanford 3 with April 2014 boundaries (red) on source photograph with previous September 2013 boundaries (orange).

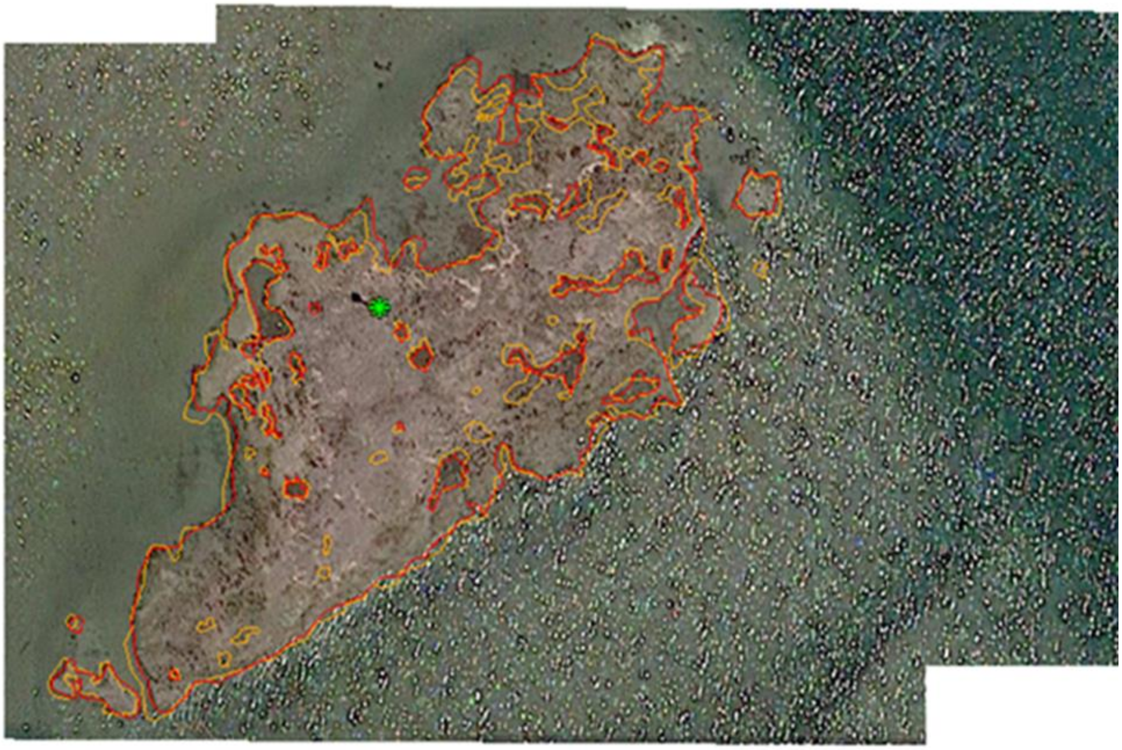

Fig. A115 North of Sanford 3 with May 2015 boundaries (red; Google Earth) on source photograph with previous April 2014 boundaries (orange).

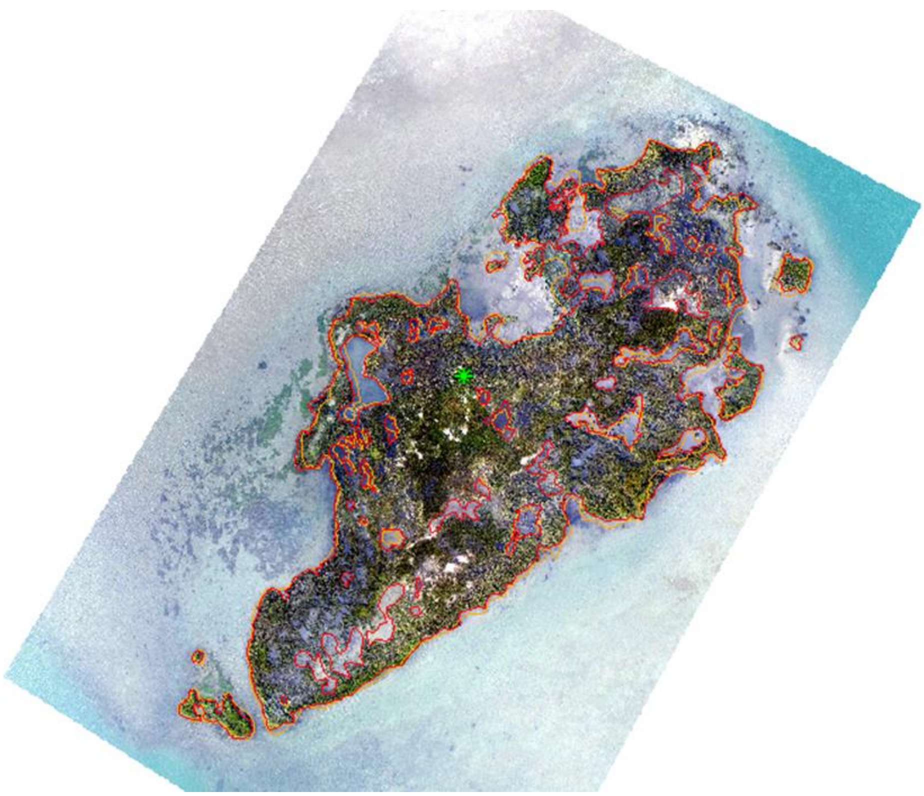

Fig. A116 North of Sanford 3 with October 2016 boundaries (red; UAV) on source photograph with previous May 2015 boundaries (orange).